UC Davis
UC Davis Electronic Theses and Dissertations

Title
Physiological Effects of Transition Metals and Serum Albumin on Proinsulin C-peptide

Permalink
https://escholarship.org/uc/item/6rx1r4p3

Author
San Juan, Jessica

Publication Date
2022

Peer reviewed|Thesis/dissertation

eScholarship.org Powered by the California Digital Library
University of California

Physiological Effects of Transition Metals and Serum Albumin on Proinsulin C-peptide

by

Jessica Ashley San Juan

DISSERTATION

Submitted in partial satisfaction of the requirements for the degree of

DOCTOR OF PHILOSOPHY

in

Chemistry and Chemical Biology

in the

OFFICE OF GRADUATE STUDIES

of the

UNIVERSITY OF CALIFORNIA

DAVIS

Approved:

Marie C. Heffern, Chair

David B. Goodin

Kit S. Lam

Committee in Charge

2023

© Jessica A. San Juan, 2023. All rights reserved.

Dedicated to Mom, Dad, and Justin who stood by my side no matter what and supported me through my education journey to become the person I am today.

“I hope that in this year to come, you make mistakes.

Because if you are making mistakes, then you are making new things, trying new things, learning, living, pushing yourself, changing yourself, changing your world. You're doing things you've never done before, and more importantly, you're Doing Something.

So that's my wish for you, and all of us, and my wish for myself. Make New Mistakes. Make glorious, amazing mistakes. Make mistakes nobody's ever made before. Don't freeze, don't stop, don't worry that it isn't good enough, or it isn't perfect, whatever it is: art, or love, or work or family or life.

Whatever it is you're scared of doing, Do it.

Make your mistakes, next year and forever.”

—Neil Gaiman

(A note to myself during my Ph.D. training)

Table of Contents

Abstract of the dissertation

Physiological Effects of Transition Metals and Serum Albumin on Proinsulin C-peptide

C-peptide exhibits beneficial effects, particularly in diabetic patients, but its clinical use has been hampered by a lack of mechanistic understanding. The work described in this thesis focuses on the advancement of C-peptide as a co-therapeutic with insulin for diabetic patients by elucidating the molecular mechanisms that drive the beneficial signaling effects of C-peptide. The work involved in understanding C-peptide's mechanisms of action during circulation, internalization, and peptide signaling include 1) identifying which metal co-factors interact with C-peptide and alter its intracellular functions, 2) analyzing how selected metal co-factors mediate ternary interactions between C-peptide and serum albumin, another potential regulatory factor, and impacts the biochemical behavior of the peptide, 3) revealing how high glucose exposure alters structure of serum albumin and modifies ternary complexations with C-peptide, and 4) determining how metal-bound C-peptide internalizes in different endocrine organs and shifts intracellular Cu trafficking levels linking to copper-related diseases.

Chapter 2 addresses the first goal in determining which essential first-row d-block transition metals play a role on the function of C-peptide using spectroscopic tools such as electronic absorption spectroscopy. Cr(III), Cu(II), and Zn(II) demonstrated binding to C-peptide with differing stoichiometries and biologically relevant binding affinities. Cr(III) and Cu(II) in particular modulated peptide internalization activity through subtle structural

changes, pointing to the biological importance of metal ions as co-factors and its impact on the function of bioactive peptides.

To this end, Chapter 3 expands on the regulatory factors associated with C-peptide by demonstrating the combined impact of Cu(II) and the serum protein albumin on the activity of C-peptide. By tackling the second goal, this chapter displays a combination of powerful tools such as FRET screening with Cu(II) and Zn(II) and spectroscopic tools. To complement the CD and electronic absorption spectroscopy studies, a collaborative effort with the Britt lab and Wang lab at UC Davis were extended to elucidate the coordination chemistry behind these ternary complexes using EPR and TDDFT studies. This work shows that Cu(II) distinctly mediates the formation of ternary complexes between albumin and C-peptide and that the resulting species depend on the order of addition. The resulting species revealed two schematics of binding, one of which is confirmed by both EPR and TDDFT simulations, whereas the other schematic points to a possible second binding site on C-peptide, as previously determined the Heffern lab. Due to differences in structure, both ternary complexes notably alter peptide activity, showing differences from the peptide or Cu(II)/peptide complexes alone in redox protection as well as in cellular internalization of the peptide. In standard clinical immunoassays for measuring C-peptide levels, the complexes inflate the quantitation of the peptide, suggesting that such adducts may affect biomarker quantitation. Altogether, our work points to the potential relevance of Cu(II)-linked C-peptide/albumin complexes in the peptide's mechanism of action and application as a clinical biomarker.

Because the focus on C-peptide mechanisms is tailored towards diabetic patients, it is crucial to consider that the structure-function of the peptide alongside its regulatory

factors may change in the presence of chronic glucose conditions. Serum albumin undergoes irreversible glycation after long-term exposure to high glucose levels, leading to modifications in its protein structure. The third goal addresses this challenge in Chapter 4, which reveals by spectroscopy (CD, UV-Vis) that glycated serum albumin alters ternary complexation with Cu(II) and C-peptide, as well as shifts cellular internalization and clinical measurements of C-peptide. To extend our understanding the molecular mechanisms of C-peptide with Cu(II) and albumin, this work looks into the impact of long-term incubation with high glucose on complexation with Cu(II), C-peptide and albumin. These studies begin to reveal formation of aggregation in collaboration with Dr. Duim at UC Davis, leading to the project development of determining what factors may drive aggregation. This warrants future studies by not only focusing on the mechanisms of C-peptide with its co-factors in normal conditions, but also considering the challenges that come with drug development of C-peptide in diabetic conditions.

As the relationship between Cu(II) and C-peptide has been thoroughly characterized in the previous chapters, Chapter 5 expands on the fourth goal by exploring the potential impact of Cu(II)-bound C-peptide on peptide internalization in different endocrine targets and Cu intracellular pathways. This work displays trends in redistributing Cu trafficking levels in the presence and absence of serum albumin, pointing to the mechanism of C-peptide as a sequestration factor, as well as linking to the impact C-peptide may have on Cu-associated diseases. Below is an abstract figure that encapsulates a visual of this thesis, and how each chapter contributes to the molecular understanding of C-peptide and its co-factors.

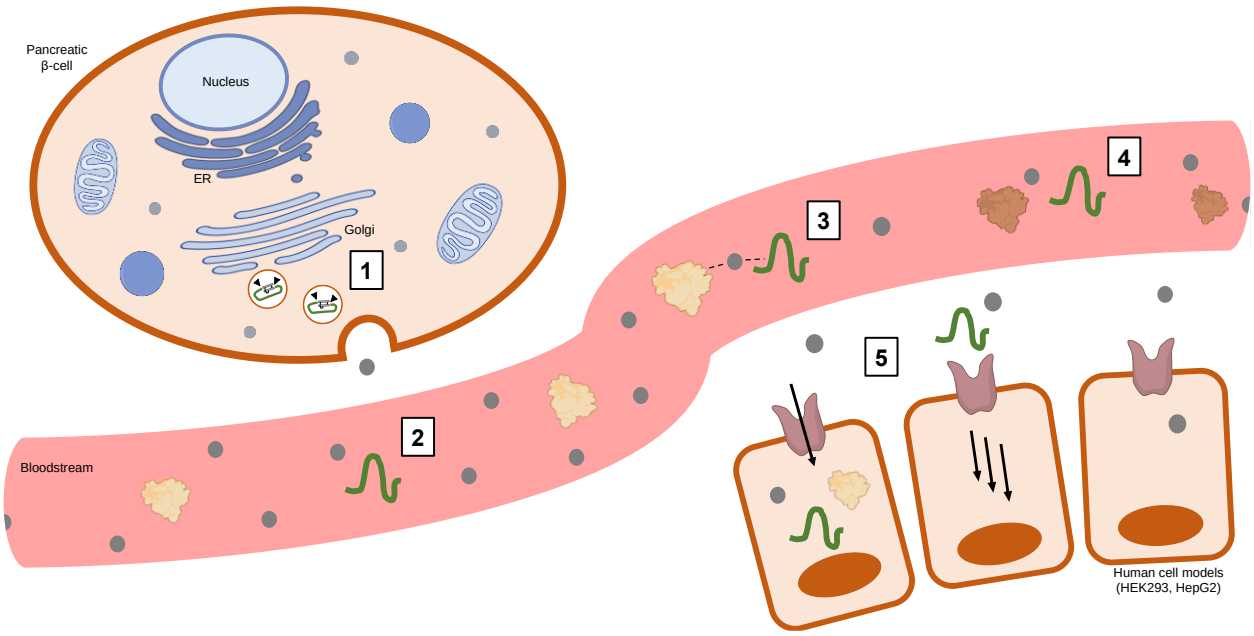

Abstract Figure. As indicated by number markers, Chapter 1 introduces the biosynthesis and discoveries made with C-peptide. Chapter 2 focuses on determining which metal co-factors interact with C-peptide. Chapter 3 expands on metal interactions with C-peptide by discussing how a metal ion may mediate ternary complexations with serum albumin. Chapter 4 explores diabetic conditions by revealing how long-term exposure to high glucose may impact ternary complexations elucidated in Chapter 3. Chapter 5 seeks to link C-peptide interactions with metals and its impact on intracellular metabolic pathways.

Acknowledgments

I am thankful for my family and friends for constantly supporting me, believing in me, and motivating me when times get tough. I would not be the successful person I am today without them. It really takes a village, and I dedicate this dissertation to them.

First, I am grateful for my PhD advisor, Marie Heffern, for letting me work with her group before my very first quarter even started. Since then, I learned many core values: recognizing my potential, trusting my intuition, and not being afraid of higher authority. With her endless support, knowledge, guidance, and mentorship, I became a confident scientist both at the bench and in front of an audience. Because of Marie, I am more detailed in my experimental designs, creative in my thinking processes, and an effective communicator. I had immense growth in both my personal and career development in my 4.5 years here and for that, I will always be grateful.

I am thankful to my dissertation committee who contributed to my confidence in growing as a scientist since my unique QE experience switching to online in less than 24 hours. They believed in me when I didn't myself at the time, and it is an experience I will always reflect on. I would like to thank David Goodin for his continued positivity and support, as well as his thought-provoking questions in how I approach my projects. I also want to thank Kit Lam for his genuine excitement and knowledge in the peptide field, and his inspiration in reaching out and networking with like-minded peptide scientists.

"If you want to go fast, go alone. If you want to go far, go together." -African Proverb. My work and knowledge would not gotten far without the help of collaborations

and mentorships. That's the best part about being in a STEM field—it is a community that comes together to use the diverse skills learned to be a part of something bigger and impact our society. First, I am thankful for my mentor in the lab, Michael Stevenson, for laying the groundwork and teaching me how to be a better scientist. I am also grateful for Job Chakarawet, Zhecheng He, Nathaniel Harder, Prof. R. Dave Britt, Prof. Lee-Ping Wang, and Prof. Whitney Duim. I also would like to thank all members of the Heffern Lab, both old and new, for cultivating a supportive and intellectually stimulating environment.

I also want to thankful those who contributed to my career journey over the years and allowed the space to explore new skills both at the bench and in my professional development: Prof. Kantorowski and Prof. Goodman at Cal Poly San Luis Obispo; Megan Wogan and my amazing co-workers at Calibr Scripps Research; Prof. Möenne-Loccoz, Prof. Ninian Blackburn and my mentor, Dr. Katherine Alwan, at Oregon Health & Science University.

Finally, I am forever grateful for my family who never stopped supporting me and constantly reminded me to celebrate my wins of all sizes—Mom, Dad, and Justin. I am also thankful to my partner, David Marchiori, who kept me grounded and supported me throughout grad school.

Thank you.

CHAPTER 1

Introduction: Effects of transition metals and serum albumin on proinsulin C-peptide activity

1.1 Therapeutic strategies using peptide hormones

Peptides have advanced the drug discovery of small molecules as a class of therapeutics that can target the undruggable due to their high potency, low toxicity, and selectivity.[1] Linked by peptide bonds, the structure of peptides vary by the number of amino acid chains ranging from dipeptides to polypeptides with molecular weights from 0.5 to 5 kDa.[2,3] Peptides typically act as growth factors, hormones, ion channel ligands, or anti-microbial agents. These systems bind with high specificity and affinity to distinct cell surface receptors and activate intracellular activities. While these mode of actions are comparable to existing biologics such as therapeutic proteins and antibodies, peptides possess the competitive advantage of lower immunogenicity, advanced peptide synthetic strategies, and effective manufacturing costs.[4–6] Below is an adaptation from Muttnethaler and colleagues[1] on milestones in peptide development and methodologies that shaped the success of peptide drug approvals in the peptide therapeutics field today (Figure 1.1).

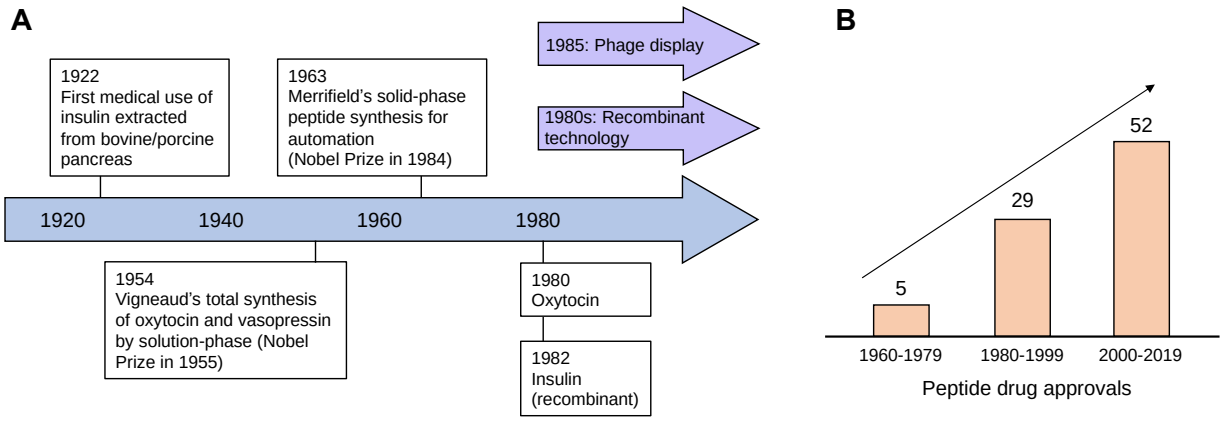

Figure 1.1. (A) The first peptide drug revolutionized the treatment for type 1 diabetes and initiated the peptide therapeutics field for clinical use. Peptides shifted to synthetic

production in the 1950s, however, processing took longer than other competing biologics. With the increase in commercial interest of peptides, automation of peptide production the use of solid-phase methods in the 1960s began to attract attention from the pharmaceutical industry. The advent of recombinant technology and phage display in the 1980s enabled effective manufacturing practices with larger peptides, leading to a surge in peptide drug approvals. (B) Peptide therapeutics now account for 5% of the pharmaceutical market, and the field continues to expand today.

1.1.1 Examples of milestone peptide therapeutics

The field of peptide therapeutics initiated in 1922 with the first discovery of insulin isolated from bovine and porcine pancreas, which plays a role regulating glucose in the bloodstream. Once its function was elucidated, insulin revolutionized clinical treatments as it became the first commercial peptide drug to treat patients with diabetes mellitus.[7] This finding led to fundamental studies of natural hormones in the 20th century centered on structure, biosynthesis, and their unique mode of action.[8] With decades of research on the elucidation on the structure and function of peptide hormones, peptide drug developments today are focused on synthetic peptide-derived analogues for clinical applications. A well-known example is oxytocin, a nonapeptide hormone first synthesized in the neurons of the hypothalamus in the brain, then transported to the posterior pituitary, where it is released to stimulate parturition and lactation.[9] Oxytocin is currently used to induce uterine contractions for childbirth, and displays promising effects for alleviating social disorders.[10,11] Similar to the peptide structure of oxytocin, vasopressin is a pituitary nonapeptide that differs by only two amino acids but produces opposite effects.[12]

Vasopressin induces changes in vasoconstriction, and acts as an anti-diuretic.[13] Figure 1.2 displays the structures of the aforementioned peptides in this section.

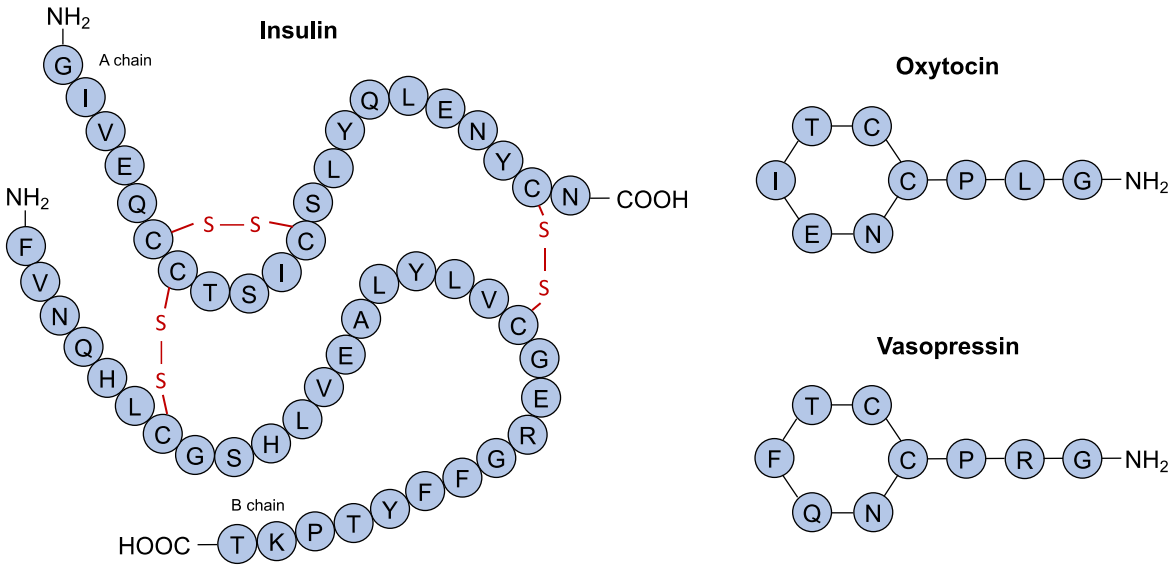

Figure 1.2. Insulin consists of two peptide chains connected by disulfide bridges: a 21-mer alpha (A)-chain and a 31-mer beta (B)-chain. Oxytocin and vasopressin are cyclic peptides with 9 AA residues. Differences of three residues between these peptide lead to juxtaposing functions.

1.2 History and significance of proinsulin C-peptide

After successful isolation of insulin, questions were raised regarding how the A- and B- chains of insulin come together to form biologically active insulin. Steiner and colleagues elucidated the mechanisms behind the biosynthesis of insulin,[14] and determined there were intermediate forms of insulin prior to secretion from the pancreas.

Their observations from labelling experiments in human pancreatic islet cells first revealed a protein molecular weight of 10.8 kDa.[14] This suggested that insulin exists as a precursor in the endoplasmic reticulum, termed as preproinsulin, where the amino acid sequence starts with a polypeptide chain at the N-terminus (N-terminal signal peptide) next to the B-chain segment of insulin, a connecting polypeptide chain between the normal insulin chain sequences, and ends with the A-chain segment of insulin. This protein precursor is what initiated the “prohormone” concept, in which active hormones exist as an inactive precursor first. Two types of proteolytic activities occur for the conversion of preproinsulin to active insulin. First, the N-terminal signal peptide is cleaved by an endopeptidase, creating proinsulin. Steiner & co-workers[15] showed that reoxidation of the fully reduced precursor produces high yields of proinsulin, indicating that the primary role of proinsulin is to facilitate the efficient formation of the disulfide bonds that link the A- and B- chains of insulin together. When active insulin is ready to be released into the bloodstream, exopeptidases cleave insulin from the connecting polypeptide chain. The free connecting segment found the middle of proinsulin was detected in equimolar amounts with active insulin post-secretion. This polypeptide chain was termed as C-peptide for its connecting properties.[16] An illustration of the production of active insulin and C-peptide, as well as the sequence of C-peptide, is shown in Figure 1.3.

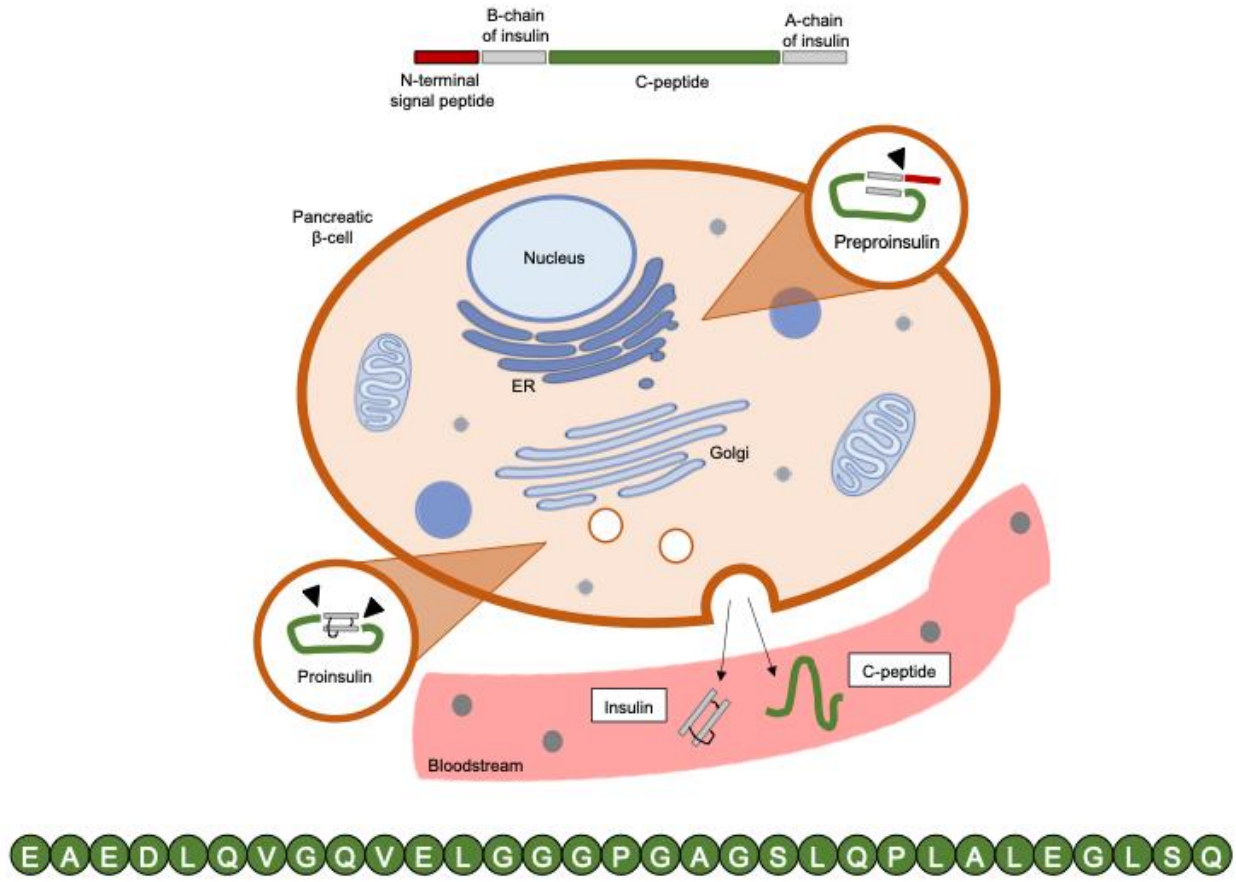

Figure 1.3. Biosynthesis of active insulin and C-peptide from the human pancreatic beta-islet cells and its intermediate prohormone products. Preproinsulin is cleaved by an endopeptidase to generate proinsulin. C-peptide brings the A- and B-chain of insulin together to form disulfide linkages. When signaled to be released to the bloodstream, an exopeptidase cleaves C-peptide from insulin to release equimolar amounts of active insulin and C-peptide. The resulting C-peptide product (green) is a 31-mer random coiled peptide.

1.2.1 C-peptide as a clinical diagnostic marker

Type 1 diabetes is an autoimmune disease in which the beta cells of the pancreas cannot produce insulin, thus requiring dependence on insulin injections to regulate blood sugar levels.[17] (CDC website). Decades ago, diagnosis of this chronic disease was difficult because insulin immunoassays were the primary diagnostic tool for measuring circulating insulin levels. These assays were more accurate for healthy subjects and diabetics with a managed diet than with insulin-treated diabetic patients who lack insulin production.[18] When it was discovered that C-peptide is released in equimolar concentrations with active insulin into the bloodstream, this opened doors to consider measurements of serum C-peptide to better understand the mechanisms behind destructed pancreatic beta cell function in patients with diabetes mellitus. Further foundational research on C-peptide revealed that the clearance rate of C-peptide was determined to be five times slower than insulin,[19] and that C-peptide production can persist decades after onset of the disease. Therefore, C-peptide peptide immunoassays became the standard measurement as an insulin marker and elucidation in beta cell functioning.[20]

1.3 Trends of beneficial effects observed on C-peptide activity

The long-term complications of Type 1 diabetes include cardiovascular (heart and blood vessel) disease, nephropathy (kidney damage), neuropathy (nerve damage), and retinopathy (eye damage).[21] Interestingly, there are diabetic patients who developed less

long-term complications than patients who are completely C-peptide deficient.[22,23] This is due to minimal endogenous beta cell activity that maintain the prolongation of C-peptide production after dysfunction of pancreatic beta cells. Researchers began to investigate if C-peptide contains any insulin-like effects. Initially thought to be inert, C-peptide now presents promising *in vivo* and *in vitro* bioactivity that could ameliorate the long-term complications of Type 1 diabetes such as blood flow regulation, glucose uptake, and increased cell growth.[24,25] An adaptation from Wahren and colleagues[25] on the summary of clinical, in vivo animal and in vitro cellular effects of C-peptide is listed in Table 1.1. Yet, despite its beneficial health effects, neither its mechanism of action nor any clear structure-function relationships have been elucidated, thus hindering its development and use as a therapeutic agent.

Table 1.1 in vivo animal and in vitro cellular effects of C-peptide

In vivo effects		*In vitro* effects	
Renal	Functional reserve ↑ Glomerular hyperfiltration ↓ Urinary albumin excretion ↓ Structural abnormalities ↓	Intracellular signaling	G-protein involvement Intracellular Ca2+ ↑ PKC, MAPK and PI-3Kγ ↑ NFκB, PPARγ, Bcl2, c-Fos, ZEB ↑
Nerve	Conduction velocity ↑ Vibration perception ↑ Blood flow ↑ Na+/K+-ATPase activity ↑ Hyperalgesia ↓ Structural abnormalities ↓	End effects	eNOS activity and protein levels ↑ Na+/K+-ATPase activity and protein levels ↑ Cell growth ↑ Apoptosis ↓ Insulinomimetic effects Anti-thrombotic effects
Circulation	Muscle blood flow ↑ Skin blood flow ↑ Myocardial blood flow and contraction rate ↑	Other	Disaggregation of insulin hexamers

1.4 Current structure-function studies of C-peptide with transition metals

Meyer and co-workers[26] first demonstrated a relationship between C-peptide and its beneficial effects on chronic diabetic complications by showing that C-peptide activates ATP release, a stimulant for nitric oxide in erythrocytes. This aids vasodilation by increasing blood flow and lowering blood pressure. The co-addition of Cr(III) and Fe(II) activated C-peptide by increasing ATP release from erythrocytes over 72 hours or 24 hours, respectively.[27] Zn(II)-activated C-peptide has also shown a similar effect by increasing ATP levels by 31%, as well as an increase in glucose uptake by 36% over

erythrocytes alone.[27,28] Recently, the Heffern lab demonstrated that Cu(II) can alter peptide internalization[29] by directly binding to E3 and D4 of C-peptide.[30] Moreover, the wild-type sequence of C-peptide is necessary for precise binding of Cu(II) to C-peptide, and mutations or truncations of the peptide lead to non-specific metal ion binding.[30] Metals clearly play a role in peptide activity, setting a paradigm in which metals should be considered when understanding the structure-function of C-peptide at a molecular level.

1.4.1 Serum albumin as a potential chaperone for C-peptide

To expand on C-peptide and Zn(II) delivery to erythrocytes for ATP release, Spence and co-workers showed that C-peptide can bind to erythrocytes in the presence or absence of Zn(II), and that Zn(II) delivery to erythrocytes only occurs in the presence of C-peptide.[31,32] However, the mechanisms of C-peptide binding to Zn(II) could not be demonstrated, indicating that another biomolecule may play a role. The physiological salt solutions used for their studies contain albumin, a protein carrier for peptides, metabolites, and drug molecules *in vivo.*[33] When working with albumin-free solutions, C-peptide and Zn(II) delivery to erythrocytes was absent, suggesting that albumin is necessary for enhanced ATP release.[31] Geiger and colleagues confirmed that with the addition of albumin/C-peptide/Zn(II) complex, ATP release in ATP-derived erythrocytes of Type 1 diabetic patients was restored to the levels of control or healthy erythrocytes.[32] Because the receptor for C-peptide remains elusive, it is now suggested that there may be a receptor for albumin/C-peptide/Zn(II) on erythrocytes.[32]

Serum albumin can become modified in hyperglycemic conditions by a process termed glycation, which may alter ligand binding capabilities.[34–36] Jacobs and co-workers demonstrated that glycation of serum albumin disrupted C-peptide and Zn(II) binding to erythrocytes and decreased ATP release in comparison to previous studies with normal serum albumin. This suggests that hyperglycemic patients with Type 1 diabetes have implications for C-peptide therapy strategies.[37]

1.5. C-peptide as a potential biomarker for copper-related disease states

Studies have shown that imbalances in C-peptide levels can serve as a risk and potentially diagnostic factor for the progression of metabolic diseases. For instance, Wang and co-workers observed that C-peptide levels decrease with the advancement of T2D, pointing to decreased function of the pancreatic beta-cells and the onset of inflammatory and fibrotic progression.[38] On the other hand, Han and colleagues demonstrated higher serum fasting C-peptide levels in obese children with non-alcoholic fatty liver disease (NAFLD) in comparison to the group without NAFLD.[39] Interestingly, copper dyshomeostasis has also been implicated in these disorders. Because the Heffern lab has characterized the Cu-binding properties of C-peptide, we hypothesize that there may be a mechanistic link between C-peptide levels and Cu regulation in DM and NAFLD.

1.5.1 Copper homeostasis

Cu is an essential metal used as a cofactor for many enzymatic functions involved in metabolic processes. When Cu is misregulated, it can be highly toxic to cells by generating reactive oxygen species (ROS).[40] ROS formation leads to protein oxidation and cleavage of DNA and RNA, peroxidation of membrane lipids, and eventually cell death.[41] Therefore, the maintenance of Cu homeostasis is crucial to avoid these chain of events. Cu ions in the bloodstream are transported through enterocytes and imported into the cell by a Cu transporter, CTR1, and is delivered to one of two Cu ATPases, ATP7A or ATP7B, for export out of the cell.[42] Cu-binding proteins in blood plasma then bind to Cu to regulate copper levels and distribution. For instance, ceruloplasmin binds tightly to 40-70% of total plasma copper and delivers copper directly to cell membrane transporters. Another example is albumin, a major constituent of exchangeable copper and accounts for 10-15% of plasma copper.[43]

1.5.2 Copper imbalance associated with DM and NAFLD

Generation of ROS such as superoxide and hydroxyl radicals is a common phenomenon associated with diabetes mellitus (DM).[44] DM leads to failure or damage of different organs and tissues such as the arteries, heart, nerves, kidneys, and retina.[45,46] It is still unclear how generation of ROS is induced in DM, but multiple studies have evaluated biologically relevant transition metals as catalysts of oxidative stress.[47,48]

Cu levels in particular exhibited a correlation with T1D studies. Streptozotocin (STZ), a common inducing agent to study T1D, destructs the function of pancreatic beta-

cells. STZ-induced rats contain elevated levels of Cu in the liver and kidney after a week of treatment, then a two to five-fold increase in Cu levels after four weeks in comparison to the control groups.[48] There was also an increase in Cu in daily urinary excretion.[49] Both of these measurements in STZ-induced rats were comparable to T1D patients, where higher serum Cu concentrations[50] and elevated ceruloplasmin plasma levels were detected in comparison to heathy subjects,[51] pointing to the systemic overload of Cu in T1D. T2D patients displayed similar trends, with higher Cu levels in serum plasma and urinary excretion, regardless of the progression path towards T2D long-term complications.[52,53] Together, these studies show that alteration of Cu levels is an important factor to consider for the onset of DM complications due to increased oxidative stress and ROS formation.[54,55]

On the other hand, Cu deficiency (CuD) is a result of abnormal cell export (ATP7A) leading to maldistribution, reduced ceruloplasmin concentrations, and decreased Cu absorption.[56–59] Because of these deleterious events, changes in lipid metabolism and increased oxidative stress are observed in both animal and human models, suggesting that CuD is a contributing factor in the pathogenesis of metabolic diseases such as non-alcoholic fatty-liver disease (NAFLD).[60,61] NAFLD is defined as the accumulation of hepatic lipidation, and is considered the leading cause of chronic liver disease in both children and adults.[62,63] However, further studies are necessary to elucidate the mechanisms that drive the imbalance of Cu in DM and NAFLD.

1.6 References

(1) Muttenthaler, M.; King, G. F.; Adams, D. J.; Alewood, P. F. Trends in Peptide Drug Discovery. *Nat. Rev. Drug Discov. 2021 204* **2021**, *20* (4), 309–325. https://doi.org/10.1038/s41573-020-00135-8.

(2) Henninot, A.; Collins, J. C.; Nuss, J. M. The Current State of Peptide Drug Discovery: Back to the Future? *J. Med. Chem.* **2018**, *61* (4), 1382–1414. https://doi.org/10.1021/ACS.JMEDCHEM.7B00318/ASSET/IMAGES/LARGE/JM-2017-00318Y_0034.JPEG.

(3) Craik, D. J.; Fairlie, D. P.; Liras, S.; Price, D. The Future of Peptide-Based Drugs. *Chem. Biol. Drug Des.* **2013**, *81* (1), 136–147. https://doi.org/10.1111/CBDD.12055.

(4) Fosgerau, K.; Hoffmann, T. Peptide Therapeutics: Current Status and Future Directions. *Drug Discov. Today* **2015**, *20* (1), 122–128. https://doi.org/10.1016/j.drudis.2014.10.003.

(5) Davda, J.; Declerck, P.; Hu-Lieskovan, S.; Hickling, T. P.; Jacobs, I. A.; Chou, J.; Salek-Ardakani, S.; Kraynov, E. Immunogenicity of Immunomodulatory, Antibody-Based, Oncology Therapeutics. *J. Immunother. Cancer* **2019**, *7* (1), 1–9. https://doi.org/10.1186/S40425-019-0586-0/TABLES/2.

(6) Waldmann, H. Human Monoclonal Antibodies: The Residual Challenge of Antibody Immunogenicity. *Methods Mol. Biol.* **2014**, *1060*, 1–8. https://doi.org/10.1007/978-1-62703-586-6_1.

(7) Scott, D. A.; Best, C. H. The Preparation of Insulin. *Ind. Eng. Chem. 17* (3).

(8) Tager, H. S.; Steiner, D. F. Peptide Hormones. *https://doi.org/10.1146/annurev.bi.43.070174.002453* **2003**, *Vol 43*, 509–538. https://doi.org/10.1146/ANNUREV.BI.43.070174.002453.

(9) Young, W. S.; Gainer, H. Transgenesis and the Study of Expression, Cellular Targeting and Function of Oxytocin, Vasopressin and Their Receptors. *Neuroendocrinology* **2003**, *78* (4), 185–203. https://doi.org/10.1159/000073702.

(10) Argiolas, A.; Gessa, G. L. Central Functions of Oxytocin. *Neurosci. Biobehav. Rev.* **1991**, *15* (2), 217–231. https://doi.org/10.1016/S0149-7634(05)80002-8.

(11) Lee, H. J.; Macbeth, A. H.; Pagani, J. H.; Scott Young, W. Oxytocin: The Great Facilitator of Life. *Prog. Neurobiol.* **2009**, *88* (2), 127. https://doi.org/10.1016/J.PNEUROBIO.2009.04.001.

(12) Baribeau, D. A.; Anagnostou, E. Oxytocin and Vasopressin: Linking Pituitary Neuropeptides and Their Receptors to Social Neurocircuits. *Front. Neurosci.* **2015**, *9* (SEP), 335. https://doi.org/10.3389/FNINS.2015.00335/XML/NLM.

(13) Robertson, G. L. The Regulation of Vasopressin Function in Health and Disease. *Recent Prog. Horm. Res.* **1977**, *Vol. 33*, 333–385. https://doi.org/10.1016/B978-0-12-571133-3.50015-5.

(14) Steiner, D. F.; Oyer, P. E. THE BIOSYNTHESIS OF INSULIN AND A PROBABLE PRECURSOR OF INSULIN BY A HUMAN ISLET CELL ADENOMA. *Proc. Natl. Acad. Sci.* **1967**, *57* (2), 473–480. https://doi.org/10.1073/PNAS.57.2.473.
(15) Rubenstein, A. H.; Clark, J. L.; Melani, F.; Steiner, D. F. Secretion of Proinsulin C-Peptide by Pancreatic β Cells and Its Circulation in Blood. *Nat. 1969 2245220* **1969**, *224* (5220), 697–699. https://doi.org/10.1038/224697a0.
(16) Brandenburg, D. History and Diagnostic Significance of C-Peptide. *Exp. Diabetes Res.* **2008**, *2008*, 576862. https://doi.org/10.1155/2008/576862.
(17) *What Is Type 1 Diabetes?* | *CDC*. https://www.cdc.gov/diabetes/basics/what-is-type-1-diabetes.html (accessed 2022-11-01).
(18) Rubenstein, A. H.; Kuzuya, H.; Horwitz, D. L. Clinical Significance of Circulating C-Peptide in Diabetes Mellitus and Hypoglycemic Disorders. *Arch. Intern. Med.* **1977**, *137* (5), 625–632. https://doi.org/10.1001/ARCHINTE.1977.03630170047014.
(19) Faber, O. K.; Hagen, C.; Binder, C.; Markussen, J.; Naithani, V. K.; Blix, P. M.; Kuzuya, H.; Horwitz, D. L.; Rubenstein, A. H.; Rossing, N. Kinetics of Human Connecting Peptide in Normal and Diabetic Subjects. *J. Clin. Invest.* **1978**, *62* (1), 197–203. https://doi.org/10.1172/JCI109106.
(20) Wang, L.; Lovejoy, N. F.; Faustman, D. L. Persistence of Prolonged C-Peptide Production in Type 1 Diabetes as Measured With an Ultrasensitive C-Peptide Assay. *Diabetes Care* **2012**, *35* (3), 465–470. https://doi.org/10.2337/DC11-1236.
(21) Deshpande, A. D.; Harris-Hayes, M.; Schootman, M. Epidemiology of Diabetes and Diabetes-Related Complications. *Phys. Ther.* **2008**, *88* (11), 1254. https://doi.org/10.2522/PTJ.20080020.
(22) Sjöberg, S.; Gunnarsson, R.; Gjötterberg, M.; Lefvert, A. K.; Persson, A.; Östman, J. Residual Insulin Production, Glycaemic Control and Prevalence of Microvascular Lesions and Polyneuropathy in Long-Term Type 1 (Insulin-Dependent) Diabetes Mellitus. *Diabetol. 1987 304* **1987**, *30* (4), 208–213. https://doi.org/10.1007/BF00270417.
(23) Zerbini, G.; Mangili, R.; Luzi, L. Higher Post-Absorptive C-Peptide Levels in Type 1 Diabetic Patients without Renal Complications. *Diabet. Med.* **1999**, *16* (12), 1048–1048. https://doi.org/10.1046/J.1464-5491.1999.00181.X.
(24) Marques, R. G.; Fontaine, M. J.; Rogers, J. C-Peptide: Much More than a Byproduct of Insulin Biosynthesis. *Pancreas* **2004**, *29* (3), 231–238. https://doi.org/10.1097/00006676-200410000-00009.
(25) Wahren, J.; Ekberg, K.; Jörnvall, H. C-Peptide Is a Bioactive Peptide. *Diabetologia* **2007**, *50* (3), 503–509. https://doi.org/10.1007/s00125-006-0559-y.
(26) Meyer, J. A.; Froelich, J. M.; Reid, G. E.; Karunarathne, W. K. A.; Spence, D. M. Metal-Activated C-Peptide Facilitates Glucose Clearance and the Release of a Nitric Oxide Stimulus via the GLUT1 Transporter. *Diabetologia* **2008**, *51* (1), 175–

182. https://doi.org/10.1007/s00125-007-0853-3.
(27) Meyer, J. A.; Subasinghe, W.; Sima, A. A. F.; Keltner, Z.; Reid, G. E.; Daleke, D.; Spence, D. M. Zinc-Activated C-Peptide Resistance to the Type 2 Diabetic Erythrocyte Is Associated with Hyperglycemia-Induced Phosphatidylserine Externalization and Reversed by Metformin. *Mol. Biosyst.* **2009**, *5* (10), 1157–1162. https://doi.org/10.1039/B908241G.
(28) Medawala, W.; McCahill, P.; Giebink, A.; Meyer, J.; Ku, C. J.; Spence, D. M. A Molecular Level Understanding of Zinc Activation of C-Peptide and Its Effects on Cellular Communication in the Bloodstream. *Review of Diabetic Studies*. Society for Biomedical Diabetes Research September 2009, pp 148–158. https://doi.org/10.1900/RDS.2009.6.148.
(29) Stevenson, M. J.; Farran, I. C.; Uyeda, K. S.; San Juan, J. A.; Heffern, M. C. Analysis of Metal Effects on C-Peptide Structure and Internalization. *ChemBioChem* **2019**, *20* (19), 2447–2453. https://doi.org/10.1002/cbic.201900172.
(30) Stevenson, M. J.; Janisse, S. E.; Tao, L.; Neil, R. L.; Pham, Q. D.; Britt, R. D.; Heffern, M. C. Elucidation of a Copper Binding Site in Proinsulin C-Peptide and Its Implications for Metal-Modulated Activity. *Inorg. Chem.* **2020**, *59* (13), 9339–9349. https://doi.org/10.1021/acs.inorgchem.0c01212.
(31) Liu, Y.; Chen, C.; Summers, S.; Medawala, W.; Spence, D. M. C-Peptide and Zinc Delivery to Erythrocytes Requires the Presence of Albumin: Implications in Diabetes Explored with a 3D-Printed Fluidic Device. *Integr. Biol. (United Kingdom)* **2015**, *7* (5), 534–543. https://doi.org/10.1039/c4ib00243a.
(32) Geiger, M.; Janes, T.; Keshavarz, H.; Summers, S.; Pinger, C.; Fletcher, D.; Zinn, K.; Tennakoon, M.; Karunarathne, A.; Spence, D. A C-Peptide Complex with Albumin and Zn2+ Increases Measurable GLUT1 Levels in Membranes of Human Red Blood Cells. *Sci. Rep.* **2020**, *10* (1), 1–9. https://doi.org/10.1038/s41598-020-74527-6.
(33) Bal, W.; Sokołowska, M.; Kurowska, E.; Faller, P. Binding of Transition Metal Ions to Albumin: Sites, Affinities and Rates. *Biochimica et Biophysica Acta - General Subjects*. 2013, pp 5444–5455. https://doi.org/10.1016/j.bbagen.2013.06.018.
(34) Anguizola, J.; Matsuda, R.; Barnaby, O. S.; Joseph, K. S.; Wa, C.; DeBolt, E.; Koke, M.; Hage, D. S. Review: Glycation of Human Serum Albumin. *Clin. Chim. Acta.* **2013**, *0*, 64. https://doi.org/10.1016/J.CCA.2013.07.013.
(35) Rondeau, P.; Bourdon, E. The Glycation of Albumin: Structural and Functional Impacts. *Biochimie* **2011**, *93* (4), 645–658. https://doi.org/10.1016/J.BIOCHI.2010.12.003.
(36) Nakajou, K.; Watanabe, H.; Kragh-Hansen, U.; Maruyama, T.; Otagiri, M. The Effect of Glycation on the Structure, Function and Biological Fate of Human Serum Albumin as Revealed by Recombinant Mutants. *Biochim. Biophys. Acta -*

Gen. Subj. **2003**, *1623* (2–3), 88–97. https://doi.org/10.1016/j.bbagen.2003.08.001.

(37) Jacobs, M. J.; Geiger, M. K.; Summers, S. E.; DeLuca, C. P.; Zinn, K. R.; Spence, D. M. Albumin Glycation Affects the Delivery of C-Peptide to the Red Blood Cells. *ACS Meas. Sci. Au* **2022**, *2* (3), 278–286. https://doi.org/10.1021/ACSMEASURESCIAU.2C00001.

(38) Wang, N.; Wang, Y.; Zhang, W.; Chen, Y.; Chen, X.; Wang, C.; Li, Q.; Chen, C.; Jiang, B.; Lu, Y. C-Peptide Is Associated with NAFLD Inflammatory and Fibrotic Progression in Type 2 Diabetes. *Diabetes. Metab. Res. Rev.* **2020**, *36* (2), e3210. https://doi.org/10.1002/DMRR.3210.

(39) Han, X.; Xu, P.; Zhou, J.; Liu, Y.; Xu, H. Fasting C-Peptide Is a Significant Indicator of Nonalcoholic Fatty Liver Disease in Obese Children. *Diabetes Res. Clin. Pract.* **2020**, *160*, 108027. https://doi.org/10.1016/j.diabres.2020.108027.

(40) Malmström, B. G.; Leckner, J. The Chemical Biology of Copper. *Curr. Opin. Chem. Biol.* **1998**, *2* (2), 286–292. https://doi.org/10.1016/S1367-5931(98)80071-9.

(41) Halliwell, B.; Gutteridge, J. M. C. Oxygen Toxicity, Oxygen Radicals, Transition Metals and Disease. *Biochem. J.* **1984**, *219* (1), 1. https://doi.org/10.1042/BJ2190001.

(42) Barnes, N.; Bartee, M. Y.; Braiterman, L.; Gupta, A.; Ustiyan, V.; Zuzel, V.; Kaplan, J. H.; Hubbard, A. L.; Lutsenko, S. CELL-SPECIFIC TRAFFICKING SUGGESTS A NEW ROLE FOR RENAL ATP7B IN THE INTRACELLULAR COPPER STORAGE. *Traffic* **2009**, *10* (6), 767. https://doi.org/10.1111/J.1600-0854.2009.00901.X.

(43) Linder, M. C. Ceruloplasmin and Other Copper Binding Components of Blood Plasma and Their Functions: An Update. *Metallomics* **2016**, *8* (9), 887–905. https://doi.org/10.1039/c6mt00103c.

(44) Mohamed, A. K.; Bierhaus, A.; Schiekofer, S.; Tritschler, H.; Ziegler, R.; Nawroth, P. P. The Role of Oxidative Stress and NF-KB Activation in Late Diabetic Complications. *BioFactors* **1999**, *10* (2–3), 157–167. https://doi.org/10.1002/BIOF.5520100211.

(45) Abcouwer, S. F.; Gardner, T. W. Diabetic Retinopathy: Loss of Neuroretinal Adaptation to the Diabetic Metabolic Environment. *Ann. N. Y. Acad. Sci.* **2014**, *1311* (1), 174–190. https://doi.org/10.1111/NYAS.12412.

(46) Song, M. K.; Davies, N. M.; Roufogalis, B. D.; Huang, T. H. W. Management of Cardiorenal Metabolic Syndrome in Diabetes Mellitus: A Phytotherapeutic Perspective. *J. Diabetes Res.* **2014**, *2014*. https://doi.org/10.1155/2014/313718.

(47) Viktorínová, A.; Tošerová, E.; Križko, M.; Ďuračková, Z. Altered Metabolism of Copper, Zinc, and Magnesium Is Associated with Increased Levels of Glycated Hemoglobin in Patients with Diabetes Mellitus. *Metabolism.* **2009**, *58* (10), 1477–

1482. https://doi.org/10.1016/j.metabol.2009.04.035.
(48) Failla, M. L.; Kiser, R. A. Hepatic and Renal Metabolism of Copper and Zinc in the Diabetic Rat. *https://doi.org/10.1152/ajpendo.1983.244.2.E115* **1983**, *7* (2). https://doi.org/10.1152/AJPENDO.1983.244.2.E115.
(49) Lau, A. L.; Failla, M. L. Urinary Excretion of Zinc, Copper and Iron in the Streptozotocin-Diabetic Rat. *J. Nutr.* **1984**, *114* (1), 224–233. https://doi.org/10.1093/JN/114.1.224.
(50) Uriu-Adams, J. Y.; Rucker, R. B.; Commisso, J. F.; Keen, C. L. Diabetes and Dietary Copper Alter 67Cu Metabolism and Oxidant Defense in the Rat. *J. Nutr. Biochem.* **2005**, *16* (5), 312–320. https://doi.org/10.1016/J.JNUTBIO.2005.01.007.
(51) Cunninghamn, J.; Leffell, M.; Mearkle, P.; Harmatz, P. Elevated Plasma Ceruloplasmin in Insulin-Dependent Diabetes Mellitus: Evidence for Increased Oxidative Stress as a Variable Complication. *Metabolism* **1995**, *44* (8), 996–999. https://doi.org/10.1016/0026-0495(95)90095-0.
(52) Ito, S.; Fujita, H.; Narita, T.; Yaginuma, T.; Kawarada, Y.; Kawagoe, M.; Sugiyama, T. Urinary Copper Excretion in Type 2 Diabetic Patients with Nephropathy. *Nephron* **2001**, *88* (4), 307–312. https://doi.org/10.1159/000046013.
(53) Cooper, G. J. S.; Chan, Y. K.; Dissanayake, A. M.; Leahy, F. E.; Keogh, G. F.; Frampton, C. M.; Gamble, G. D.; Brunton, D. H.; Baker, J. B.; Poppitt, S. D. Demonstration of a Hyperglycemia-Driven Pathogenic Abnormality of Copper Homeostasis in Diabetes and Its Reversibility by Selective ChelationQuantitative Comparisons Between the Biology of Copper and Eight Other Nutritionally Essential Elements in Normal and Diabetic Individuals. *Diabetes* **2005**, *54* (5), 1468–1476. https://doi.org/10.2337/DIABETES.54.5.1468.
(54) Lowe, J.; Taveira-da-Silva, R.; Hilário-Souza, E. Dissecting Copper Homeostasis in Diabetes Mellitus. *IUBMB Life* **2017**, *69* (4), 255–262. https://doi.org/10.1002/IUB.1614.
(55) Squitti, R.; Negrouk, V.; Perera, M.; Llabre, M. M.; Ricordi, C.; Rongioletti, M. C. A.; Mendez, A. J. Serum Copper Profile in Patients with Type 1 Diabetes in Comparison to Other Metals. *J. Trace Elem. Med. Biol.* **2019**, *56*, 156–161. https://doi.org/10.1016/j.jtemb.2019.08.011.
(56) Danks, D. M. Copper Deficiency in Humans. *https://doi.org/10.1146/annurev.nu.08.070188.001315* **2003**, *8*, 235–257. https://doi.org/10.1146/ANNUREV.NU.08.070188.001315.
(57) Song, M.; Schuschke, D. A.; Zhou, Z.; Chen, T.; Pierce, W. M.; Wang, R.; Johnson, W. T.; McClain, C. J. High Fructose Feeding Induces Copper Deficiency in Sprague-Dawley Rats: A Novel Mechanism for Obesity Related Fatty Liver. *J. Hepatol.* **2012**, *56* (2), 433–440. https://doi.org/10.1016/J.JHEP.2011.05.030.
(58) Gletsu-Miller, N.; Broderius, M.; Frediani, J. K.; Zhao, V. M.; Griffith, D. P.; Davis, S. S.; Sweeney, J. F.; Lin, E.; Prohaska, J. R.; Ziegler, T. R. Incidence and

Prevalence of Copper Deficiency Following Roux-En-y Gastric Bypass Surgery. *Int. J. Obes. (Lond).* **2012**, *36* (3), 328–335. https://doi.org/10.1038/IJO.2011.159.

(59) Kumar, N.; Crum, B.; Petersen, R. C.; Vernino, S. A.; Ahlskog, J. E. Copper Deficiency Myelopathy. *Arch. Neurol.* **2004**, *61* (5), 762–766. https://doi.org/10.1001/ARCHNEUR.61.5.762.

(60) Morrell, A.; Tallino, S.; Yu, L.; Burkhead, J. L. The Role of Insufficient Copper in Lipid Synthesis and Fatty-Liver Disease. *IUBMB Life* **2017**, *69* (4), 263–270. https://doi.org/10.1002/iub.1613.

(61) Aigner, E.; Strasser, M.; Haufe, H.; Sonnweber, T.; Hohla, F.; Stadlmayr, A.; Solioz, M.; Tilg, H.; Patsch, W.; Weiss, G.; Stickel, F.; Datz, C. A Role for Low Hepatic Copper Concentrations in Nonalcoholic Fatty Liver Disease. *Am. J. Gastroenterol.* **2010**, *105* (9), 1978–1985. https://doi.org/10.1038/AJG.2010.170.

(62) Musso, G.; Gambino, R.; Cassader, M. Recent Insights into Hepatic Lipid Metabolism in Non-Alcoholic Fatty Liver Disease (NAFLD). *Prog. Lipid Res.* **2009**, *48* (1), 1–26. https://doi.org/10.1016/J.PLIPRES.2008.08.001.

(63) Tiniakos, D. G.; Vos, M. B.; Brunt, E. M. Nonalcoholic Fatty Liver Disease: Pathology and Pathogenesis. *Annu. Rev. Pathol.* **2010**, *5*, 145–171. https://doi.org/10.1146/ANNUREV-PATHOL-121808-102132.

CHAPTER 2

Analysis of Metal Effects on C-Peptide Structure and Internalization

Adapted with permission from:

*Stevenson, M. J., Farran, I. C., Uyeda, K. S., **San Juan, J. A.,** & Heffern, M. C. (2019). Analysis of Metal Effects on C-Peptide Structure and Internalization. ChemBioChem, 20(19), 2447-2453.*

Copyright © 2019 Wiley-VCH GmbH, Weinheim

2.1 Introduction

Proinsulin C-peptide is a clinical marker for understanding pancreatic β-cell function and to help distinguish between Type 1 and Type 2 diabetes. Biosynthesized between the A- and B-chains of insulin, C-peptide acts as the connecting linker by bringing the A- and B-chains of insulin together by disulfide bond formation. As glucose levels rise, active insulin and C-peptide are cleaved in the secretory vesicles, then exocytosed in equimolar amounts. Using this action as an advantage, the strategy of measuring C-peptide production is combined with screening for the presence of remaining islet-cells and other autoantibodies to provide accurate assessments of residual beta-cell function.[1]

C-peptide was initially thought to be biologically inert. Strong evidence now suggests that C-peptide acts as a solubilizing agent for insulin and demonstrates hormone-like roles post secretion such as glucose uptake, blood flow regulation by stimulation of the eNOS pathway, release of ATP from erythrocytes, and increased cell growth.[1,2] In addition, there is debate about the signaling effects of C-peptide, whether it binds classically to a G-protein coupled receptor on the cell surface to trigger signaling cascades,[3,4] or if C-peptide undergoes nonclassical peptide internalization then localizes to the cytoplasm.[5] With over a decade of work supporting the beneficial physiological effects of C-peptide,[6,7] its therapeutic advances are hindered by a lack of mechanistic understanding.[6] Therefore, it is important to investigate the molecular mechanisms of C-peptide activity to make the connection between the biological activities of C-peptide and its structural functions.

In elucidating the peptide's mode of action, previous studies have shown that C-peptide function depends on the co-addition of essential divalent metal ions. In the presence of Zn(II), C-peptide can prevent islet amyloid polypeptide (IAPP) aggregation in pancreatic β-cells.[8] C-peptide activation of ATP release from erythrocytes is enhanced when in the presence of Cr(III), Fe(II), or Zn(II),[9–11] to which Spence and co-workers speculated that this mode of action may require a chaperone such as serum albumin while C-peptide is being transported in the bloodstream.[12,13] Despite these observations, the structural consequences and peptide functions of C-peptide when a metal ion binds remain elusive. Recent studies have supported that essential d-block transition metals can perturb and alter function of bioactive peptides at a molecular level such as insulin, oxytocin, and hepcidin.[14–17] Because the sequence of C-peptide (EAEDLQVGQVELGGGPGAGSLQPLALEGSLQ) includes possible metal-binding contenders, such as negatively charged glutamic and aspartic acid, this work highlights how the inorganic biochemistry of metal ions may impact the function of C-peptide. While the complete published work assesses the effects of all the first-row d-block metals, this chapter focuses on my key contribution to the work, which is the investigation to the the direct metal binding stoichiometries and affinities of metal ions that showed visible interactions with C-peptide.

2.2 Results and Discussion

2.2.1 Characterization of metal binding stoichiometries and affinities to C-peptide

To gain a better understanding of the structure/function dependence of metal-peptide interactions responsible for C-peptide activation of ATP release from erythrocytes, we characterized resulting species from Zn(II) addition to C-peptide. Previous mass spectrometry studies suggested a Zn(II)/C-peptide complex could form.[10] To determine the binding affinity of optically silent Zn(II), we used a chromophoric ligand, Zincon (ZI). ZI binds to labile Zn(II) and exhibits a metal-ligand charge-transfer (MLCT) peak in the visible region of the electronic absorption spectrum. ZI was used as a competitive ligand to assess binding parameters of Zn(II)/C-peptide. When C-peptide is titrated into a solution of preformed ZI-Zn(II), the MLCT band of ZI-Zn(II) at 618 nm decreases (Figure 2.1). This suggests that C-peptide is competing with ZI for Zn(II). The calculated formation constant[18] of the Zn(II)/C-peptide complex is estimated to be log *K* between 4.0 and 5.0, or $K_{d,\ app}$ = 10-100 uM. Because the Zn(II) concentration range is from picomolar to micromolar in plasma, the dissociation constant range of the Zn(II)/C-peptide complex indicates that Zn(II) can interact with C-peptide in solution and plasma.

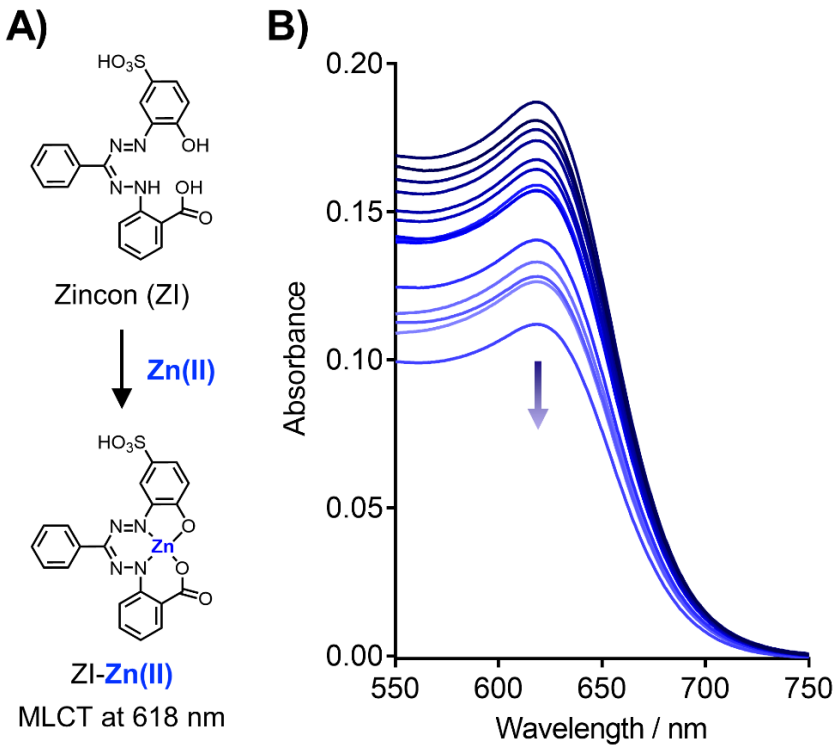

Figure 2.1. Binding affinity of Zn(II) to C-peptide. (A) Zn(II) binds to Zincon (ZI) at one equivalence, and the binding affinity is determined to be log *K* = 5.7. The ZI-Zn(II) complex produces a MLCT at 618 nm, providing a colorimetric method to measure Zn(II) affinities with other complex systems. (B) Electronic absorption spectra when 5 μM of C-peptide is titrated up to 80 μM into a solution containing 10 μM Zn and 20 μM ZI in 50 mM HEPES at pH 7.4. C-peptide competition for Zn(II) is displayed by the absorption decrease at 618 nm. The estimated binding affinity of Zn(II)/C-peptide is log *K* between 4.0 and 5.0 or $K_{d,app}$ = 10-100 μM.

Immunofluorescence demonstrated that out of all the d-block transition metals, Cr(III) and Cu(II) were the only metal ions that altered C-peptide internalization in human embryonic kidney (HEK-293) cells.(add citation) To determine whether this effect was due

to direct metal/peptide interactions, we probed the presence and approximate affinities of such binding using electronic absorption (UV-Vis). To prepare samples for analysis, metal salts were titrated from sub- to super- stoichiometric amounts into solutions containing 300 μM C-peptide in 50 mM phosphate buffer (pH 7.4). All essential d-block transition metals (Cr(III), Mn(II), Fe(II), Fe(III), Co(II), Ni(II), Cu(II)) were titrated into C-peptide to determine any direct metal binding. Based on the observed altered intracellular peptide behavior by Cr(III) and Cu(II), results from UV-Vis studies indicate a 1:1 Cu(II)/C-peptide stoichiometric ratio and Cr(III) shows a stoichiometric ratio of a 2:1 Cr(III)/C-peptide (Figure 2.2).

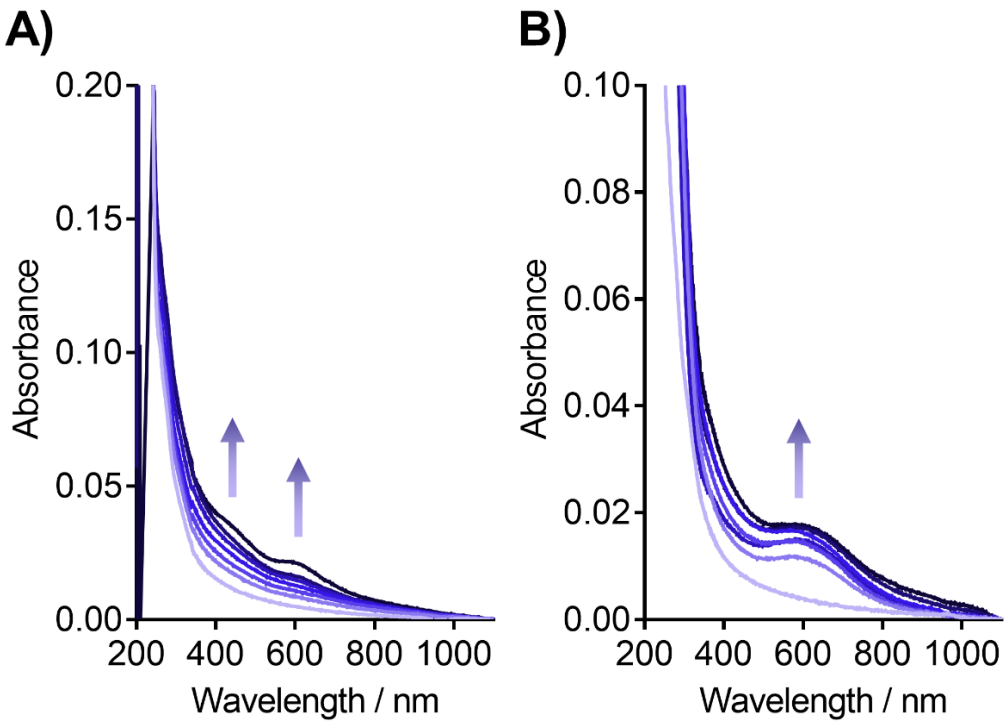

Figure 2.2. Electronic absorption spectra of C-peptide in 50 mM phosphate buffer (pH 7.4) when titrated with (A) Cr(III) and (B) Cu(II). Metal solutions were titrated into 300 μM

C-peptide from sub- to super-stoichiometric ratios (0.5 to 5 equivalences). A large band at 220 nm is attributed to peptide backbone absorption. Arrows portray an increase in d-d bands, suggesting interactions of the metal with C-peptide. (A) Addition of Cr(III) display an increase in two bands at 431 and 585 nm. (B) Titration of Cu(II) caused an increase in absorbance at 600 nm.

Because these metals display direct binding to C-peptide, we sought to determine its binding affinity. While a $K_{d,\ app}$ could not be determined for Cr(III), we applied the same method for determination of Zn(II)/C-peptide affinity using the chromophoric ligand 1,10-phenanthroline (phen) for Cu(II)/C-peptide. Cu(II)-phen has a charge transfer band at 265 nm. When C-peptide is titrated into Cu(II)-phen solution, the loss of the charge band is monitored to determine if the peptide can compete with phen for Cu(II) (Figure 2.3). Cu(II)/C-peptide was calculated to be between log K of 7.4 and 7.8, or $K_{d,\ app}$ = 15-40 nM. With this estimation, Cu(II) has a biologically relevant affinity for C-peptide.

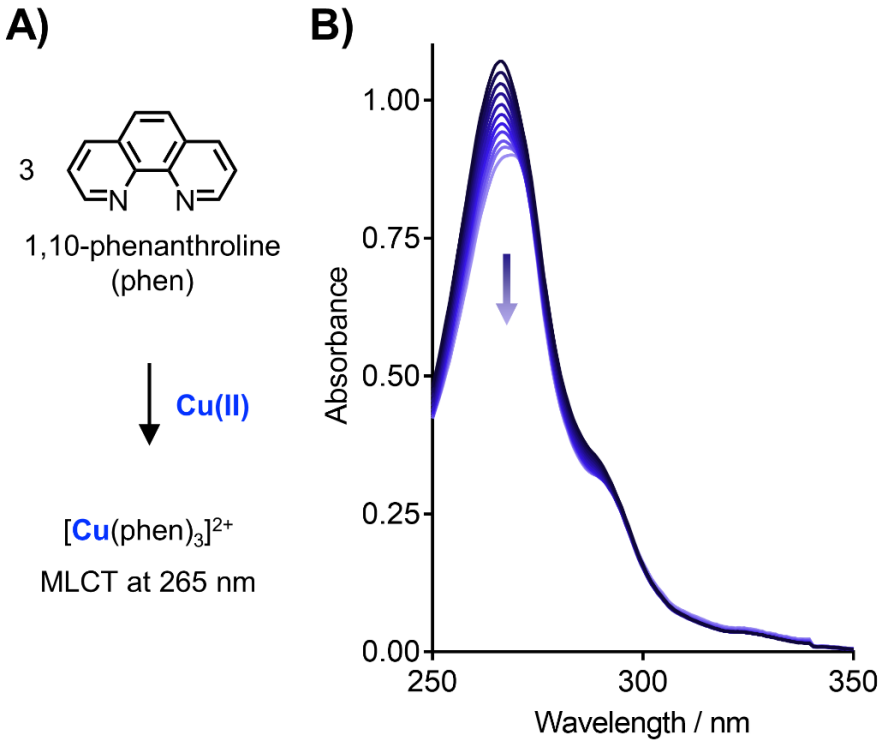

Figure 2.3. Binding affinity of Cu(II) to C-peptide. (A) Cu(II) binds to 1,10-phenanthroline (phen) up to three equivalences, with K_1, β_2, and β_3 of 9.0, 15.7, and 20.8, respectively. $[Cu(phen)_3]^{2+}$ exhibits a charge transfer band at 265 nm ($\varepsilon \approx 90{,}000\ M^{-1}\ cm^{-1}$). (B) Electronic absorption spectra when 5 μM of C-peptide is titrated up to 80 μM into a solution containing 10 μM Cu(II) and 40 μM phen in 50 mM bisTris at pH 7.4. C-peptide competition for Cu(II) is displayed by the absorption decrease at 265 nm. As C-peptide chelates Cu(II) from a 1:1 $Cu(phen)^{2+}$ complex, the estimated binding affinity of Cu(II)/C-peptide is log K between 7.4 and 7.8 or $K_{d,\ app}$ = 15-40 nM.

2.3 Conclusions

This work highlights the molecular mechanisms of how metals may influence C-peptide activity. Because Cr(III) and Cu(II) altered peptide internalization, electronic absorption spectroscopy was applied to probe how these metals affected C-peptide at the molecular level. Direct binding of Cr(III) and Cu(II) was observed, to which an approximate biologically relevant binding constant was determined for Cu(II). As the mechanisms of peptide hormones are commonly difficult to elucidate due to its random coiled structure and modifications, this study brings enhances our understanding the structure-function relationship of peptide hormones by demonstrating that metals can modulate peptide activity; a slight structural change can alter peptide internalization, and in turn alter its signaling pathways. As the extracellular space contains concentrations of various essential metal ions through import and export of regulated channels and transporters, it is important to consider the possible bioinorganic interactions peptides may encounter. The exact signaling pathways impacted from metal/C-peptide interactions remains unknown, but these studies provide a paradigm on metal-binding effects that will help direct future work (see Chapter 5).

An extension of this work was also used for an educational article on metal-binding interactions. This work can be found in the cited article below:

Choi, S., **San Juan, J. A.,** Heffern, M. C., & Stevenson, M. J. (2022). Quantifying the Binding Interactions Between Cu (II) and Peptide Residues in the Presence and Absence of Chromophores. *Journal of Visualized Experiments: Jove*, (182).

2.4 Materials and Methods

Chemicals and Reagents. All chemicals, reagents, and kits were purchased from Fisher Scientific, Sigma-Aldrich, or Spectrum Chemicals, unless otherwise noted. Specifically, dimethylformamide (DMF), 4-methylpiperidine, N,N,N′,N′-tetramethyl-O-(1H-benzotriazol-1-yl)uronium hexafluorophosphate (HBTU), N,N-diisopropylethylamine (DIEA), dichloromethane (DCM), 2,2,2-trifluoroacetic acid (TFA), diethyl ether, methanol, formic acid (FA), dimethylsulfoxide (DMSO), $CrCl_3 \cdot 6H_2O$, $MnCl_2$, $(NH_4)_2Fe(SO_4)_2 \cdot 6H_2O$, $CoCl_2$, $NiCl_2$, $CuCl_2$, 2-carboxy-2′-hydroxy-5′-sulfoformazylbenzene monosodium salt (Zincon, ZI), 2,2,2-Trifluoroethanol (TFE), Na_2HPO_4, 2-[Bis(2-hydroxyethyl)amino]-2-(hydroxymethyl)propane-1,3-diol (bisTris), 4-(2-hydroxyethyl)-1-piperazineethanesulfonic acid (HEPES), NaOH, HCl, ethylenediaminetetraacetic acid (EDTA), and 1,10-phenanthroline (phen) were purchased from ThermoFisher; $ZnCl_2$ and $FeCl_3$ were purchased from Sigma-Aldrich; and piperidine was purchased from Spectrum Chemicals. Wang resin preloaded with Fmoc-Gln(Trt)-OH, along with Fmoc-protected amino acids were purchased from ThermoFisher but manufactured by ChemImpex. Buffered solutions and metal salt solutions were made using Direct-Q 3 deionized water (>18 MΩ, Millipore).

Solid-phase peptide synthesis and RP-HPLC purification of C-peptide. Human wild-type C-peptide (EAEDLQVGQVELGGGPGAGSLQPLALEGSLQ) was synthesized via a heated Fmoc-based solid-phase peptide synthesis (SPPS) method. For a 0.2 mmol synthesis, Wang resin with preloaded Fmoc-Gln(Trt)-OH was swelled overnight in 5x DMF. Resin was washed 5 times with 2x resin volume of DMF. The N-terminal residue was deprotected with 20% piperidine in DMF or 25% 4-methylpiperidine in DMF, first

shaken for 1 minute then repeated and placed on shaker for 10 minutes. The resin was washed 10x with 2x resin volume of DMF. Amino acids (4.0 equivalents) and HBTU (3.9 equivalents) were dissolved in minimal DMF, then DIEA (10.0 eq) was added. Resin was then suspended in the amino acid/HBTU solution and heated for 10 minutes at 95 °C, shaken after 5 minutes, then placed on a shaker for 2 minute to cool. The resin was washed 10x with 2x resin volume with DMF. The process was repeated from the deprotection step for each amino acid. After the last amino acid was added to the peptide, the resin was washed 10x with 2x resin volume of DMF, followed by 10x washes with 2x resin volume of DCM and dried overnight. Cleavage of the protecting groups and peptide from the resin was carried out in minimal solution of 95:5 TFA:water with 1-4 hours of shaking. The solution was separated from the resin and precipitated in chilled diethyl ether and the suspension was centrifuged at 3900 rpm for 10 minutes at 4 °C. The supernatant was decanted and the pellet was washed thrice with chilled diethyl ether followed by centrifugation after each wash. The pellet was dried under a stream of air overnight. Purification was performed with RP-HPLC on an Agilent Technologies 1260 Infinity II HPLC with coupled Agilent Technologies 1260 Infinity II UV-Vis detection system. Purification of crude C-peptide was performed using an Agilent Zorbax SB-C3 column (9.4 x 250 mm) at a flow rate of 3.4 mL min^{-1} using a nonlinear gradient of water with 0.1% FA (Solvent A) and methanol with 0.1% FA (Solvent B). The column was equilibrated and crude C-peptide loaded onto the column in 50% Solvent B held constant for 5 minutes. Solvent B increased from 50% to 75% from 5-30 minutes and from 75% to 100% from 30-35 minutes. C-peptide eluted off of the column at 63% Solvent B. Fractions containing C-peptide were confirmed by electrospray ionization

mass spectrometry (ESI-MS) using an Agilent Technologies 1260 Infinity II coupled with an Agilent Technologies InfinityLab LC/MSD (Figure S12), dried, and stored at -20 °C until use.

UV-Visible spectroscopy. All measurements were recorded on either a UV-1800 or UV-1900 (Shimadzu) at room temperature using quartz cuvettes with 1 cm path length (Starna Cells). For metal titrations into apo C-peptide, C-peptide was dissolved to 300 µM in either 50 mM phosphate, pH 7.4 or 50 mM bisTris, pH 7.4. All metal solutions were dissolved in Milli-Q water. Sub-stoichiometric (150 µM) to super-stoichiometric (up to 1.5 mM) equivalents of metal salts were added to C-peptide, allowed to equilibrate for 3-5 minutes at room temperature, and measured. Water was used as the spectral reference. Following data collection, the buffer spectrum with water as reference was subtracted from all spectra and all spectra were normalized to account for dilution. For competition studies of C-peptide with the preformed ZI-Zn(II) complex, C-peptide was dissolved in 50 mM HEPES, pH 7.4 at a concentration of 100 µM. ZI was dissolved in DMSO. A solution of 500 µM Zn(II) and 1 mM ZI was made by diluting Zn(II) and ZI in 50 mM HEPES, pH 7.4. Equilibria were established by addition of Zn(II) and ZI to final concentrations 10 and 20 µM, respectively. C-peptide was added at varying concentrations from 0 to 80 µM. Absorbance was measured with a reference of water followed by subtraction of buffer with a reference of water and normalized for dilution. [ZI-Zn(II)] monitored at 618 nm as detailed by Kocyła et al.[1] All samples were kept under dark conditions throughout the experiment. Calculation for the formation constant of Zn(II)/C-peptide complex are shown in Table S1. Similarly, C-peptide was dissolved in 50 mM bisTris, pH 7.4 to a concentration of 300 uM and titrated into 10 µM Cu(II) with

40 μM phen. Absorbance was measured with a reference of water followed by subtraction of buffer with a reference of and normalized for dilution.

2.5 References

(1) Marques, R. G.; Fontaine, M. J.; Rogers, J. C-Peptide: Much More than a Byproduct of Insulin Biosynthesis. *Pancreas* **2004**, *29* (3), 231–238. https://doi.org/10.1097/00006676-200410000-00009.

(2) Wahren, J.; Ekberg, K.; Jörnvall, H. C-Peptide Is a Bioactive Peptide. *Diabetologia* **2007**, *50* (3), 503–509. https://doi.org/10.1007/s00125-006-0559-y.

(3) Yosten, G. L. C.; Kolar, G. R.; Redlinger, L. J.; Samson, W. K. Evidence for an Interaction between Proinsulin C-Peptide and GPR146. *J. Endocrinol.* **2013**, *218* (2). https://doi.org/10.1530/JOE-13-0203.

(4) Lindfors, L.; Sundström, L.; Fröderberg Roth, L.; Meuller, J.; Andersson, S.; Kihlberg, J. Is GPR146 Really the Receptor for Proinsulin C-Peptide? *Bioorganic Med. Chem. Lett.* **2020**, *30* (13), 127208. https://doi.org/10.1016/j.bmcl.2020.127208.

(5) Lindahl, E.; Nyman, U.; Melles, E.; Sigmundsson, K.; Ståhlberg, M.; Wahren, J.; Öbrink, B.; Shafqat, J.; Joseph, B.; Jörnvall, H. Cellular Internalization of Proinsulin C-Peptide. *Cell. Mol. Life Sci.* **2007**, *64* (4), 479–486. https://doi.org/10.1007/s00018-007-6467-6.

(6) Pinger, C. W.; Entwistle, K. E.; Bell, T. M.; Liu, Y.; Spence, D. M. C-Peptide Replacement Therapy in Type 1 Diabetes: Are We in the Trough of Disillusionment? *Molecular BioSystems*. Royal Society of Chemistry 2017, pp 1432–1437. https://doi.org/10.1039/c7mb00199a.

(7) Washburn, R. L.; Mueller, K.; Kaur, G.; Moreno, T.; Moustaid-moussa, N.; Ramalingam, L.; Dufour, J. M. C-peptide as a Therapy for Type 1 Diabetes Mellitus. *Biomedicines*. MDPI AG 2021, pp 1–24. https://doi.org/10.3390/biomedicines9030270.

(8) Ge, X.; Kakinen, A.; Gurzov, E. N.; Yang, W.; Pang, L.; Pilkington, E. H.; Govindan-Nedumpully, P.; Chen, P.; Separovic, F.; Davis, T. P.; Ke, P. C.; Ding, F. Zinc-Coordination and C-Peptide Complexation: A Potential Mechanism for the Endogenous Inhibition of IAPP Aggregation. *Chem. Commun.* **2017**, *53* (68), 9394–9397. https://doi.org/10.1039/C7CC04291D.

(9) Meyer, J. A.; Froelich, J. M.; Reid, G. E.; Karunarathne, W. K. A.; Spence, D. M. Metal-Activated C-Peptide Facilitates Glucose Clearance and the Release of a Nitric Oxide Stimulus via the GLUT1 Transporter. *Diabetologia* **2008**, *51* (1), 175–182. https://doi.org/10.1007/s00125-007-0853-3.

(10) Keltner, Z.; Meyer, J. A.; Johnson, E. M.; Palumbo, A. M.; Spence, D. M.; Reid, G. E. Mass Spectrometric Characterization and Activity of Zinc-Activated Proinsulin C-Peptide and C-Peptide Mutants. *Analyst* **2010**, *135* (2), 278–288. https://doi.org/10.1039/b917600d.

(11) Medawala, W.; McCahill, P.; Giebink, A.; Meyer, J.; Ku, C. J.; Spence, D. M. A

Molecular Level Understanding of Zinc Activation of C-Peptide and Its Effects on Cellular Communication in the Bloodstream. *Review of Diabetic Studies*. Society for Biomedical Diabetes Research September 2009, pp 148–158. https://doi.org/10.1900/RDS.2009.6.148.

(12) Geiger, M.; Janes, T.; Keshavarz, H.; Summers, S.; Pinger, C.; Fletcher, D.; Zinn, K.; Tennakoon, M.; Karunarathne, A.; Spence, D. A C-Peptide Complex with Albumin and Zn2+ Increases Measurable GLUT1 Levels in Membranes of Human Red Blood Cells. *Sci. Rep.* **2020**, *10* (1). https://doi.org/10.1038/s41598-020-74527-6.

(13) Liu, Y.; Chen, C.; Summers, S.; Medawala, W.; Spence, D. M. C-Peptide and Zinc Delivery to Erythrocytes Requires the Presence of Albumin: Implications in Diabetes Explored with a 3D-Printed Fluidic Device. *Integr. Biol. (United Kingdom)* **2015**, *7* (5), 534–543. https://doi.org/10.1039/c4ib00243a.

(14) Dunn, M. F. Zinc–Ligand Interactions Modulate Assembly and Stability of the Insulin Hexamer – A Review. *Biometals 2005 184* **2005**, *18* (4), 295–303. https://doi.org/10.1007/S10534-005-3685-Y.

(15) Liu, D.; Seuthe, A. B.; Ehrler, O. T.; Zhang, X.; Wyttenbach, T.; Hsu, J. F.; Bowers, M. T. Oxytocin-Receptor Binding: Why Divalent Metals Are Essential. *J. Am. Chem. Soc.* **2005**, *127* (7), 2024–2025. https://doi.org/10.1021/JA046042V/SUPPL_FILE/JA046042VSI20041022_061739.PDF.

(16) Tselepis, C.; Ford, S. J.; McKie, A. T.; Vogel, W.; Zoller, H.; Simpson, R. J.; Diaz Castro, J.; Iqbal, T. H.; Ward, D. G. Characterization of the Transition-Metal-Binding Properties of Hepcidin. *Biochem. J.* **2010**, *427* (2), 289–296. https://doi.org/10.1042/BJ20091521.

(17) Stevenson, M. J.; Uyeda, K. S.; Harder, N. H. O.; Heffern, M. C. Metal-Dependent Hormone Function: The Emerging Interdisciplinary Field of Metalloendocrinology. *Metallomics* **2019**, *11* (1), 85–110. https://doi.org/10.1039/C8MT00221E.

(18) Kocyła, A.; Pomorski, A.; Krężel, A. Molar Absorption Coefficients and Stability Constants of Zincon Metal Complexes for Determination of Metal Ions and Bioinorganic Applications. *J. Inorg. Biochem.* **2017**. https://doi.org/10.1016/j.jinorgbio.2017.08.006.

CHAPTER 3

Copper(II) affects the biochemical behavior of proinsulin C-peptide by forming ternary complexes with serum albumin

Collaborations done with Job Chakarawet of the Britt lab (EPR), Zhecheng He of the Wang lab (TDDFT), and Michael Stevenson formerly in the Heffern lab (C-peptide EPR)

At the time of the writing of this thesis, the enclosed chapter was submitted to the Journal of the American Chemical Society and was under review.

3.1 Introduction

Peptide hormones are key chemical messengers in all forms of life, driving vital functions such as energy homeostasis, reproduction, and stress response.[1] Several FDA-approved drugs have been derived from these hormones, including oxytocin for labor induction and insulin for glucose regulation.[2–4] A number of endogenous peptide hormones have been identified in recent years via combined bioinformatic and structural approaches, but for many of these, their function and mode of action remain elusive.[5] One example is C-peptide, a 31-mer peptide derived from the same prohormone as insulin. Over two decades of research support its physiological effects, including beneficial impacts on glucose uptake, blood flow regulation, and cell growth,[6–9] but its therapeutic advancement has been hindered by a lack of mechanistic understanding,[8] including debate over the identity of its cognate receptor.[10–12] It has been suggested that the elusive activity of the peptide may be due to overlooked regulators and binding partners that modulate function.[8] We and others have recently shown that the activity of C-peptide is influenced by metal ions, warranting further investigations on the molecular basis of these interactions.[13–16]

The signaling activity of bioactive peptides like C-peptide is influenced by its rate of production and secretion, circulation half-life, and the resulting concentration at the target site.[17] Fundamental to the latter two are the potential interactions with plasma proteins. Abundant plasma proteins such as albumin, IgG, and transferrin are versatile carriers of low-molecular metabolites, peptides, and proteins.[18] Serum albumin, in particular, contains four sites where biometals can bind, including one N-terminal site (NTS, Figure 3.1) containing the classical Amino-Terminal Cu(II)- and Ni(II) (ATCUN)

binding motif, a Zn(II) binding site at Cys34, and two multi-metal binding sites: Site A (MBSA, Figure 3.1, which can bind both Cu(II) and Zn(II), and Site B (MBSB) which can bind Zn(II).[19,20]

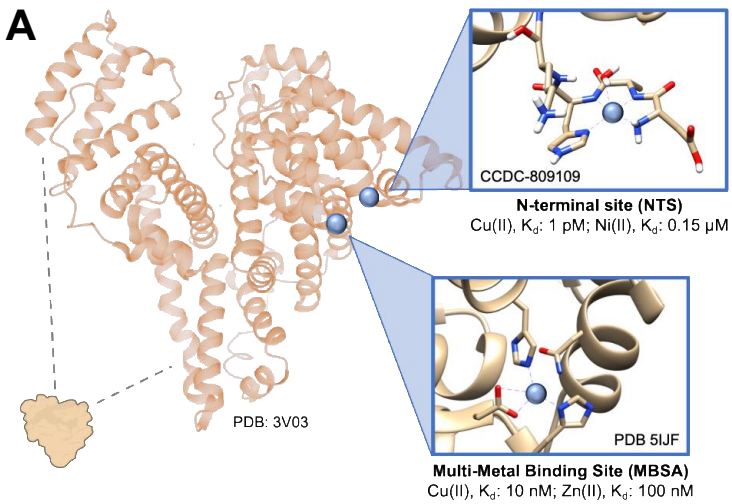

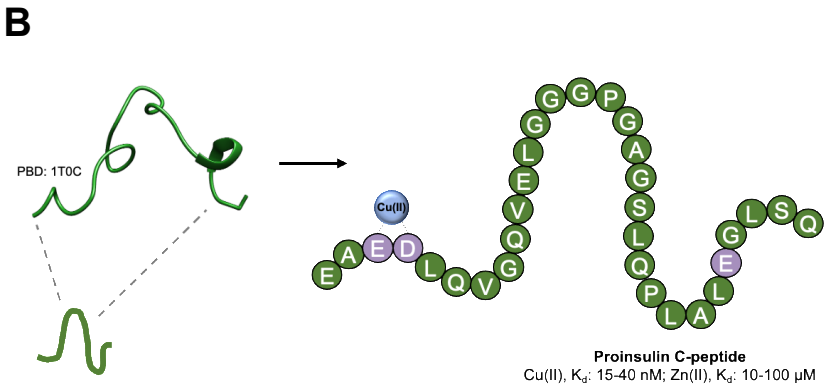

Figure 3.1. Model structures and metal-binding sites of BSA and C-peptide. (A) BSA is a heart-shaped molecule comprised of mainly alpha-helical domains. The protein contains many binding sites for various classes of ligands. Particularly, BSA has two metal-binding sites: N-terminal site (NTS) and Multi-Metal Binding Site A (MBSA). NTS binds to Cu(II) at K_d = 1 pM and Ni(II) at K_d = 0.15 μM. MBSA binds to Cu(II) at K_d = 10 nM and Zn(II) at K_d = 100 nM. (B) C-peptide is a random coiled 31-mer peptide that coordinates to Cu(II) at E3 and D4 with a K_d = 10 nM, and indirectly with E27 when E3 and E4 are mutated. C-peptide also binds to Zn(II) at K_d = 10-100 μM, but the coordinating ligands remain elusive.

Considering its metal binding capacity, albumin is posited to be the major transporter of endogenous and exogenous metals alike. In addition to metal ions, these binding sites have been investigated for their effects on the bioavailability and distribution of small molecule metallodrugs, including platinum-based anti-cancer agents.[21,22] Less studied is the chemical nature of how metal-binding peptides may interact with these sites in albumin. In a two-species binding pair model, the high-affinity metal-binding sites on albumin may be considered ligand-exchange competitors for the peptide-bound metal ions. Choi and colleagues recently demonstrated that serum albumin can bind to and sequester metal ions from Zn(II) and Cu(II)-loaded amyloid-beta (Aβ), a peptide implicated in the pathologies associated with Alzheimer's disease. The metal-bound Aβ/albumin interaction affects the peptide's cytotoxicity, pointing to a possible regulatory role of albumin in the metal/Aβ pathophysiology.[23–27] Recently, another binding model between albumin and metal-binding peptides was presented by Bossak-Ahmad and co-

workers with the Cu(II)-containing tripeptide, GHK, namely that the metal center may serve as a bridge in a peptide-metal-albumin ternary complex.[28]

The activity of C-peptide has indeed been linked both to metal ions and the presence of albumin.[13] Spence and coworkers first demonstrated that the activity of C-peptide in modulating blood vessel physiology is activated by the addition of Zn(II).[29,30] Interestingly, the ability of C-peptide to increase GLUT1 levels and ATP release in red blood cells were further elevated by the co-addition of bovine serum albumin (BSA) alongside Zn(II).[13,14] They proposed that the C-peptide receptor may actually recognize the peptide complexed to albumin rather than the peptide alone;[13,14] but the molecular nature of such a complex and whether Zn(II) is involved in its formation require further characterization. We recently demonstrated that Cu(II) can directly bind to C-peptide and alter the cellular internalization of the peptide.[16] We identified that the binding interaction was focused on the N-terminal region of the peptide involving the E3 and D4 residues, forming a 1N3O square planar Cu(II) complex. While we determined that Zn(II) could also bind to the peptide directly via the peptide backbone, Cu(II) addition displaces the Zn(II). Moreover, the full-length sequence of C-peptide is necessary for precise binding of Cu(II) to C-peptide, with mutations or truncations of the metal-binding region leading to reshuffling of the binding site (Figure 3.1).[15]

Herein, we sought to assess whether Cu(II) or Zn(II) could facilitate interactions between C-peptide and albumin, and characterize the molecular nature of the species formed. We demonstrate that Cu(II) facilitates the formation of ternary complexes between C-peptide and BSA which do not form in the absence of Cu(II), and that such an interaction is not observed with Zn(II). Interestingly, the resulting complexes depend on

the order of addition. Characterization via circular dichroism and UV-Vis absorption spectroscopy in conjunction with time-dependent density functional theory (TDDFT) calculations support the formation of distinct species when a C-peptide/Cu(II) complex is added to BSA versus when Cu(II)-coordinated BSA is added to C-peptide. Electron paramagnetic resonance (EPR) spectra show that, in either case, the coordination environment around the Cu(II) center shows close similarity to the Cu(II)-albumin sites. Taken together, the data indicate that the ternary complexes form via ligand exchange of an Asp residue from the Cu(II)-binding site of albumin for a carboxylate-bearing residue in C-peptide. Regardless of order of addition, the ternary complexes exhibit higher protection of the Cu(II) center from reduction than albumin or C-peptide alone, suggesting a possible metal sequestration function. Within the cellular context, inclusion of serum albumin alters internalization of the peptide into human embryonic kidney cells, with the complexes showing distinct activity from one another. Finally, we demonstrate the potential clinical relevance of the ternary complexes with their effects on bioanalytical immunoassays for C-peptide. C-peptide is a well-accepted secondary biomarker for insulin,[31,32] as the two are co-released with C-peptide exhibiting a higher circulation lifetime.[33] Our results show that the presence of the ternary complexes significantly affects the read-out in these assays, conveying their potential importance to diagnostic measurements. Overall, the presented data point to the impact of the albumin/Cu(II)/C-peptide complexes both in its molecular mechanisms as well as its clinical applications.

3.2 Results & Discussion

3.2.1 Cu(II) facilitates interactions between C-peptide and albumin

We first assayed whether Cu(II) or Zn(II) could facilitate interactions between C-peptide and albumin differently than in the absence of either metal by application of Förster resonance energy transfer (FRET). The FRET phenomenon is widely used in fluorescence spectrophotometry to assess protein-ligand interactions. In these applications, two species of interest are independently labeled with two parts of a FRET pair. FRET efficiency is used to determine if the two species come in close enough proximity, (within the Förster distance) for energy transfer to occur.[34] To apply this approach to C-peptide and albumin, we generated C-peptide labeled with the fluorescent dye TAMRA (TAMRA-C-peptide; λ_{ex} = 546 nm, λ_{em} = 579 nm) to be used as a FRET acceptor alongside BSA that has been labeled with fluorescein isothiocyanate (FITC-albumin, λ_{ex} = 495 nm, λ_{em} = 520 nm), an established FRET donor for TAMRA (R_0 = 49-56 Å).[35,36] In screening for binding interactions between TAMRA-C-peptide and FITC-albumin, the FRET efficiency was measured with increasing ratios of donor-to-acceptor. We used the calculated FRET efficiency (FRET efficiency = 1 - F/F_o, where F is the fluorescence intensity of the presence of the acceptor while F_o is the fluorescence intensity in the absence of the acceptor) to assess relative proximities of albumin and C-peptide under varying ratios of the donor-to-acceptor. While additional conditions and information are required to calculate a quantitative distance, the FRET efficiency with

varying donor-to-acceptor ratios can be used to infer whether a binding interaction between two unlinked molecules facilitates FRET. In this scenario, FRET efficiency is positively correlated with donor-to-acceptor ratios (Figure 3.1). Thus an increase in FRET efficiency with higher ratios of TAMRA-C-peptide to FITC-BSA is suggestive of a binding interaction between the two species. When TAMRA-C-peptide is preincubated with Cu(II), then added to FITC-albumin, an increase in the FRET efficiency is observed with increasing donor-to-acceptor ratios (Figure 3.1B), suggesting energy transfer through binding between the two species. Such an increase was not observed with the addition of Zn(II) nor in the absence of either metal (Figure 3.1A & 3.1C). Furthermore, the addition of metal ions does not quench FRET output with increasing ratios of donor/acceptor (Figure 3.2). Altogether, this assay indicated that Cu(II) may mediate the formation of a C-peptide/albumin complex that does not otherwise occur under the other conditions tested. We thus sought to further characterize the interaction with fluorophore-free forms of the peptide and protein.

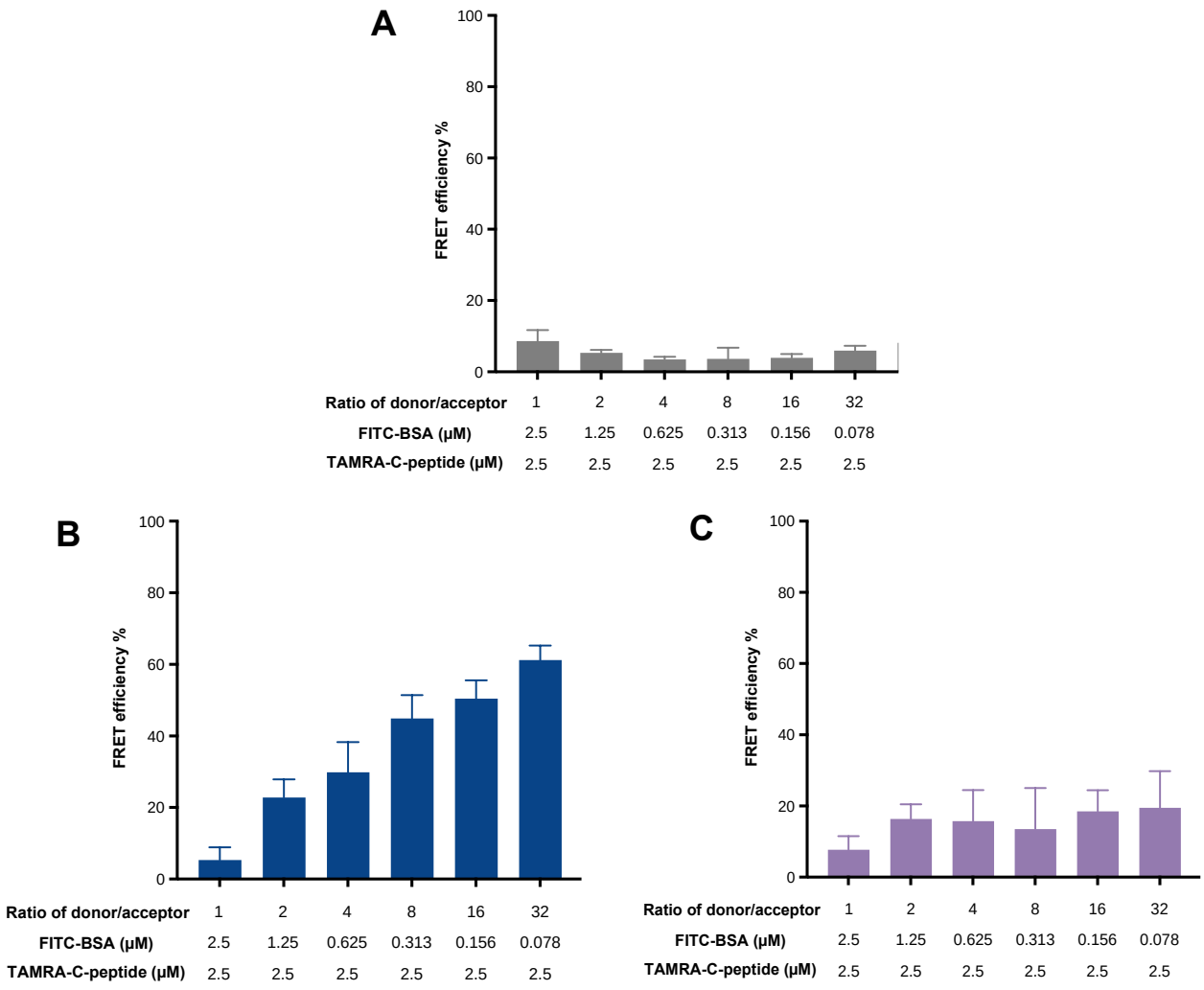

Figure 3.1. FRET efficiency of FITC-BSA and TAMRA-C-peptide in the absence and presence of Cu(II) or Zn(II). (A) Preincubation of apo-TAMRA-C-peptide and apo-FITC-BSA demonstrated little to no FRET efficiency. (B) Preincubation of Cu(II) with TAMRA-C-peptide followed by the addition of FITC-BSA showed increasing FRET efficiency with increasing ratio of donor/acceptor. (C) Preformed Zn(II) with TAMRA-C-peptide followed by the addition of FITC-BSA displayed minimal FRET efficiency in comparison to Cu(II). Data is shown as mean ± SD with n = 3.

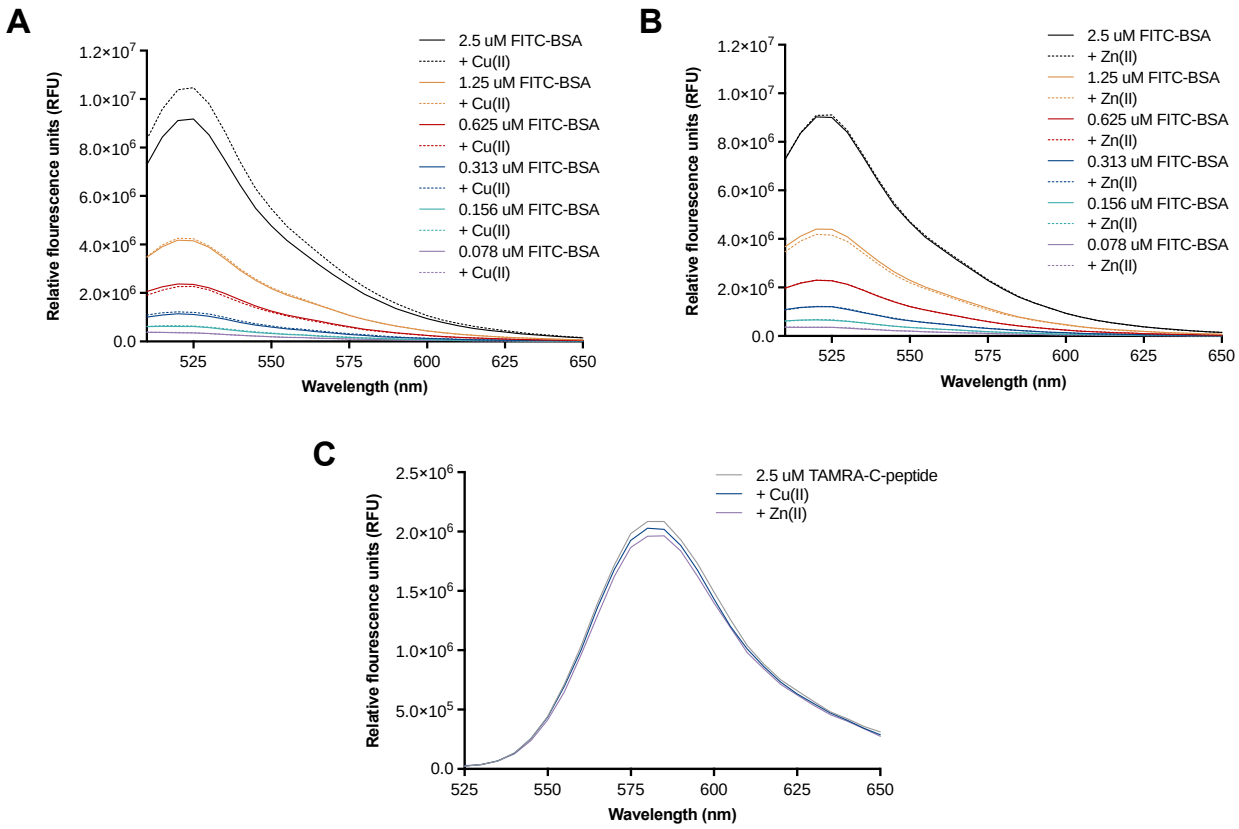

Figure 3.2. Fluorescence readout of FITC-BSA and TAMRA-C-peptide with or without Cu(II) or Zn(II). (A) Addition of Cu(II) to FITC-BSA quenches the fluorescence output at 2.5 μM FITC-BSA, but not at lower concentrations. (B) Fluorescence output of FITC-BSA is not quenched by the addition of Zn(II). (C) Addition of Cu(II) or Zn(II) minimally quenches TAMRA-C-peptide at 2.5 μM.

Changes to the secondary structure of BSA is frequently used as a proxy for characterizing the binding of drug metabolites and co-factors, including Cu(II) to the protein.[19,37,38] We thus applied circular dichroism (CD) spectroscopy to screen for impacts

of Cu(II) on interactions between C-peptide and albumin. The CD spectrum of BSA in the absence of Cu(II) (apo-BSA) exhibits two negative bands at approximately λ = 208 and 222 nm, characteristic of the α-helical structures that make up the protein.[39,40] These negative bands arise from contributions of the n→π* transition of a peptide bond within the α-helices of the protein.[41] Under the conditions we tested, the 208 nm band is slightly red-shifted to 212 nm (Figure 3.3A). We estimated the mean residue ellipticities (MRE) at 212 and 222 nm and their ratios using the following Equation (1),

$$MRE_{212\ or\ 222\ nm} = \frac{observed\ CD\ (mdegs)}{C_p\ n\ l \times 10} \quad (1)$$

where C_p is the molar concentration, n is number of amino acid residues, and l is the pathlength. From the MRE, the helical content can be approximated using Equation (2):

$$\alpha - helix\ (\%) = \frac{MRE - 4000}{33000 - 4000} \times 100 \quad (2)$$

This method has been used to assess ligand effects on albumin structure in a semi-quantitative manner.[42–44] We estimated the helical content of apo-BSA to be 71.1% and 68.2% at 212 and 222 nm, respectively (Figure 3.3A, Table 3.2). Serum albumin can bind up to two equivalents of Cu(II). Consistent with literature,[45] we observed that the addition of one equivalent of Cu(II) (1:1 Cu(II)-BSA) induces a modest reduction in negative molar ellipticity at 212 nm (corresponding to an overall 1.8% decrease in helicity), while two equivalents of Cu(II) (2:1 Cu(II)-BSA) induce notable reductions in the negative ellipticity

at both 212 and 222 nm (corresponding to an overall 5.7% and 4.9% decrease in helicity) (Figure 3.3A, Table 3.1).

We compared the helicity values of BSA and Cu(II)-BSA with addition of C-peptide in the presence or absence of Cu(II). In the absence of BSA, the CD spectra of metal-free C-peptide (apo-C-peptide) and 1:1 or 2:1 Cu(II)-C-peptide yield CD spectra representing primarily random coil conformations with no detectable helical content (Figure 3.4). When apo-C-peptide is added to apo-BSA, the resulting CD spectral traces and helical content closely overlaps with apo-BSA at both the 212 and 222 nm peak regions (Figure 3.3C and Table 3.2). This suggests that the molar ellipticity of apo-C-peptide is minimally detectable in the presence of apo-BSA, and that the two species do not interact in a way that perturbs the secondary structure of apo-BSA. In contrast, addition of apo-C-peptide to 1:1 Cu(II)-BSA decreases the helical content at 212 and 222 nm by 6.5% and 4.9% respectively relative to 1:1 Cu(II)-BSA alone (Figure 3.3B, Table 3.1). The helicity content of 2:1 Cu(II)-BSA at 212 and 222 nm similarly shifts in the presence of C-peptide albeit to a lesser degree than at 1:1 Cu(II)-BSA (an overall 1% decrease and 1.6% increase over 2:1 Cu(II)-BSA alone) (Figure 3.3B, Table 3.1). These shifts indicate that addition of apo-C-peptide to Cu(II)-BSA may result in new species that are distinct from Cu(II)-BSA alone at either equivalence.

As we had previously observed direct binding of Cu(II) to C-peptide ($K_{d,\ Cu(II)/C\text{-}peptide}$ = 10 nM at pH 7.4),[15] we investigated whether similar shifts in the apo-BSA structure could be observed if Cu(II) pre-complexed to C-peptide were introduced to BSA. Our prior work supports the binding of at least 1 equivalent of Cu(II);[16] while we did not elucidate the nature of 2nd binding site, we observed that mutating or truncating the binding site of

the first Cu(II) does not eradicate, but rather, reshuffles the binding site, pointing to a possibility of the peptide binding a 2nd Cu(II) equivalent.[15] We thus pre-incubated C-peptide with Cu(II) at both 1 or 2 equivalents prior to addition to apo-BSA and the CD spectra were monitored and compared to apo-BSA alone. The addition of 1:1 and 2:1 Cu(II)-C-peptide to apo-BSA reduces the negative ellipticity of apo-BSA. Relative to apo-BSA, addition of 1:1 Cu(II)-C-peptide notably decreases helical content at 212 and 222 nm by 8% and 5.7%, respectively, while the addition of 2:1 Cu(II)-C-peptide decreases helical content further at 212 and 222 nm by 8.4% and 6.5% (Figure 3.3D, Table 3.2).

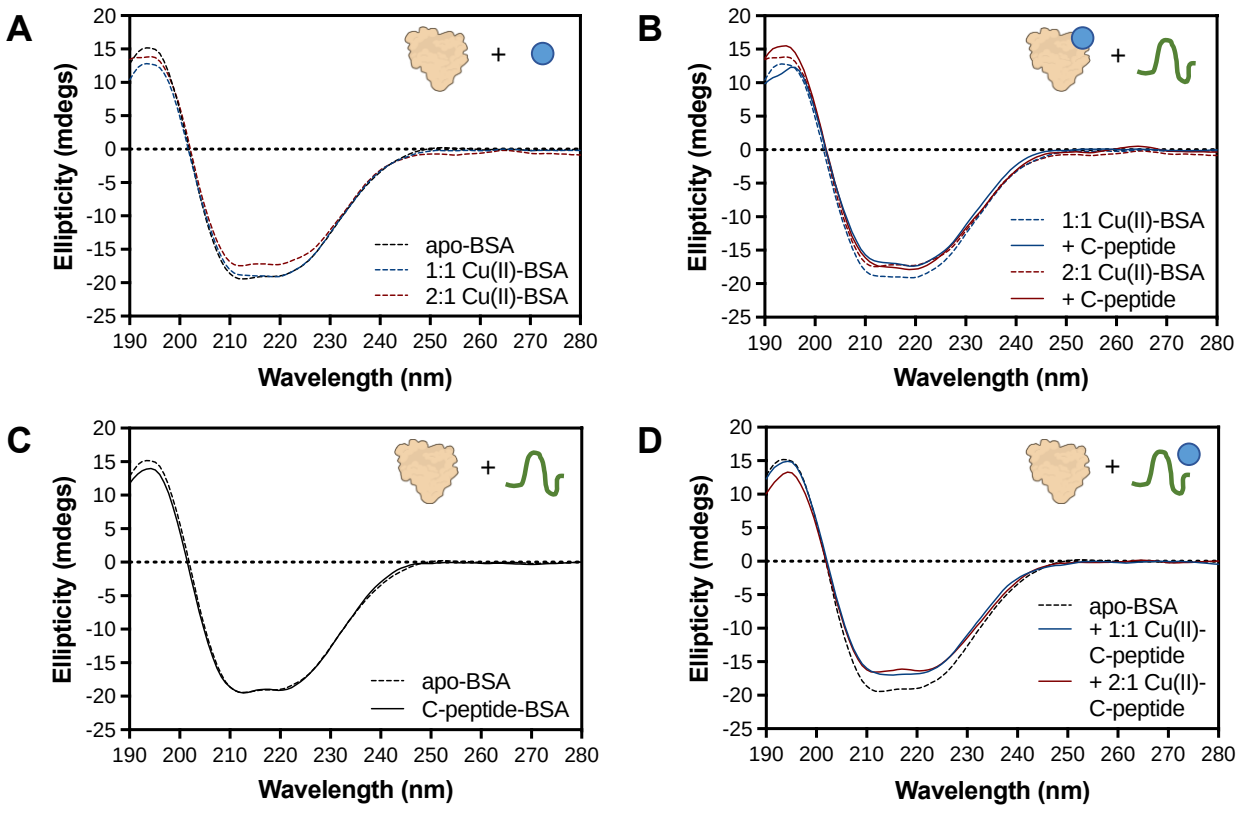

Figure 3.3. Circular dichroism spectra of 2 μM BSA display structural changes in α-helicity as shown by shifts in ellipticity at 212 and 222 nm. Inset figures show the associated schemes with BSA (orange protein); Cu(II) (blue circle); C-peptide (green peptide). (A) Minimal reduction of negative ellipticity occurs at 1 equivalent Cu(II), with further reduction at 2 equivalents Cu(II). (B) The addition of apo-C-peptide to 1:1 Cu(II)-BSA shows perturbations in secondary structure, while 2:1 Cu(II)-BSA displays modest shifts. (C) In the absence of Cu(II), the CD spectra of apo-C-peptide and apo-BSA overlaps to the spectra of apo-BSA alone. (D) With the addition of 1:1 and 2:1 Cu(II)-C-peptide to apo-BSA, similar decreases in ellipticity occur.

Table 3.1. Alpha helical content for BSA with the addition of 1 and 2 equivalents of Cu(II), followed by the addition of apo-C-peptide

Wavelength (nm)	1:1 Cu(II)-BSA	1:1 Cu(II)-BSA + Apo-C-peptide	2:1 Cu(II)-BSA	2:1 Cu(II)-BSA + Apo-C-peptide
212 nm	69.3	62.8	65.4	64.4
222 nm	68.3	63.4	63.3	64.9

Table 3.2. Alpha helical content for BSA with the addition of apo-C-peptide or 1 and 2 equivalents of Cu(II)-C-peptide

Wavelength (nm)	Apo-BSA	Apo-BSA + Apo-C-peptide	Apo-BSA + 1:1 Cu(II)-C-peptide	Apo-BSA + 2:1 Cu(II)-C-peptide
212 nm	71.1	71.1	63.1	62.7
222 nm	68.2	69.2	62.5	61.7

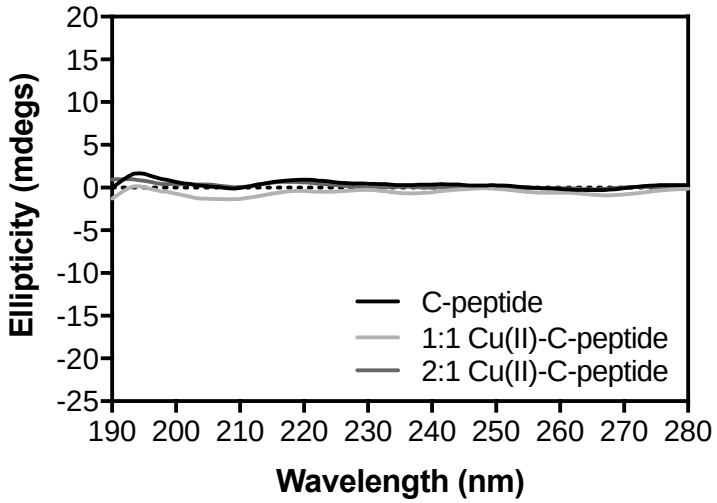

Figure 3.4. CD spectra of C-peptide bound to 1 or 2 eq. Cu(II). CD spectra of C-peptide (2 μM) treated with one or two equivalents of Cu(II) show no notable differences in ellipticity compared to apo-C-peptide.

Interestingly, the resulting spectra of Cu(II)-C-peptide adducts added to apo-BSA are distinct from the spectra when apo-C-peptide is added to Cu(II)-treated BSA at the same Cu(II) equivalents. Taken together, the CD data points to the ability of Cu(II) to mediate the formation of a complex between C-peptide and BSA that otherwise does not occur in the absence of the metal ion, and that both the Cu(II) stoichiometry as well as the order of addition impacts the resulting species. We thus present two schemes by which a C-peptide/albumin/Cu(II) complex may form: either C-peptide binds to metallated sites on Cu(II)-BSA (Scheme 1 or S1, Figure 3.5) or Cu(II)-C-peptide coordinates to available sites on BSA (Scheme 2 or S2, Figure 3.5).

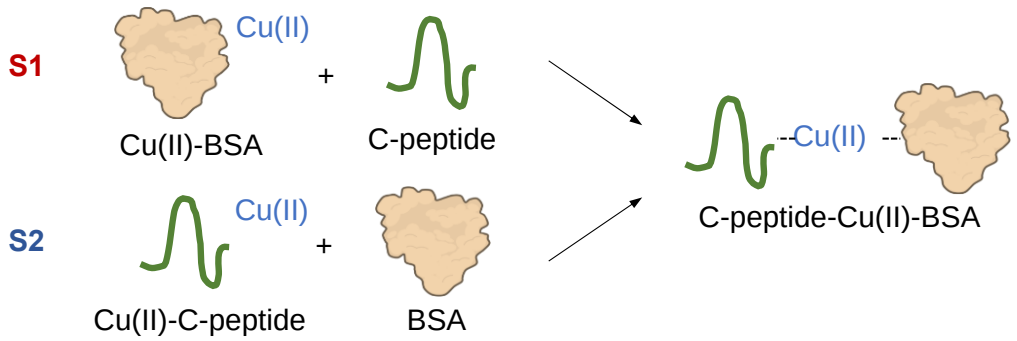

Figure 3.5. Schematic representations of two potential binding interactions that may result in ternary complexation between C-peptide and BSA, with Cu(II) serving as a bridge. The order of addition (whether Cu(II) is added to C-peptide or BSA first prior to the addition of the other) affects the structure of the resulting species.

3.2.2 Order and equivalence of Cu(II) produces distinct metal coordination sites

We next determined whether the Cu(II) binding sites differ between the distinct C-peptide/albumin/Cu(II) complexes. We assessed the Cu(II) coordination sites using the d-d region in the electronic absorption spectra, which is sensitive to coordination geometry and ligand identity. BSA is known to bind Cu(II) at two sites, which can be distinguished by their spectroscopic signatures: a high affinity N-terminal Site (NTS, K_d = 1 pM), which is metallated by the addition of one equivalent of Cu(II), and a lower-affinity Multi-Metal Binding Site A (MBSA, K_d = 10 nM), which is metallated at higher equivalents of Cu(II).[19] At pH 7.4 in phosphate buffer, we observe that population of the NTS with (1:1 Cu(II)/BSA) yields a d-d band with λ_{max} at 540 nm (Figure 3.6B, Table 3.3, Figure 3.7), characteristic of a strong square-planar ligand field. Further addition of Cu(II) (2:1

Cu(II)/BSA) produces a red-shifted band with λ_{max} at 555 nm, a charge transfer (CT) transition band at 385 nm, and a second band with λ_{max} at 680 nm (Figure 3.6A & 3.6B, Table 3.4, Figure 3.7). The CT transition and second band is indicative of a weaker ligand field consistent with the ligand set of the MBSA.[38,46] While a d-d band with λ_{max} at 650 nm and 725 nm is observed upon addition of 1 and 2 equivalents Cu(II) respectively to apo-C-peptide (Figure 3.6B, Table 3.3 & 3.4), the extinction coefficient of these peaks are significantly lower than that of the Cu(II)-BSA sites. We thus used the Cu(II)-BSA signatures as a point of comparison to assess the C-peptide/BSA/Cu(II) complexes.

Spectral traces of the S1 and S2 complexes were subtracted from the summation of the apo-C-peptide and apo-BSA spectra to focus the analysis on the Cu(II) d-d bands (Figure 3.8). Relative to the spectra of metallated BSA, the S1 complex at one equivalent Cu(II) shows a red shift in the λ_{max} from 540 nm to 545 nm (Figure 3.6B, Table 3.3), indicative of a weaker field ligand environment compared to 1:1 Cu(II)-BSA. However, at two equivalents Cu(II), the S1 spectrum closely overlaps with that of the 2:1 Cu(II)-BSA spectra with minimal shifts in λ_{max} at 388 nm, 556 nm, and 678 nm (Figure 3.6A & 3.6B, Table 3.4). In contrast, the S2 complex at one equivalent of Cu(II) blue-shifts the λ_{max} to 525 nm relative to the 540-nm peak of 1:1 Cu(II)/BSA and interestingly produces a CT band at 360 nm (Figure 3.6A, Table 3.3), suggesting a stronger field ligand set compared to 1:1 Cu(II)-BSA. At two equivalents of Cu(II), the spectrum of the S2 complex yield blue-shifted absorption maxima at 375 nm and 530 nm relative to the 385 nm and 555 nm bands of 2:1 Cu(II)-BSA, while a 690 nm peak is observed red-shifted from the 680 nm band of Cu(II)-BSA (Figure 3.6A, Table 3.4). To ensure that the S1 and S2 spectra are not merely the additive spectra of the species in solution, we summed the independent

traces of C-peptide, BSA, or their Cu(II) complexes accordingly to mimic the sample preparation conditions of each scheme (Figure 3.9, Table 3.5 and 3.6). The addition spectra show marked differences in the experimental spectra, both in terms of overall spectral profile and absorption maxima, suggesting that the S1 and S2 preparations do indeed result in new species and that the spectra are not merely mixtures of the individual species added to the solution.

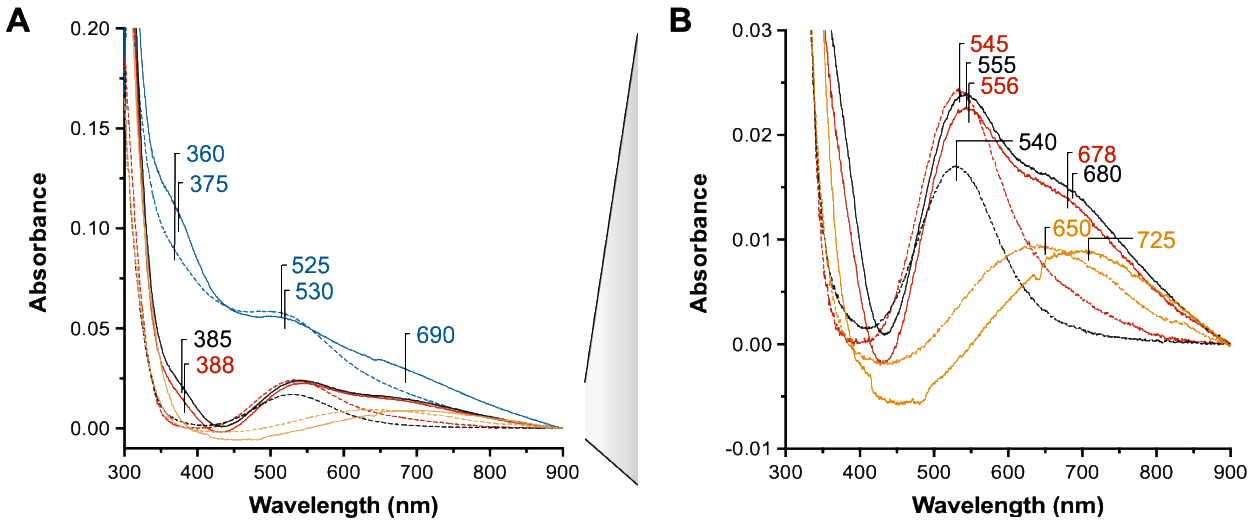

Figure 3.6. UV-Visible spectra of Cu(II)-C-peptide (orange), Cu(II)-BSA (black), S1 (red), and S2 (blue) at one (dashed line) and two (solid line) equivalents of Cu(II). (A) Overlay display of all spectra in the 300-900 nm range, alongside an (B) inset to highlight subtle blue- or red-shifts in wavelength in the 500-700 nm range.

Table 3.3. Maximum absorbance values of the UV-Vis spectra with the addition of one equivalence of Cu(II) (dashed line)

One equivalence of Cu(II) (dashed)		
Sample	Abs_{max} (nm)	
Cu(II)-C-peptide	—	650
Cu(II)-BSA	—	540
S1: 1:1 Cu(II)-BSA + apo-C-peptide	—	545
S2: apo-BSA + 1:1 Cu(II)-C-peptide	360	525

Table 3.4. Maximum absorbance values of the UV-Vis spectra with the addition of two equivalences of Cu(II) (solid line)

Two equivalences of Cu(II) (solid)			
Sample	Abs_{max} (nm)		
Cu(II)-C-peptide	—	—	725
Cu(II)-BSA	385	555	680
S1: 2:1 Cu(II)-BSA + apo-C-peptide	388	556	678
S2: apo-BSA + 2:1 Cu(II)-C-peptide	375	530	690

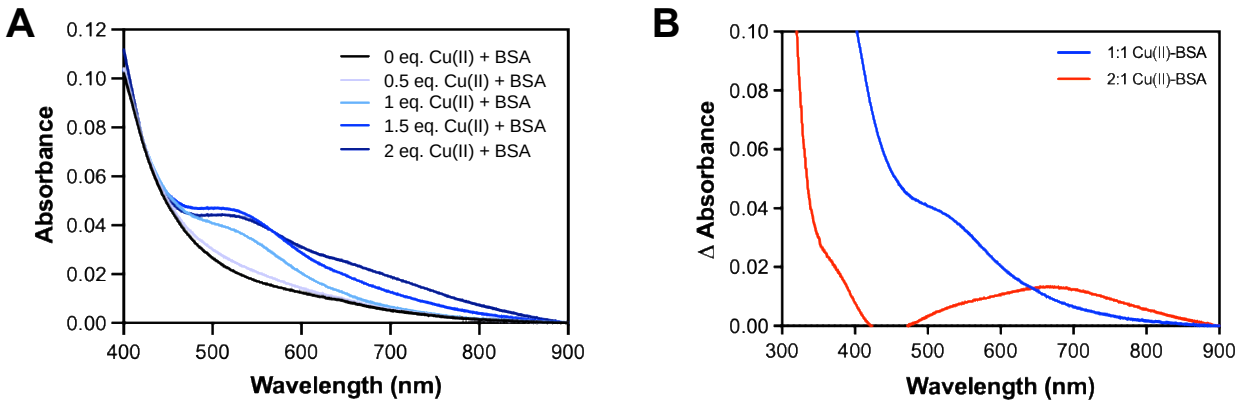

Figure 3.7. UV-Visible spectra of Cu(II) titrations into BSA. (A) Substoichiometric additions of Cu(II) was titrated into BSA. (B) Resulting spectra of 2:1 Cu(II)-BSA and 1:1 Cu(II)-BSA after subtraction from 1:1 Cu(II)-BSA and apo BSA respectively.

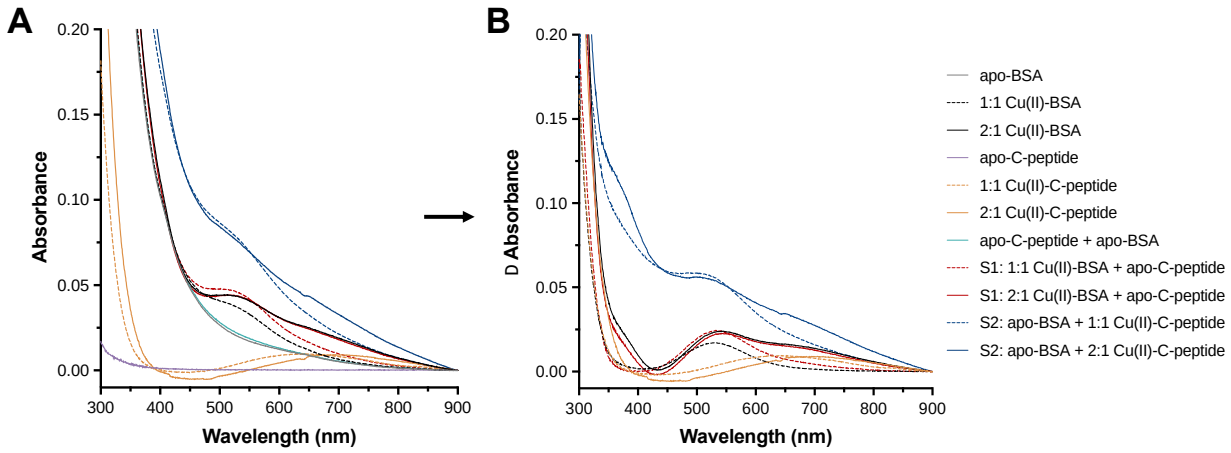

Figure 3.8. UV-Visible spectra of Figure 3 without subtraction of the protein/peptide spectra. (A) Raw spectra traces of 1:1 and 2:1 Cu(II)-BSA before subtraction from apo-BSA, 1:1 and 2:1 Cu(II)-C-peptide prior to subtraction from apo-C-peptide, as well as 1:1 and 2:1 S1 or S2 before subtraction from apo-C-peptide + apo-BSA. (B) Resulting spectra after subtraction.

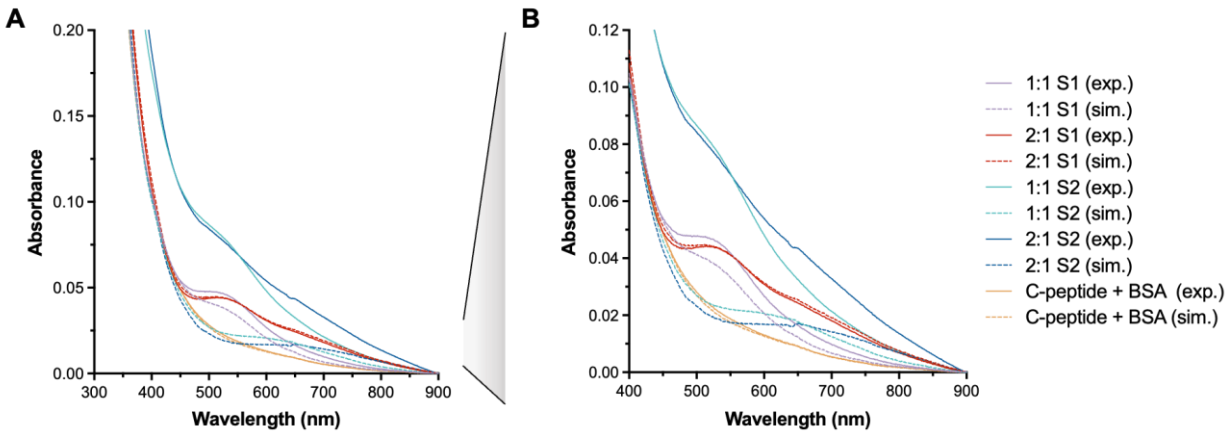

Figure 3.9. Overlay of UV-Visible experimental spectra of S1 and S2 at 1 and 2 equivalences of Cu(II) to the simulated (sim.) addition spectra corresponding to the species present in solution if no interaction were to occur. (A) Simulation data (dashed) entail spectra addition of control sample traces, resulted in differences in absorbance maximum peaks and lack of CT transition bands in comparison to experimental traces of S1 and S2 (solid). (B) Inset of spectra region of (A). Absorbance maximum values of the simulations are listed in Table S1 and S2.

Table 3.5. Addition spectra simulation of S1 and S2 at one equivalence of Cu(II).

One equivalence of Cu(II)		
Sample	Abs_{max} (nm)	
S1: 1:1 Cu(II)-BSA + apo-C-peptide		545
S1: 1:1 Cu(II)-BSA + apo-C-peptide (simulation)		548
S2: apo-BSA + 1:1 Cu(II)-C-peptide	360	525
S2: apo-BSA + 1:1 Cu(II)-C-peptide (simulation)	—	663

Table 3.6. Addition spectra simulation of S1 and S2 at two equivalences of Cu(II).

Two equivalences of Cu(II)			
Sample	Abs_{max} (nm)		
S1: 2:1 Cu(II)-BSA + apo-C-peptide	388	556	678
S1: 2:1 Cu(II)-BSA + apo-C-peptide (simulation)	—	555	694
S2: apo-BSA + 2:1 Cu(II)-C-peptide	375	530	690
S2: apo-BSA + 1:1 Cu(II)-C-peptide (simulation)	—	—	695

We further probed the coordination environment and geometry around the Cu(II) center of the complexes with electron paramagnetic resonance (EPR) spectroscopy.

Previous work has shown that the NTS of serum albumin is composed of nitrogen ligands which include the N-terminus, two backbone amide nitrogen atoms, and one His residue, making a 4N square planar coordination site (Figure 3.9).[47] The MBSA contains two nitrogen ligands, both from His residues, one oxygen ligand from an Asn residue and a second oxygen ligand from an Asp residue to make a tetrahedral 2N2O site (Figure 3.9).[48]

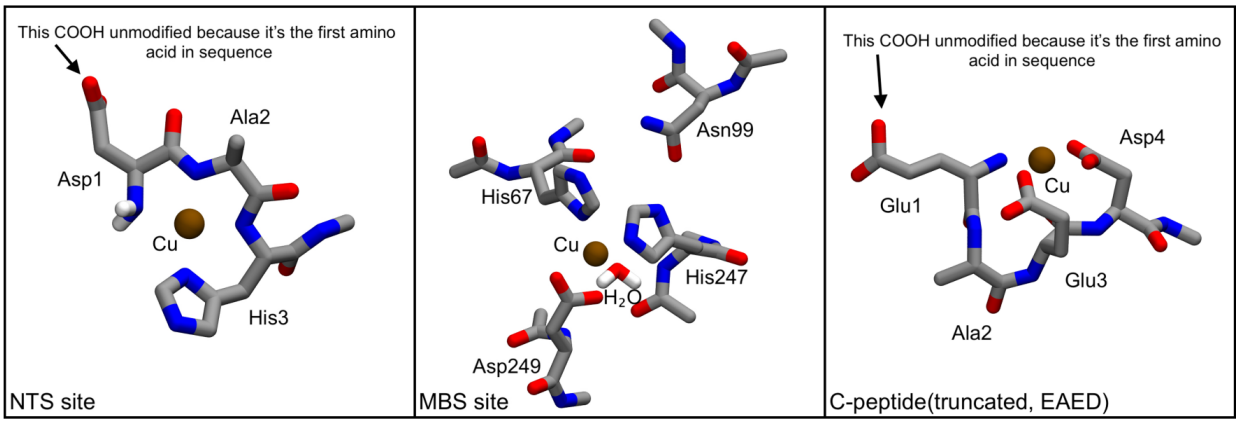

Figure 3.9. TDDFT results of the NTS site and MBSA site of BSA, as well as truncated C-peptide (EAED). (A) Copper coordination models of the NTS site (left), MBSA site (middle), and C-peptide (EAED) (right) are achieved by replacing terminal COOH with $(C=O)NHCH_3$ and terminal NH_2 with $NH(C=O)CH_3$. COOH of the first amino acid of the NTS site (Asp1) and truncated C-peptide (Glu1) remains unmodified, and selected hydrogens are hidden for visibility. All geometries are optimized (cam-b3lyp functional/def2-tzvp-f basis) in TeraChem software by utilizing the PCM model (dielectric constant = 4) for lowest energy geometry.

We compared the Cu(II) coordination environment of S1 and S2 to that of BSA alone. At X-band frequency (9.39 GHz), the EPR spectra S1 and S2 complexes at one equivalent Cu(II) are identical to that of Cu(II)-BSA; all species exhibit an axial signal with hyperfine interactions to the Cu(II) nucleus. Simulation was achieved using $g_{||}$ = 2.183 and $A_{||}$ = 601 MHz. This result indicates no change in coordination modes at the NTS of BSA in either complex.

Upon addition of two equivalents Cu(II), a second paramagnetic copper species with $g_{||}$ = 2.27, $g_{\perp}$ = 2.055 and $A_{||}$ = 545 MHz was detected in all samples (Figure 3.10A, Table 3.7). For Cu(II)-BSA, this is consistent with metalation of the MBSA as previously observed.[49] No change in EPR spectra were observed upon the addition of C-peptide, which suggests similarities in the coordination environment around the Cu(II) center to the MBSA in Cu(II)-BSA. In addition, the parameters from the Cu(II)-C-peptide EPR spectrum at X-band frequency did not overlap with those of either the S1 or S2 complex, confirming that Cu(II)-C-peptide species were not present or detected (Figure 3.11, Table 3.8).[15]

To discern subtle differences, the samples were investigated at higher frequencies. At Q-band frequency, the EPR spectra of S1 and S2 remain similar to that of Cu(II)-BSA (Figure 3.10B). We further interrogated Cu(II)-BSA and the S2 complexes at D-band frequency (130 GHz) (Figure 3.10C) due to the differences observed in the UV-Vis absorption spectra (Figure 3.6A). To our knowledge, this is the first time that Cu(II)-BSA complex has been investigated with high-field EPR. The resulting spectra allow a precise determination of $g_{\perp}$ = 2.042 for the NTS and 2.055 for the MBSA. The simultaneous simulation of all EPR spectra yield $g_{||}$ and $A_{||}$ values (Table 3.7) indicative of a neutral 4N

coordination for the first site, and a neutral 2N2O coordination for the second site,[50] which is in agreement with the assignment of the NTS and MBSA, respectively. These parameters do not change significantly in S1 or S2, suggesting conserved coordination environments around the Cu(II) centers compared to the equimolar Cu(II)-BSA complex.

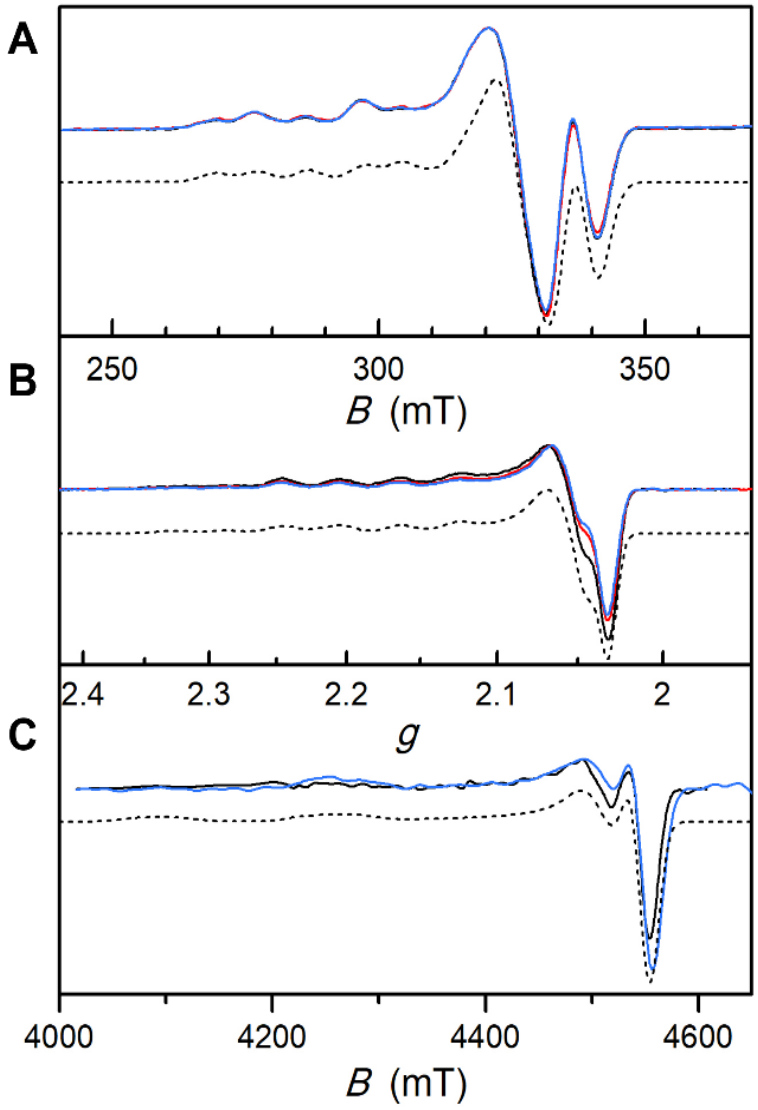

Figure 3.10. Determination of coordination modes using EPR at X-, Q-, and D-band. (A) X-band continuous-wave EPR spectra of Cu(II)-BSA (black), S1 (red), and S2 (blue) at

2 equivalents Cu(II) concentration measured at 20 K. (B) Q-band field-sweep echo-detected EPR spectra of Cu(II)-BSA, S1, and S2 measured at 25 K. The spectra were taken at microwave frequencies 34.296, 33.958, and 34.293 GHz, respectively, and were overlaid onto the common *g*-factor abscissa. The spectra were pseudo-modulated at 3 mT. (C) D-band field-sweep echo detected EPR spectra of Cu(II)-BSA and S2 at 10 and 13 K, respectively. The spectra were pseudo-modulated at 20 mT. Black dashed lines are simulations of the data using the parameters given in Table 3.7.

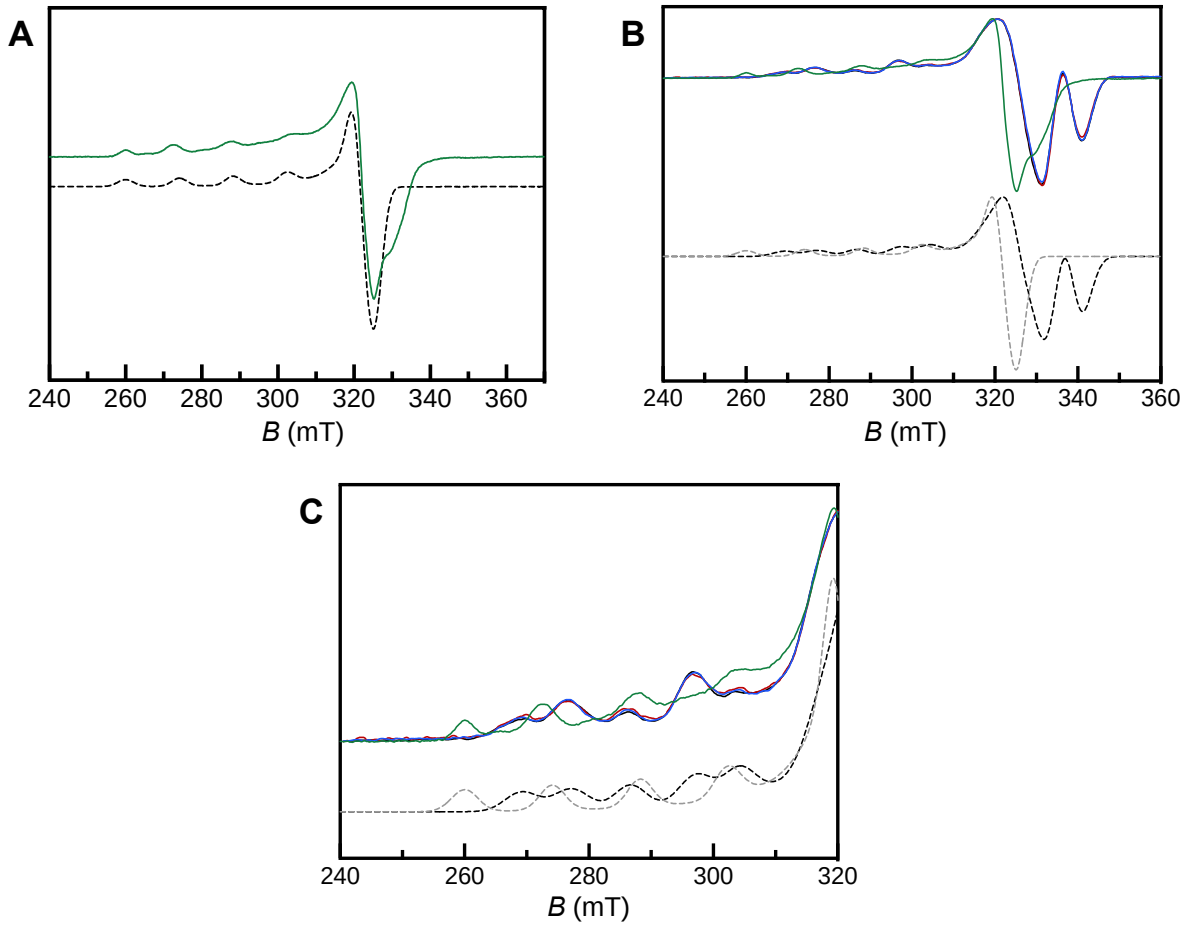

Figure 3.11. Electron paramagnetic resonance spectra of Cu(II)-C-peptide. (A) X-band continuous-wave EPR spectra of Cu(II)-C-peptide (green) measured at 20 K. Black dashed lines are simulations to the data using the parameters given in Table 3.8. (B) Overlay of Cu(II)-C-peptide spectra with X-band EPR spectra of S1 (red) and S2 (blue) from Figure 4A. Dashed lines are simulations to the data for C-peptide (gray, Table 3.8) as well as the data for S1 and S2 (black, Table 5) (C) Inset of $g_{||}$ region of (B

Table 3.7. EPR simulation parameters for Cu(II)-BSA, S1, and S2.

	NTS site	MBSA site
$g_{\|}$	2.183	2.270
$g_{\perp}$	2.0418	2.055
$A_{\|}$ (MHz)	601	545
$A_{\perp}$ (MHz)	80	0
linewidth (X-band, mT)	5	5
linewidth (Q-band, mT)	6	11
linewidth (D-band, mT)	15	35
Relative ratio	0.5	0.5

Table 3.8. EPR simulation parameters for Cu(II)-C-peptide.

$g_{\parallel}$	2.38
$g_{\perp}$	2.078
$A_{\parallel}$ (MHz)	460
$A_{\perp}$ (MHz)	0
linewidth (X-band, mT)	4

The EPR and electronic absorption data together suggest that while the Cu(II) species in both S1 and S2 complexes are distinct from metallated BSA, they exhibit similar geometries and atom identities. To help understand what leads to the slight shifts in the absorption maxima of the UV-Vis spectra of the C-peptide/BSA/Cu(II) complexes relative to Cu(II)/BSA alone, we applied time-dependent density functional theory (TDDFT) to predict the visible spectra of hypothesized binding modes.[51] Geometry optimization and TDDFT calculations were constructed for both Cu(II) binding sites of BSA and Cu(II)-C-peptide. The TDDFT calculations reveal that displacement of Asp249 at the MBSA of BSA (Figure 3.12A) by Asp4 of C-peptide (Figure 3.12B), results in a modest blue shift in the λ_{max} from 721 to 688 nm (Figure 3.12C), which resembles the observed experimental shift in the spectrum of the 2:1 S1 complex (Figure 3.6B). Modifications of TDDFT calculations with other residues of the C-peptide terminus yield various models and electronics that does not support this experimental shift. Rather, the subtle change in the λ_{max} value may be attributed to a shift in sterics in the outer coordination sphere as Asp4 of C-peptide coordinates.[52,53]

In addition, this model is also consistent with the minimal perturbations in the primary coordination sphere observed by EPR. DFT calculation of EPR parameters using PBE0 functional[54] gives $g_{||}$ = 2.237 for Cu(II) center in the MBSA, and $g_{||}$ = 2.233 for Cu(II) ternary complex with the MBSA and C-peptide Asp4 residue (Table 3.9). There is a slight discrepancy in the $g_{||}$ value from the experimental value, but the difference in $g_{||}$ of the Cu site with and without C-peptide is minimal, in congruence with the experimental observation. Calculation of $A_{||}$ parameter performed with B3LYP functional[54] give $|A_{||}|$ = 546 and 549 MHz for Cu/BSA and C-peptide/Cu(II)/BSA models, respectively, in excellent agreement with the experimental value (Table 3.9). Altogether, this supports the role of Cu(II) in bridging the interaction between C-peptide and BSA at the MBS via retention of a coordinating Asp from C-peptide and replacement of the remaining Cu(II) ligand set of C-peptide with the MBSA ligands of BSA. Conversely, the red shift to λ_{max} at 690 nm observed in the experimental spectrum of the 2:1 S2 complex (Figure 3.6A) does not match the predicted spectra of the model structures. In our previous work, we had observed C-peptide mutants or truncates where the E3 and D4 binding sites are removed still bind to Cu(II) but at different sites that yield red-shifted spectra. One possible reason for the red shift in the spectra of the S2 complex is that BSA addition may also induce a reshuffling of the Cu(II)-binding ligands from C-peptide similarly to what was observed with the analogues.

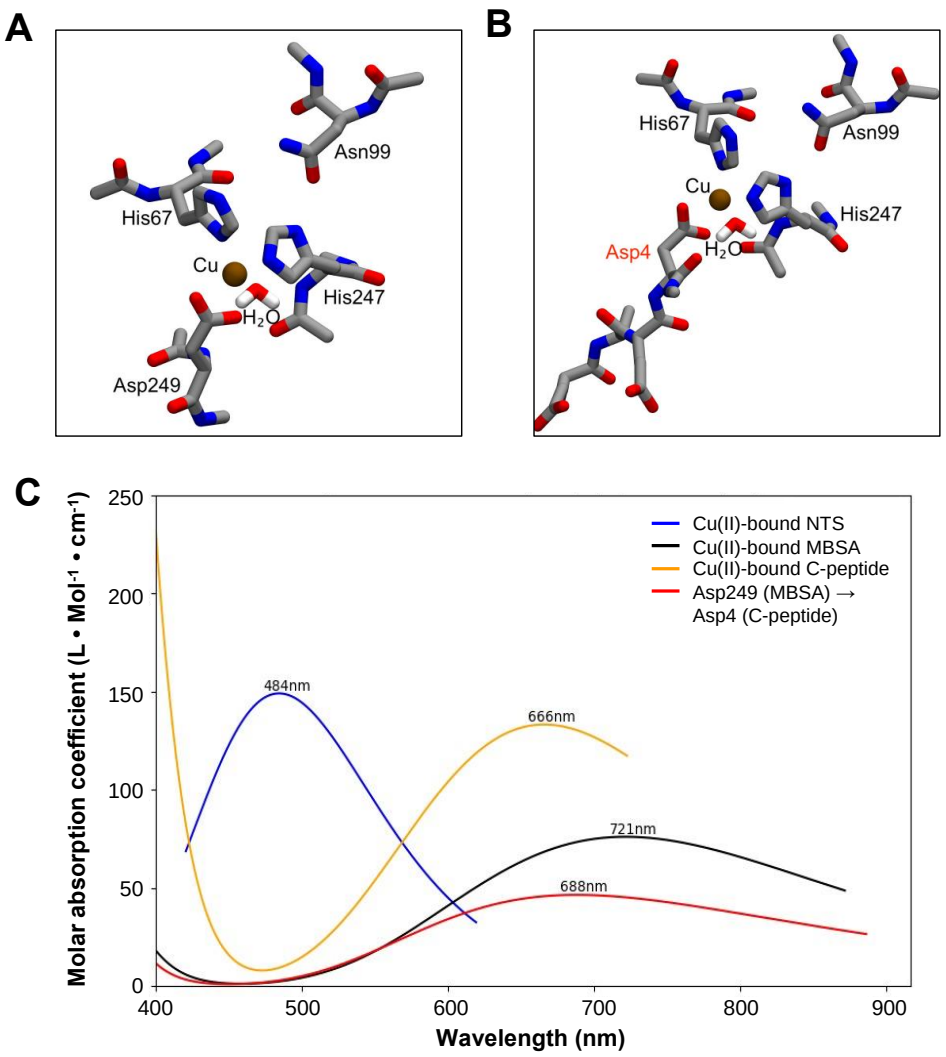

Figure 3.12. Modeled copper coordination ligand sets between C-peptide and BSA using TDDFT calculations. (A) Established structure of the copper-binding MBSA in BSA (PDB: 5IJF), where His67, His247, Asp249, and H2O are coordinated to the copper center following a tetrahedral 2N2O site, and Asn99 is displaced. (B) Hypothetical coordination model of the displacement of Asp249 from the MBSA to Asp4 of C-peptide. (C) Resulting TDDFT calculations of predicted wavelengths based on optimized geometries of the Cu(II)-bound NTS (blue) and the Cu(II)-bound MBSA (black) of BSA, as well as Cu(II)-bound C-peptide (orange). The displacement of Asp249 in the MBSA of BSA to Asp4 of

C-peptide results in a blue-shifted λ_{max} at 688 nm (red) from the MBSA trace at 721 nm (black).

Table S8. Experimental EPR parameters from multifrequency EPR measurements and calculated parameters from the DFT-optimized structures of Cu(II) in the MBSA and in the ternary complex with BSA MBSA site and C-peptide Asp4 residue.

	Functional	$g_{\|\|}$	$g_{\perp}$	$A_{\|\|}$ (MHz)	$A_{\perp}$ (MHz)
Experimental		2.270	2.055	545[a]	0[b]
DFT-optimized Cu/BSA (MBSA)	PBE0	2.237	2.067 2.075	−576	19 −27
DFT-optimized C-peptide/Cu(II)/BSA (MBSA)	PBE0	2.233	2.064 2.077	−579	5 −4
DFT-optimized Cu/BSA (MBSA)	B3LYP	2.212	2.061 2.067	−546	−1 45
DFT-optimized C-peptide/Cu(II)/BSA (MBSA)	B3LYP	2.209	2.058 2.069	−549	20 37

3.2.3 Ternary complexes exhibit modified biochemical and cellular C-peptide behavior

We sought to determine whether the Cu(II) center in the S1 and S2 complexes could convey differences in biochemical and cellular function. Cu(II) coordination to peptides have been previously shown to alter the redox susceptibilities of metal ions relative to its "free" aquated form. Both Cu(II) and C-peptide have independently been

shown to impact oxidative balance with biological systems. Thus, we assessed and compared the ability of C-peptide, BSA, and the S1 and S2 complexes to affect Fenton-type chemistry of Cu(II). In its "free" form (e.g. the addition of $CuCl_2$ to a buffered aqueous solution), Cu(II) ions in solution are reduced to Cu(I) in the presence of a reducing agent such as ascorbic acid. In the presence of dissolved O_2, the resulting Cu(I) can catalyze the production of reactive oxygen species (ROS) such as $OH^{\bullet}$ radicals via Fenton-type reactions (Equations 3-6).

$$Red + Cu(II) \rightarrow Ox + Cu(I) \quad (3)$$

$$Cu(I) + O_2 \rightarrow Cu(II) + O_2^- \quad (4)$$

$$2\,O_2^- + 2\,H^+ \rightarrow H_2O_2 + O_2 \quad (5)$$

$$Cu(I) + H_2O_2 \rightarrow Cu(II) + HO^- + HO^{\cdot} \quad (6)$$

In this way, the production of ROS by Cu(II) in the presence of a reducing agent has been used as an indicator of Cu(II) ion availability in solution. Non-fluorescent coumarin-3 carboxylic acid (3-CCA) is oxidized to fluorescent 7-OH-CCA (excitation at 388 nm, emission at 450 nm) in the presence of $HO^{\bullet}$ radicals, and has been applied as a probe for this process.[55,56] We evaluated the ability of C-peptide, BSA, and the S1 and S2 complex to affect Cu(II) redox susceptibility with this assay. C-peptide displays greater protective copper redox abilities than phosphate buffer, indicating that the peptide decreases free Cu(II) availability (Figure 3.13A). BSA is able to reduce protect from ROS generation to a more appreciable extent. In testing the S1 and S2 complexes, the resulting

species show even lower ROS generation than both C-peptide and BSA alone (Figure 3.13A and B), further supporting the presence of distinct Cu(II)-bridged species.

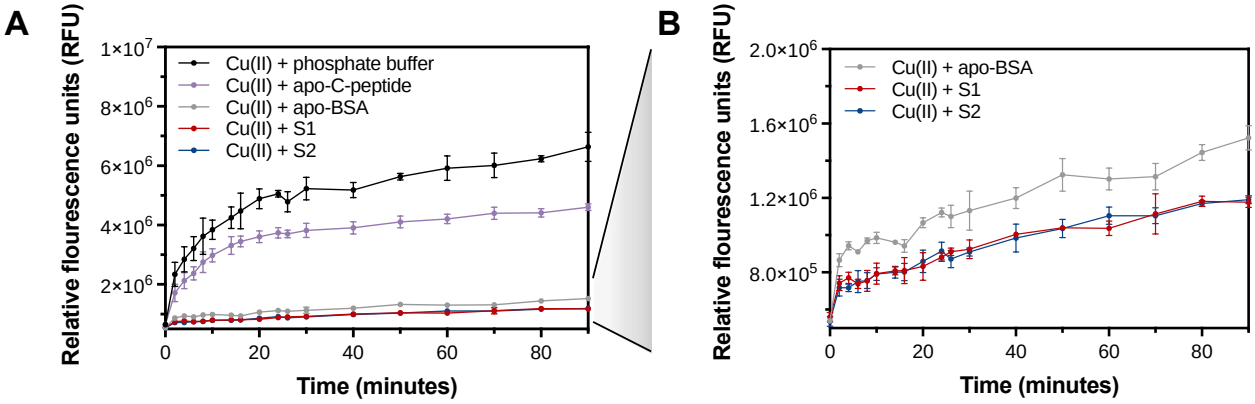

Figure 3.13. Fluorescent 7-OH-CCA assay (ex. 338 nm, em. 450 nm; *n* = 3) for measuring redox protection from Cu(II)-induced $OH^{\cdot}$ generation by solutions containing 1 eq. Cu(II) and 2 μM C-peptide and/or BSA in 10 mM phosphate buffer at pH 7.4. (A) RFU of C-peptide decreases in comparison to phosphate buffer, but not to the same extent as either BSA or the ternary complexes. (B) Inset of (A) highlights that S1 and S2 show increased redox protection as compared to Cu(II)-BSA. Data is shown as mean ± SD with n = 3.

To determine whether copper-bridged C-peptide/BSA complexes have biological relevance in the cellular context, we assessed whether the presence of albumin could impact peptide internalization via immunofluorescence staining of the peptide. C-peptide internalizes into HEK-293 (human embryonic kidney) at 30 minutes via endocytosis;[57] we previously showed that Cu(II) addition decreases this internalization.[16] HEK-293 cells

grown in serum-free media were treated with solutions containing apo-C-peptide or Cu(II)-C-peptide in the absence or presence of BSA (Figure 3.14A). To detect peptide uptake, cells were fixed, permeabilized, and incubated with C-peptide primary antibodies, followed by secondary antibodies conjugated with Alexa Fluor 488 fluorophore (Figure 3.14A). Mean pixel intensities (MPI) of each sample condition were used to determine shifts in C-peptide internalization (Figure 3.14B). In comparison to apo-C-peptide, the S1 complex shows a decrease in MPI, although to a lesser degree than Cu(II)/C-peptide in the absence of BSA. In contrast, the S2 complex shows a marked increase in internalization, even relative to apo-C-peptide in starvation media (Figure 3.14A & 3.14B). The data confirms that the Cu(II)-bridged albumin/C-peptide complexes are distinct from one another and influence the pathway by which C-peptide interacts with cells.

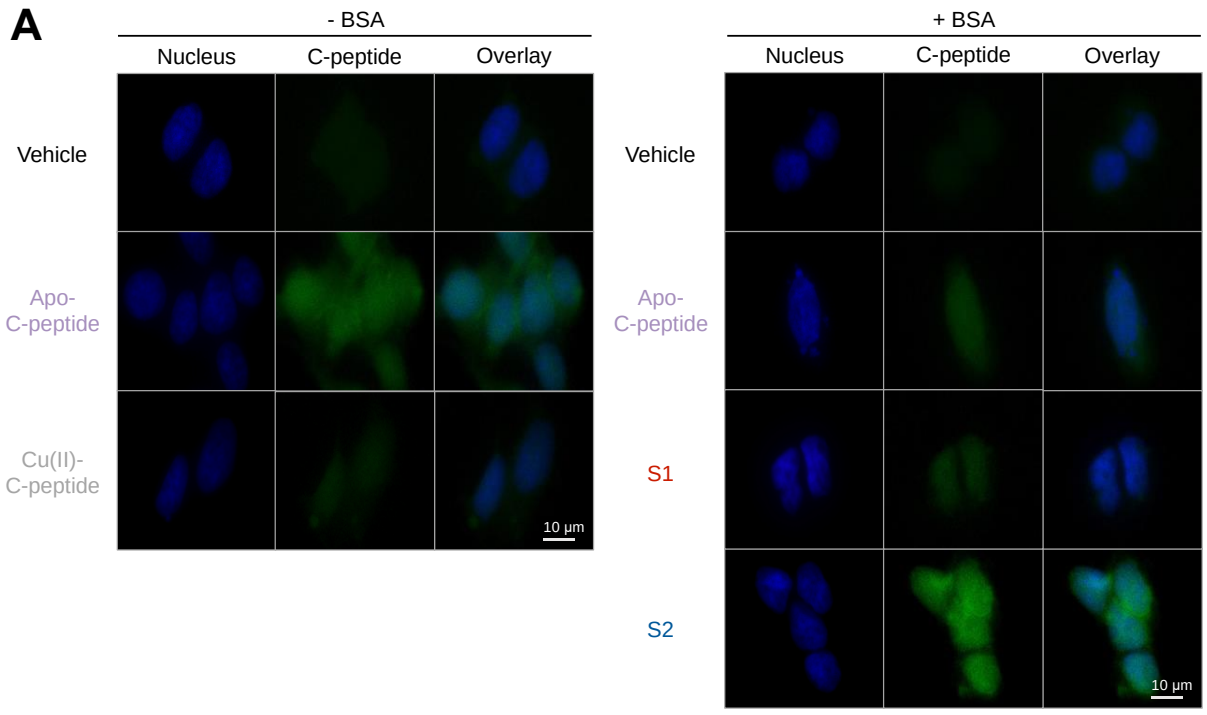

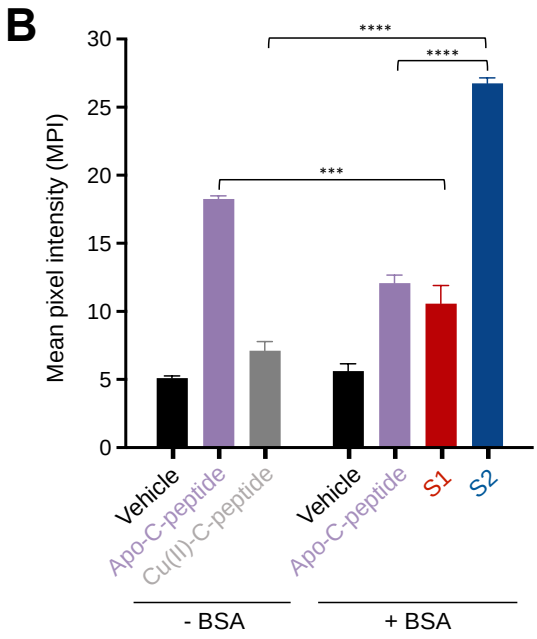

Figure 3.14. Immunofluorescence imaging of C-peptide uptake into HEK-293 cells when stimulated with 10 μM C-peptide, 11 μM $CuCl_2$, and/or 100 μM BSA. (A) Fixed cells were immunolabeled with C-peptide primary antibodies followed by secondary antibodies conjugated to Alexa Fluor 488. (B) Comparisons of fluorescence intensity of Alexa Fluor 488 immuno-labeled C-peptide. Data represent mean pixel intensities in regions of interest as mean ± SD with n = 3. Significance is analyzed by unpaired t test; *** $p < 0.005$, **** $p < 0.0001$. Uptake of S1 is lower in comparison to apo-C-peptide while S2 shows a marked increase relative to all conditions tested.

Given that previous studies have shown Zn(II) to influence the cellular behavior of C-peptide, we also assessed whether Zn(II) could similarly affect cellular internalization of the peptide in the presence of albumin. In the absence of albumin, Zn(II) modestly

decreases cellular internalization of C-peptide albeit not to the same extent as Cu(II). A Zn(II)/C-peptide/albumin preparation according to S1 shows a decrease in peptide internalization when compared to Zn(II)/C-peptide alone, but comparable to the internalization of C-peptide in the presence of albumin (Figure 3.15A & 3.15B). In contrast, a Zn(II)-containing preparation according to S2 results in an increase in internalization relative to Zn(II)/C-peptide alone, but comparable to the internalization of C-peptide in the absence of albumin (Figure 3.15A & 3.15B). In either case, order of addition and the presence of albumin may also influence interactions between Zn(III) and C-peptide at the cellular level, but perhaps not via a ternary complex detectable by the FRET-based assay (Figure 3.1C), warranting additional studies on the molecular regulation of the Zn(II)/C-peptide/albumin interaction.

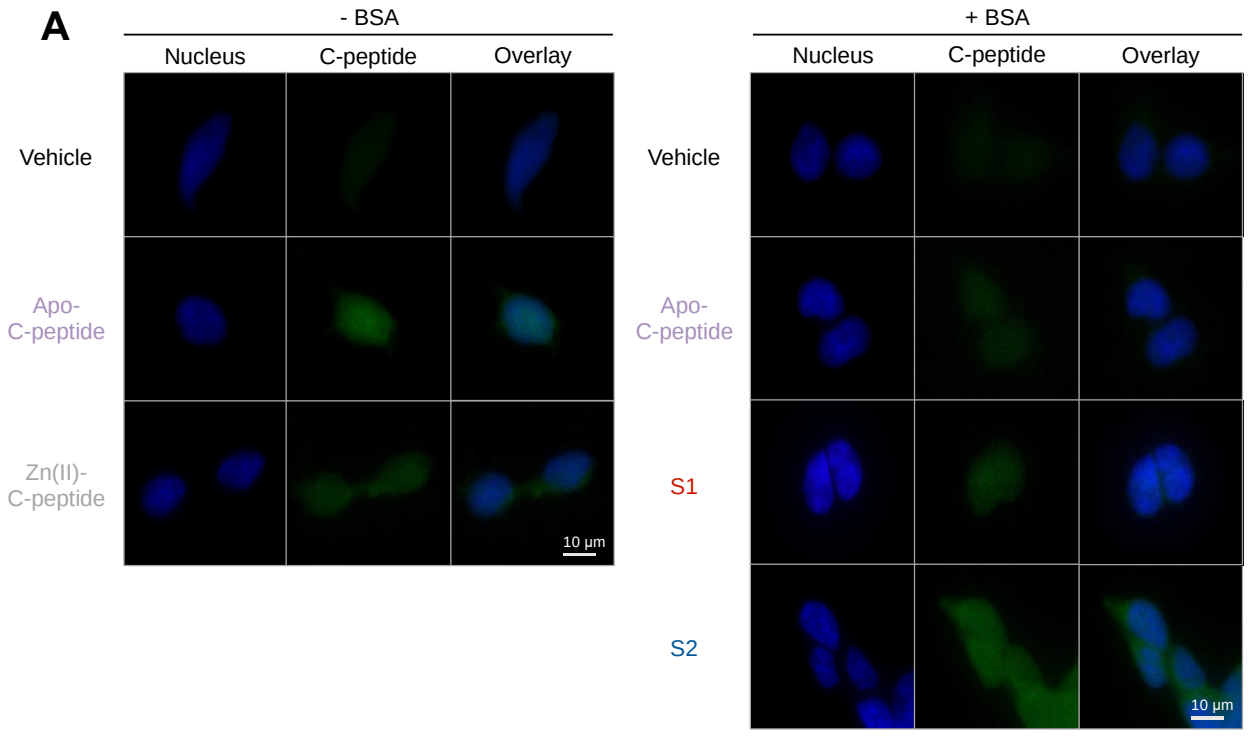

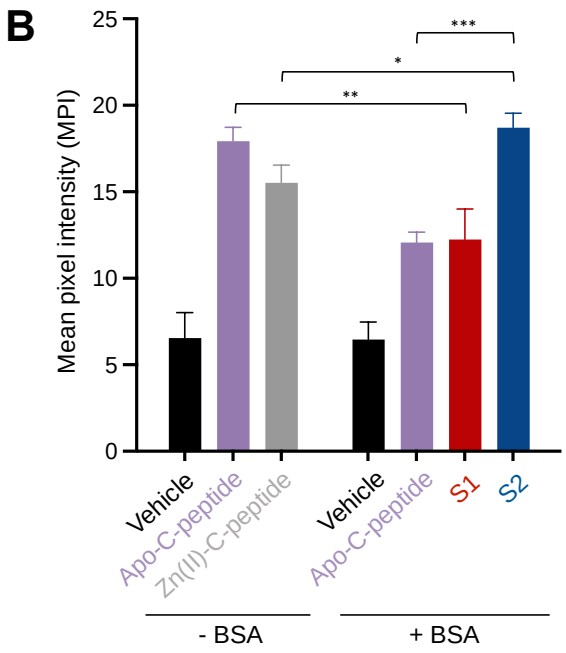

Figure 3.15. Immunofluorescence imaging of C-peptide uptake into HEK-293 cells when stimulated with 10 μM C-peptide, 11 μM $ZnCl_2$, and/or 100 μM BSA. (A) Fixed cells were immunolabeled with C-peptide primary antibodies followed by secondary antibodies conjugated to Alexa Fluor 488 in green. Nuclei were stained with Hoescht 33342 dye as a counterstain in blue. (B) Comparisons of fluorescence intensity of Alexa Fluor 488 immuno-labeled C-peptide. Data represent mean pixel intensities in regions of interest (n = 3). Significance is analyzed by unpaired t test; * $p < 0.05$, ** $p < 0.01$, *** $p < 0.001$. The uptake of S1 is lower in comparison to apo-C-peptide while S2 shows a relative increase to C-peptide/BSA. Data is shown as mean ± SD with n = 3.

The uptake pathways that initiate the cellular activity of C-peptide remain elusive as several internalization methods have been proposed but not substantiated at the

molecular level—passive diffusion, receptor-independent endocytosis, and receptor-dependent endocytosis.[57–59] Previous studies have shown that under stress conditions, albumin can internalize into cells via endocytosis.[60] This goes alongside with Spence and coworkers' hypothesis that the C-peptide receptor may interact with the peptide complexed to albumin than the peptide alone.[13,14] The immunofluorescence data points to the possibility that copper-stabilization of a C-peptide complex with albumin may direct uptake of the peptide via an albumin-associated pathway, and that this pathway may diverge when cells are treated with the peptide in the absence of albumin. As debate remains whether C-peptide uptake is receptor-mediated, and if so, which receptor serves as the peptide's cognate, additional work is required to fully elucidate the impact of metal ions on cellular activity. However, our work suggests the potential importance of considering metal ions as mediators of C-peptide signaling, and their inclusion into future studies to better facilitate our understanding of the peptide's mode of action.

3.2.4 Formation of ternary species inflates C-peptide measurements

Perhaps the most widespread clinical application of C-peptide to date is as a secondary biomarker for insulin,[31,32] given that the two are co-released from the pancreas and C-peptide bears a significantly longer half-life.[33] As we demonstrated that C-peptide may be present in blood as a copper-linked complex with albumin, we investigated whether the formation of these species would affect the measurement of C-peptide levels with a standard clinical immunoassay. C-peptide enzyme-linked immunosorbent assay (ELISA) measures C-peptide by immobilized immunoaffinities of the peptide. We

compared the detection of C-peptide in its apo-form to the addition of Cu(II), BSA, and the S1 and S2 complexes. The presence of either Cu(II) or albumin does not significantly affect the ELISA-based detection of C-peptide. However, when both are present either by the S1 and S2 preparations, the ELISA registers significantly higher C-peptide levels than was added into the solution, showing 4.7- and 4.1-fold increases in measured C-peptide levels, respectively (Figure 3.16). In contrast, the addition of Zn(II) following these same conditions does not significantly shift ELISA-based detection of C-peptide (Figure 3.17). Altogether, these observations point to the possibility that the presence of these ternary complexes may impact quantification of these biomarkers, potentially impacting diagnoses and treatment regimens.

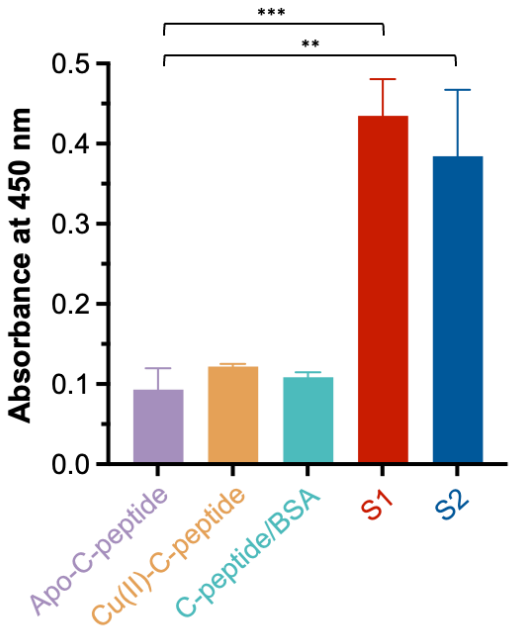

Figure 3.16. C-peptide ELISA (abs. at 450 nm) for detecting C-peptide by antibody recognition in solutions containing 50 pg/mL of apo-C-peptide, Cu(II), and BSA. Measurements were done in biological replicates (n = 3), and ELISA detection was normalized to apo-C-peptide. The presence of Cu(II) (orange) or BSA (teal) with C-peptide minimally shifts C-peptide detection. When C-peptide is copper-bridged to BSA following S1 (red) or S2 (blue), C-peptide detection significantly increases. Significance is analyzed by unpaired t test; ** $p < 0.01$, *** $p < 0.005$. Data is shown as mean ± SD with n = 3.

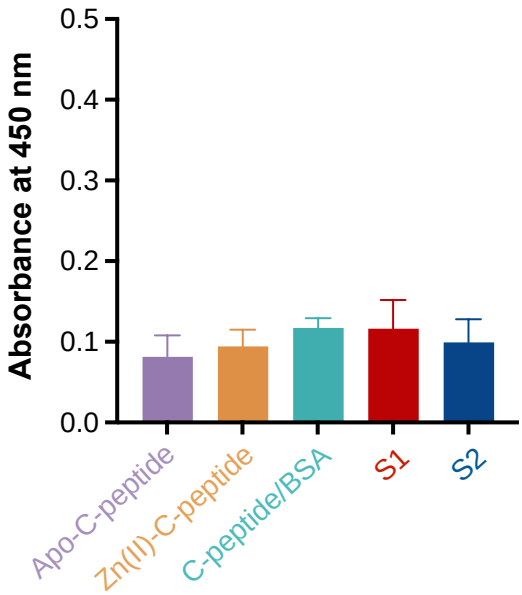

Figure S13. C-peptide ELISA (450 nm) for detecting C-peptide by antibody recognition in solutions containing 50 pg/mL of apo-C-peptide, $ZnCl_2$, and BSA. Measurements were done in biological triplicates (n = 3), and ELISA detection was normalized to apo-C-peptide. The presence of Zn(II) (orange) or BSA (teal) with C-peptide minimally shifts C-

peptide detection. When C-peptide is prepared with the following S1 and S2 sample conditions, C-peptide detection does not significantly shift in comparison to Cu(II). Data is shown as mean ± SD with n = 3.

3.3 Conclusions

In this work, we present evidence for the formation of ternary complexes involving C-peptide, Cu(II), and albumin. The complexes are unique to the presence of Cu(II) in contrast to Zn(II) addition or under metal-free conditions. The structure of albumin is altered in the presence of Cu(II) and C-peptide and distinct species are formed based on the order of addition. While the Cu(II) binding environments show similarities to the Cu(II)-BSA complex, spectroscopic and computational work suggest differences in ligand identities. The S1 complex (C-peptide added to a Cu(II)-BSA complex) corresponds to a binding scenario wherein the Asp249 of the MBSA in BSA is exchanged with the Asp4 of C-peptide. The S2 complex (Cu(II)-C-peptide complex added to albumin) is spectroscopically distinct from S1 and Cu(II)-BSA alone, however, the exact ligand identities require further investigation.

These ternary complexes exhibit biological activity that differ from metallated C-peptide or BSA. Both the S1 and S2 species impact the biochemical activity of the bound Cu(II) to a similar degree, exhibiting higher redox protection on Cu(II) than either C-peptide or BSA. However, the complexes differ in their effects on cellular behavior: while the S1 complex shows a reduction in internalization of C-peptide similarly to addition of Cu(II) to the peptide in the absence of BSA, the S2 complex has the opposite behavior,

enhancing C-peptide internalization over that of C-peptide alone. This observation may support the notion that a cognate receptor recognizes the albumin-associated C-peptide rather than the apo-peptide,[13,14] and that Cu(II) may be an important factor in stabilizing this complex. Taken together, consideration of the ternary complexes may be essential to untangling C-peptide's mechanism of action.

The S1 and S2 complexes may also bear clinical relevance to C-peptide measurements by standard bioassays. As C-peptide is used as a proxy for assessing insulin secretory health, these assays are most frequently conducted in patients with insulin-associated dysfunctions such as diabetes.[31,32] Of note, many of these disorders are associated with elevated serum copper levels.[61–63] Independently of copper levels, shifts in albumin levels have been linked to diabetes risk and progression.[64–66] As both complexes significantly increased the observed C-peptide levels in comparison to C-peptide alone, our data points to the importance of considering C-peptide measurements alongside copper and albumin levels. While further investigations are required to determine if the S1 or S2 species form in vivo, the concomitant changes in copper, albumin, and C-peptide in diabetic states may point to a potential value of such ternary complexes as biomarkers. Beyond C-peptide, this work offers additional opportunities to investigate the impact of plasma proteins on metal-binding peptides in extracellular signaling, further highlighting a need for studies on the biological and clinical implications of regulatory partners associated with peptide hormones.

3.4 Materials and Methods

Chemicals and reagents. All chemicals and reagents were purchased from Fisher Scientific. Dimethylformamide (DMF), 4-methylpiperidine, *N,N*-diisopropylethylamine (DIEA), dichloromethane (DCM), *N,N,N′,N′*-tetramethyl-O-(1H-benzotriazol-1-yl)uronium hexafluorophosphate (HBTU), 2,2,2-trifluoroacetic acid (TFA), diethyl ether, methanol, formic acid (FA), dimethylsulfoxide (DMSO), 5(6)-carboxytetramethylrhodamine succinimidyl ester (TAMRA), $CuCl_2$, Na_2HPO_4, H_2CO_3, NaOH, HCl, coumarin-3-carboxylic acid (3-CCA), L-ascorbic acid (Asc), and bovine serum albumin fatty acid-free powder (BSA) were purchased from ThermoFisher. Albumin-fluorescein isothiocyanate conjugate (FITC-albumin) was purchased from Sigma-Aldrich. Wang resin preloaded with Fmoc-Gln(Trt)-OH and Fmoc-Gly-OH, along with Fmoc-protected amino acids were purchased from ChemImpex. All buffered solutions and copper salt solutions were created using Direct-Q 3 deionized water (>18 MΩ, Millipore).

Solid-phase peptide synthesis and purification of C-peptide. SPPS and purification protocol were adapted from Stevenson et al.[3,4] Human wild-type C-peptide (EAEDLQVGQVELGGGPGAGSLQPLALEGSLQ), double mutant E3AD4A C-peptide, and N-terminus (N-term, EAEDLQVGQVELG) and C-terminus (C-term, LALEGSLQ) truncations were synthesized at a 0.2 mmol scale using a heated Fmoc-based solid-phase peptide synthesis (SPPS) method. Wang resin with preloaded Fmoc-Gln(Trt)-OH was swelled overnight in 5x DMF. Resin was washed 10 times with DMF. The C-terminal residue was deprotected with 25% 4-methylpiperidine in DMF, first hand-shaken for 1 minute then placed on the shaker for 10 minutes. The resin was washed 10x with 2x resin volume of DMF. Amino acids (4 eq.) and HBTU (3.9 eq.) were dissolved in minimal DMF,

then DIEA (10 eq.) was added. Resin was suspended in the amino acid/HBTU/DIEA solution and heated for 5 minutes at 95°C, shaken, and incubated again at 95 °C for another 5 minutes. The solution was placed on a shaker to cool for 2 minutes. The resin was washed 10x with 2x resin volume with DMF. The protocol was repeated from the Fmoc deprotection step for each additional amino acid. After the last amino acid coupling, the resin was washed 10x with 2x resin volume of DMF, followed by 10x washes with 2x resin volume of DCM and dried overnight. Cleavage of the protecting groups and peptide from the resin was carried out in minimal solution of 95:5 TFA:H_2O with 1-4 hours shaking. The solution was poured into chilled diethyl ether to precipitate, then the suspension was centrifuged at 3900 rpm for 10 minutes at 4°C. The supernatant was decanted and the pellet was washed again with chilled diethyl ether followed by centrifugation after each wash (3x). The pellet was dried under a stream of air overnight. Purification was performed with RP-HPLC on an Agilent Technologies 1260 Infinity II HPLC with coupled Agilent Technologies 1260 Infinity II UV-Vis detection system. Purification of crude C-peptide was performed using an Agilent Zorbax SB-C3 column (9.4 x 250 mm) at a flow rate of 3.4 mL min-1 using a nonlinear gradient of water with 0.1% FA (Solvent A) and methanol with 0.1% FA (Solvent B). The column was equilibrated and crude C-peptide loaded onto the column in 50% Solvent B held constant for 5 minutes. Solvent B increased from 50% to 75% from 5-30 minutes and from 75% to 100% from 30-35 minutes. C-peptide eluted off of the column at 63% Solvent B. Fractions containing C-peptide were confirmed by electrospray ionization mass 2 spectrometry (ESI-MS) using an Agilent Technologies 1260 Infinity II coupled with an Agilent Technologies InfinityLab LC/MSD then dried and stored at -20°C until ready for use.

Synthesis and purification of TAMRA-C-peptide. 2 mg/mL of purified C-peptide was diluted in 0.1 M H_2CO_3 buffer, and 10x molar excess of TAMRA was dissolved in DMSO. Reactive dye solution was slowly added to the C-peptide solution, and incubated for 1 hour with constant stirring. The mixed reaction was quenched using 1.5 M hydroxylamine (pH 8.5) then incubated for another hour. Sep-Pak C18 1 cc Vac cartridges (Waters) were activated with MeOH then equilibrated with H_2O + 0.1% FA. Once the reaction mixture is loaded onto the column and flowed through, the column was washed 3x with H_2O + 0.1% FA. The column was then eluted with MeOH in H_2O + 0.1% FA at 20%, 40%, 60%, 80%, then 100%. Purification was achieved using RP-HPLC on an Agilent Technologies 1260 Infinity II HPLC with coupled Agilent Technologies 1260 Infinity II UV-Vis detection system. Purification of crude C-peptide was performed using an Agilent Zorbax SB-C3 column (9.4 x 250 mm) using a nonlinear gradient of water with 0.1% FA (Solvent A) and MeOH with 0.1% FA (Solvent B). The column was equilibrated and TAMRA-C-peptide was loaded onto the column in 100% Solvent A and held constant for 5 minutes. Solvent B increased from 0% to 100% from 5-55 minutes and maintained at 100% Solvent B for another 5 minutes. from 75% to 100% from 30-35 minutes. TAMRA-C-peptide eluted off of the column between 60-80% Solvent B. The absorbance of TAMRA-labeled C-peptide was monitored at 214 nm and 280 nm, and TAMRA was monitored at 555 nm. Fractions containing TAMRA-C-peptide were verified by electrospray ionization mass spectrometry (ESI-MS) using Agilent Technologies 1260 Infinity II coupled with an Agilent Technologies InfinityLab LC/MSD then dried and stored at -20°C until ready for use.

Preparation of samples following each schematic. Concentrations of C-peptide and BSA were first determined by molecular weight, then dissolved in 10 mM phosphate buffer

(Fisher) at pH 7.4 for CD, UV-Vis, EPR, and CCA fluorescence, as well as in DPBS (Gibco) for immunofluorescence. $CuCl_2$ (Fisher) was dissolved in Milli-Q water followed by solutions containing C-peptide and/or BSA to achieve 1 or 2 eq. Cu(II). Treatments following each schematic include: (S1) 15 minute incubation of preformed Cu(II)-BSA at 1 or 2 eq. Cu(II) in solution followed by the addition of C-peptide for another 15 minutes incubation at 37°C; and (S2) 15 minute incubation of preformed Cu(II)-C-peptide at 1 or 2 eq. Cu(II) in solution followed by the addition of BSA for another 15 minute incubation at 37°C.

Förster resonance energy transfer assay for screening C-peptide/albumin interactions. 5 µM TAMRA-C-peptide and FITC-BSA were dissolved in 10 mM phosphate buffer at pH 7.4. Concentrations and stoichiometric range of TAMRA-C-peptide and FITC-BSA were first optimized to detect observable fluorescent output by serial dilution with a factor of 2 using a 96-well microplate (Greiner Bio-One). Fluorescent intensity was monitored at λex = 495 nm and λem = 520 nm for FITC-albumin, and at λex = 546 nm and λem = 579 nm for TAMRA-C-peptide using a fluorescent platereader (Molecular Devices i3x). Because TAMRA-C-peptide displayed a detectable fluorescence output at 2.5 µM only, the FRET assay was then optimized with TAMRA-C-peptide at this concentration. Serial dilutions of FITC-BSA by a factor of 2 was added to 2.5 µM TAMRA-C-peptide in the presence and absence of Cu(II) or Zn(II), then FRET efficiency % was measured. When R_0 = 49-56 Å, FRET efficiency is achieved at 50%. Statistics were performed on Prism 9.1 (GraphPad).

Circular dichroism. All measurements were recorded on a DSM 20 Circular Dichroism spectrophotometer (Olis) at RT using 1 mm path-length cuvettes (Starna Cells). The

following samples were made: (1) 2 µM (1 eq.) or 4 µM (2 eq.) of Cu(II)-BSA (2) 2 µM of preformed C-peptide and BSA, and (3) 2 µM (1 eq.) or 4 µM (2 eq.) of Cu(II) with 2 µM of C-peptide and BSA following (S1) and (S2) conditions. For each spectra acquisition, 4 scans were averaged with a bandwidth of 0.5 nm. The buffer spectrum was subtracted from all spectra, then all spectra were smoothened using GraphPad Prism 8.

UV-Visible spectroscopy. All measurements were recorded on UV-1900 (Shimadzu) using quartz cuvettes with 1 cm path-length cuvettes (Starna Cells). Samples include (1) 300 µM (1 eq.) or 600 µM (2 eq.) of Cu(II) with 300 µM BSA to make preformed Cu(II)-BSA, and (2) 300 µM (1 eq.) or 600 µM (2 eq.) of Cu(II) with 300 µM of C-peptide and BSA following (S1) and (S2) conditions. Milli-Q water was used as a spectral reference. After data collection, the phosphate buffer spectrum with water as reference was subtracted from all spectra. All spectra were normalized to account for dilution.

Electron paramagnetic resonance. EPR spectra were recorded at the CalEPR center at the University of California, Davis. Samples include (1) 50 µM (0.5 eq., “1 eq.”) or 150 µM (1.5 eq., “2 eq.”) of Cu(II) with 100 µM BSA to make preformed Cu(II)-BSA, (2) 50 µM (0.5 eq., “1 eq.”) or 150 µM (1.5 eq., “2 eq.”) of Cu(II) with 100 µM of C-peptide and BSA following (S1) and (S2) conditions, and (3) 0.5 mM of Cu(II) with 1 mM C-peptide. Continuous wave (CW) X-Band (9.39 GHz) spectra were collected using a Bruker EleXsys-II E500 (Billerica, MA) equipped with a super high Q resonator (ER4122SHQE). Spectra were recorded at 20 K with a modulation frequency of 100 kHz, and a modulation amplitude of 1 mT, with a 10 µW microwave power. Cryogenic temperatures were controlled and maintained through the use of an ESR900 liquid helium cryostat in conjunction with a temperature controller (Oxford Instruments ITC503) and a gas flow

controller. Echo-detected field sweep spectra at Q-band (34 GHz) were collected using a Bruker EleXsys E580 spectrometer equipped with a 10 W amplifier and an R. A. Isaacson-built cylindrical TE011 resonator mounted in an Oxford CF935 cryostat. The standard Hahn echo sequence ($\pi/2 - \tau - \pi -$ echo) was applied to each sample via the XEPR software at 25 K and with π = 24 ns and τ = 320 ns at various magnetic field values. The resulting field sweeps were pseudomodulated using a modulation amplitude of 3 mT. Echo-detected field sweep spectra at D-band (130 GHz) were collected using a home-built 130 GHz EPR spectrometer equipped with an Oxford-CF935 liquid helium cryostat as described previously.[5] Magnetic field-swept echo-detected EPR spectrum was acquired using the Hahn echo pulse sequence: $\pi/2 - \tau - \pi -$ echo, with a π = 45 ns and τ = 300 ns at various magnetic field values. The resulting field sweeps were pseudomodulated using a modulation amplitude of 20 mT. Simulations of the EPR spectra were generated using the Easyspin 6.0.0 toolbox[6] in the Matlab R2021b software suite (Mathworks Inc., Natick, MA).

Assay for measuring copper(I)-catalyzed $OH^{\bullet}$ radical formation. C-peptide and BSA were diluted in 10 mM phosphate buffer at pH 7.4. Samples for the time-dependent fluorescence readouts were added to a 96-well microplate (Greiner Bio-One) which include (1) 2 μM $CuCl_2$, (2) 2 μM of Cu(II)-C-peptide, and (3) 2 μM of Cu(II), C-peptide, and BSA following (S1) and (S2) conditions. Coumarin-3-carboxylic acid (3-CCA) was dissolved in 100 mM NaOH then back-titrated to a pH of 7.4, and L-ascorbic acid (Asc) was dissolved in Milli-Q water. A premixed solution of 100 μM Asc:500 μM 3-CCA was then added to each sample well, and time-dependent fluorescent intensity was monitored

at 450 nm with an excitation at 388 nm using a fluorescent platereader (Molecular Devices i3x) for 1.5 hours. Statistics were performed on Prism 9.1 (GraphPad).

Cell line maintenance. Human embryonic kidney (HEK-293) cells were grown in complete DMEM media + 4.5 g/L glucose (ThermoFisher Scientific) with the addition of 10% Avantor Seradigm Premium Grade Fetal Bovine Serum (VWR), 1 mM sodium pyruvate (ThermoFisher Scientific), 100 IU penicillin and 100 µg/mL streptomycin (ThermoFisher Scientific), and 2 mM L-glutamine (Gibco). Cells were subcultured every 2 to 3 days at 70 to 80% confluence. All experiments were performed on HEK-293 cells between passage 5 and 35. Cells were maintained in a sterile environment and grown in 5% CO2 at 37°C in a Heracell 150l incubator (ThermoFisher Scientific).

Immunofluorescence. The immunofluorescence protocol was adapted from Stevenson et al.[4] HEK-293 cells were plated into 12-well plates with acid-washed coverslips at 200,000 cells/well and grown to 50-70% confluence, then starved in serum-free DMEM media with the same culturing formulation overnight. Cells were washed with DPBS and treated with the following treatments for 30 minutes: (1) $CuCl_2$ diluted in serum-free media to final concentration of 11 µM Cu(II), (2) 10 µM C-peptide diluted with serum-free media, (3) preformed Cu(II)-C-peptide diluted in serum-free media to final concentrations of 10 µM C-peptide and 11 µM Cu(II), (4) 100 µM BSA diluted in serum-free media, (5) preformed Cu(II)-BSA diluted with serum-free media to make 100 µM BSA and 11 µM Cu(II), (6) 15 minute incubation of preformed C-peptide-BSA followed by dilution with serum-free media to make 10 µM C-peptide and 100 µM BSA, and (7) 10 µM C-peptide, 11 µM Cu(II), and 100 uM BSA following S1 or S2 conditions. Cells were then fixed with 4% paraformaldehyde at RT for 10 minutes, then washed twice with cold DPBS. Cells

were permeabilized with 0.3% Triton X-100 (Fisher) in DPBS at RT for 10 minutes, then washed thrice with cold DPBS. HEK-293 cells were blocked for 1 hour using blocking solution that contains 3% BSA (Fisher),10 mM HEPES (Gibco), and 0.3% Triton X-100 in DPBS. Cells were incubated overnight with primary anti-human C-peptide antibody (4593, Cell Signaling Technology) at 1:400 dilution in blocking buffer at 4°C. Cells were rinsed thrice with DPBS at 5 minutes each, incubated with Alexa Fluor 488 goat anti-rabbit ReadyProbes secondary antibody (Invitrogen) for 30 minutes, then washed twice with DBPS. Cells were stained with NucBlue Live ReadyProbes (Hoescht 33342, R37605, Invitrogen), washed twice with DPBS, then mounted with ProLong Gold Antifade Mountant (Invitrogen). Cells were imaged on an EVOS FL microscope with 40x magnification using DAPI and GFP Fluorescent light cubes (Invitrogen). ImageJ was used for image processing such as contrasting the DAPI and GFP channels, overlaying images, and zooming images by 200%. ImageJ was also used to determine the mean pixel intensity of treated cells. Statistics were performed on Prism 9.1 (GraphPad).

Antibody recognition of C-peptide. C-peptide, BSA, and $CuCl_2$ were diluted in DPBS to prepare 200 pg/mL stock solutions. Samples were incubated to final concentration of 50 pg/mL including (1) apo-C-peptide, (2) Cu(II)/C-peptide (1 eq.), (3) C-peptide and BSA (1 eq.), Cu(II) with C-peptide and BSA following (4) (S1) and (5) (S2) conditions (1 eq.). Samples were assessed for antibody recognition of C-peptide by ELISA (ab260064, Abcam). All experiments were performed in three independent biological replicates, and statistics were done on Prism 9.1 (GraphPad).

3.5 References

(1) Fricker, L. D.; Devi, L. A. Orphan Neuropeptides and Receptors: Novel Therapeutic Targets. *Pharmacol. Ther.* **2018**, *185*, 26. https://doi.org/10.1016/j.pharmthera.2017.11.006.

(2) Fosgerau, K.; Hoffmann, T. Peptide Therapeutics: Current Status and Future Directions. *Drug Discov. Today* **2015**, *20* (1), 122–128. https://doi.org/10.1016/j.drudis.2014.10.003.

(3) Saltiel, A. R.; Kahn, C. R. Insulin Signalling and the Regulation of Glucose and Lipid Metabolism. *Nat. 2001 4146865* **2001**, *414* (6865), 799–806. https://doi.org/10.1038/414799a.

(4) Manning, M.; Stoev, S.; Chini, B.; Durroux, T.; Mouillac, B.; Guillon, G. Peptide and Non-Peptide Agonists and Antagonists for the Vasopressin and Oxytocin V1a, V1b, V2 and OT Receptors: Research Tools and Potential Therapeutic Agents. *Prog. Brain Res.* **2008**, *170*, 473–512. https://doi.org/10.1016/S0079-6123(08)00437-8.

(5) Mirabeau, O.; Perlas, E.; Severini, C.; Audero, E.; Gascuel, O.; Possenti, R.; Birney, E.; Rosenthal, N.; Gross, C. Identification of Novel Peptide Hormones in the Human Proteome by Hidden Markov Model Screening. *Genome Res.* **2007**, *17* (3), 320. https://doi.org/10.1101/gr.5755407.

(6) Wahren, J.; Ekberg, K.; Jörnvall, H. C-Peptide Is a Bioactive Peptide. *Diabetologia*. Springer March 18, **2007**, pp 503–509. https://doi.org/10.1007/s00125-006-0559-y.

(7) Marques, R. G.; Fontaine, M. J.; Rogers, J. C-Peptide: Much More than a Byproduct of Insulin Biosynthesis. *Pancreas* **2004**, *29* (3), 231–238. https://doi.org/10.1097/00006676-200410000-00009.

(8) Pinger, C. W.; Entwistle, K. E.; Bell, T. M.; Liu, Y.; Spence, D. M. C-Peptide Replacement Therapy in Type 1 Diabetes: Are We in the Trough of Disillusionment? *Molecular BioSystems*. Royal Society of Chemistry **2017**, pp 1432–1437. https://doi.org/10.1039/c7mb00199a.

(9) Washburn, R. L.; Mueller, K.; Kaur, G.; Moreno, T.; Moustaid-moussa, N.; Ramalingam, L.; Dufour, J. M. C-peptide as a Therapy for Type 1 Diabetes Mellitus. *Biomedicines*. MDPI AG **2021**, pp 1–24. https://doi.org/10.3390/biomedicines9030270.

(10) Lindfors, L.; Sundström, L.; Fröderberg Roth, L.; Meuller, J.; Andersson, S.; Kihlberg, J. Is GPR146 Really the Receptor for Proinsulin C-Peptide? *Bioorganic Med. Chem. Lett.* **2020**, *30* (13), 127208. https://doi.org/10.1016/j.bmcl.2020.127208.

(11) Yosten, G. L. C.; Kolar, G. R.; Redlinger, L. J.; Samson, W. K. Evidence for an Interaction between Proinsulin C-Peptide and GPR146. *J. Endocrinol.* **2013**, *218*

(2). https://doi.org/10.1530/JOE-13-0203.
(12) Rossiter, J. L.; Redlinger, L. J.; Kolar, G. R.; Samson, W. K.; Yosten, G. L. C. The Actions of C-Peptide in HEK293 Cells Are Dependent upon Insulin and Extracellular Glucose Concentrations. *Peptides* **2022**, *150*. https://doi.org/10.1016/j.peptides.2021.170718.
(13) Liu, Y.; Chen, C.; Summers, S.; Medawala, W.; Spence, D. M. C-Peptide and Zinc Delivery to Erythrocytes Requires the Presence of Albumin: Implications in Diabetes Explored with a 3D-Printed Fluidic Device. *Integr. Biol. (United Kingdom)* **2015**, *7* (5), 534–543. https://doi.org/10.1039/c4ib00243a.
(14) Geiger, M.; Janes, T.; Keshavarz, H.; Summers, S.; Pinger, C.; Fletcher, D.; Zinn, K.; Tennakoon, M.; Karunarathne, A.; Spence, D. A C-Peptide Complex with Albumin and Zn2+ Increases Measurable GLUT1 Levels in Membranes of Human Red Blood Cells. *Sci. Rep.* **2020**, *10* (1), 1–9. https://doi.org/10.1038/s41598-020-74527-6.
(15) Stevenson, M. J.; Janisse, S. E.; Tao, L.; Neil, R. L.; Pham, Q. D.; Britt, R. D.; Heffern, M. C. Elucidation of a Copper Binding Site in Proinsulin C-Peptide and Its Implications for Metal-Modulated Activity. *Inorg. Chem.* **2020**, *59* (13), 9339–9349. https://doi.org/10.1021/acs.inorgchem.0c01212.
(16) Stevenson, M. J.; Farran, I. C.; Uyeda, K. S.; San Juan, J. A.; Heffern, M. C. Analysis of Metal Effects on C-Peptide Structure and Internalization. *ChemBioChem* **2019**, *20* (19), 2447–2453. https://doi.org/10.1002/cbic.201900172.
(17) Kleine, B.; Rossmanith, W. G. Hormones and the Endocrine System. *Horm. Endocr. Syst.* **2016**. https://doi.org/10.1007/978-3-319-15060-4.
(18) Zolla, L. Proteomics Studies Reveal Important Information on Small Molecule Therapeutics: A Case Study on Plasma Proteins. *Drug Discov. Today* **2008**, *13* (23), 1042. https://doi.org/10.1016/j.drudis.2008.09.013.
(19) Bal, W.; Sokołowska, M.; Kurowska, E.; Faller, P. Binding of Transition Metal Ions to Albumin: Sites, Affinities and Rates. *Biochimica et Biophysica Acta - General Subjects*. 2013, pp 5444–5455. https://doi.org/10.1016/j.bbagen.2013.06.018.
(20) Stefaniak, E.; Płonka, D.; Drew, S. C.; Bossak-Ahmad, K.; Haas, K. L.; Pushie, M. J.; Faller, P.; Wezynfeld, N. E.; Bal, W. The N-Terminal 14-Mer Model Peptide of Human Ctr1 Can Collect Cu(Ii) from Albumin. Implications for Copper Uptake by Ctr1. *Metallomics* **2018**, *10* (12), 1723–1727. https://doi.org/10.1039/c8mt00274f.
(21) Krause-Heuer, A. M.; Price, W. S.; Aldrich-Wright, J. R. Spectroscopic Investigations on the Interactions of Potent Platinum(II) Anticancer Agents with Bovine Serum Albumin. *J. Chem. Biol.* **2012**, *5* (3), 105. https://doi.org/10.1007/S12154-012-0074-1.
(22) Shahabadi, N.; Hadidi, S. Mechanistic and Conformational Studies on the Interaction of a Platinum(II) Complex Containing an Antiepileptic Drug,

Levetiracetam, with Bovine Serum Albumin by Optical Spectroscopic Techniques in Aqueous Solution. *Appl. Biochem. Biotechnol.* **2015**, *175* (4), 1843–1857. https://doi.org/10.1007/S12010-014-1423-Z.

(23) Choi, T. S.; Lee, H. J.; Han, J. Y.; Lim, M. H.; Kim, H. I. Molecular Insights into Human Serum Albumin as a Receptor of Amyloid-β in the Extracellular Region. *J. Am. Chem. Soc.* **2017**, *139* (43), 15437–15445. https://doi.org/10.1021/jacs.7b08584.

(24) Rózga, M.; Bal, W. The Cu(II)/Abeta/Human Serum Albumin Model of Control Mechanism for Copper-Related Amyloid Neurotoxicity. *Chem. Res. Toxicol.* **2010**, *23* (2), 298–308. https://doi.org/10.1021/TX900358J.

(25) Perrone, L.; Mothes, E.; Vignes, M.; Mockel, A.; Figueroa, C.; Miquel, M. C.; Maddelein, M. L.; Faller, P. Copper Transfer from Cu-Abeta to Human Serum Albumin Inhibits Aggregation, Radical Production and Reduces Abeta Toxicity. *Chembiochem* **2010**, *11* (1), 110–118. https://doi.org/10.1002/CBIC.200900474.

(26) Lu, N.; Yang, Q.; Li, J.; Tian, R.; Peng, Y. Y. Inhibitory Effect of Human Serum Albumin on Cu-Induced Aβ(40) Aggregation and Toxicity. *Eur. J. Pharmacol.* **2015**, *767*, 160–164. https://doi.org/10.1016/J.EJPHAR.2015.10.020.

(27) Han, J.; Yoon, J.; Shin, J.; Nam, E.; Qian, T.; Li, Y.; Park, K.; Lee, S. H.; Lim, M. H. Conformational and Functional Changes of the Native Neuropeptide Somatostatin Occur in the Presence of Copper and Amyloid-β. *Nat. Chem.* **2022**, *14* (9). https://doi.org/10.1038/S41557-022-00984-3.

(28) Bossak-Ahmad, K.; Bal, W.; Frączyk, T.; Drew, S. C. Ternary Cu2+Complexes of Human Serum Albumin and Glycyl- l -Histidyl- l -Lysine. *Inorg. Chem.* **2021**, *60* (22), 16927–16931. https://doi.org/10.1021/acs.inorgchem.1c03084.

(29) Meyer, J. A.; Froelich, J. M.; Reid, G. E.; Karunarathne, W. K. A.; Spence, D. M. Metal-Activated C-Peptide Facilitates Glucose Clearance and the Release of a Nitric Oxide Stimulus via the GLUT1 Transporter. *Diabetologia* **2008**, *51* (1), 175–182. https://doi.org/10.1007/s00125-007-0853-3.

(30) Meyer, J. A.; Subasinghe, W.; Sima, A. A. F.; Keltner, Z.; Reid, G. E.; Daleke, D.; Spence, D. M. Zinc-Activated C-Peptide Resistance to the Type 2 Diabetic Erythrocyte Is Associated with Hyperglycemia-Induced Phosphatidylserine Externalization and Reversed by Metformin. *Mol. Biosyst.* **2009**, *5* (10), 1157–1162. https://doi.org/10.1039/B908241G.

(31) Jones, A. G.; Hattersley, A. T. The Clinical Utility of C-Peptide Measurement in the Care of Patients with Diabetes. *Diabet. Med.* **2013**, *30* (7), 803–817. https://doi.org/10.1111/dme.12159.

(32) Leighton, E.; Sainsbury, C. A.; Jones, G. C. A Practical Review of C-Peptide Testing in Diabetes. *Diabetes Ther.* **2017**, *8* (3), 475–487. https://doi.org/10.1007/s13300-017-0265-4.

(33) Faber, O. K.; Hagen, C.; Binder, C.; Markussen, J.; Naithani, V. K.; Blix, P. M.;

Kuzuya, H.; Horwitz, D. L.; Rubenstein, A. H.; Rossing, N. Kinetics of Human Connecting Peptide in Normal and Diabetic Subjects. *J. Clin. Invest.* **1978**, *62* (1), 197–203. https://doi.org/10.1172/JCI109106.

(34) Lakowicz, J. R. *Principles of Fluorescence Spectroscopy, 3rd Edition, Joseph R. Lakowicz, Editor*; 2006. https://doi.org/10.1007/978-0-387-46312-4.

(35) Berney, C.; Danuser, G. FRET or No FRET: A Quantitative Comparison. *Biophys. J.* **2003**, *84* (6), 3992. https://doi.org/10.1016/S0006-3495(03)75126-1.

(36) Foley, T. L.; Burkart, M. D. A Homogeneous Resonance Energy Transfer Assay for Phosphopantetheinyl Transferase. *Anal. Biochem.* **2009**, *394* (1), 39–47. https://doi.org/10.1016/j.ab.2009.06.037.

(37) Liu, Y.; Chen, M.; Song, L. Comparing the Effects of Fe(III) and Cu(II) on the Binding Affinity of Erlotinib to Bovine Serum Albumin Using Spectroscopic Methods. *J. Lumin.* **2013**, *134*, 515–523. https://doi.org/10.1016/j.jlumin.2012.07.036.

(38) Zhang, Y.; Wilcox, D. E. Thermodynamic and Spectroscopic Study of Cu(II) and Ni(II) Binding to Bovine Serum Albumin. *J. Biol. Inorg. Chem.* **2002**, *7* (3), 327–337. https://doi.org/10.1007/s00775-001-0302-6.

(39) Masuoka, J.; Saltman, P. Zinc(II) and Copper(II) Binding to Serum Albumin: A Comparative Study of Dog, Bovine, and Human Albumin. *J. Biol. Chem.* **1994**, *269* (41), 25557–25561. https://doi.org/10.1016/S0021-9258(18)47285-7.

(40) Greenfield, N. J. Using Circular Dichroism Collected as a Function of Temperature to Determine the Thermodynamics of Protein Unfolding and Binding Interactions. *Nat. Protoc. 2006 16* **2006**, *1* (6), 2527–2535. https://doi.org/10.1038/nprot.2006.204.

(41) Kelly, S. M.; Jess, T. J.; Price, N. C. How to Study Proteins by Circular Dichroism. *Biochim. Biophys. Acta - Proteins Proteomics* **2005**, *1751* (2), 119–139. https://doi.org/10.1016/j.bbapap.2005.06.005.

(42) Buddanavar, A. T.; Nandibewoor, S. T. Multi-Spectroscopic Characterization of Bovine Serum Albumin upon Interaction with Atomoxetine. *J. Pharm. Anal.* **2017**, *7* (3), 148–155. https://doi.org/10.1016/j.jpha.2016.10.001.

(43) Varlan, A.; Hillebrand, M. Bovine and Human Serum Albumin Interactions with 3-Carboxyphenoxathiin Studied by Fluorescence and Circular Dichroism Spectroscopy. *Mol. 2010, Vol. 15, Pages 3905-3919* **2010**, *15* (6), 3905–3919. https://doi.org/10.3390/molecules15063905.

(44) Shahabadi, N.; Hadidi, S.; Kalar, Z. M. Biophysical Studies on the Interaction of Platinum(II) Complex Containing Antiviral Drug Ribavirin with Human Serum Albumin. *J. Photochem. Photobiol. B Biol.* **2016**, *160*, 376–382. https://doi.org/10.1016/j.jphotobiol.2016.05.006.

(45) Jing, M.; Liu, R.; Yan, W.; Tan, X.; Chen, Y. Investigations on the Effects of Cu2+ on the Structure and Function of Human Serum Albumin. *Luminescence* **2016**, *31*

(2), 557–564. https://doi.org/10.1002/BIO.2995.
(46) Peters, T.; Blumenstock, F. A. Copper-Binding Properties of Bovine Serum Albumin and Its Amino-Terminal Peptide Fragment. *J. Biol. Chem.* **1967**, *242* (7), 1574–1578. https://doi.org/10.1016/S0021-9258(18)96130-2.
(47) Kozlowski, H.; Bal, W.; Dyba, M.; Kowalik-Jankowska, T. Specific Structure-Stability Relations in Metallopeptides. *Coord. Chem. Rev.* **1999**, *184*, 319–346. https://doi.org/10.1016/S0010-8545(98)00261-6.
(48) Handing, K. B.; Shabalin, I. G.; Kassaar, O.; Khazaipoul, S.; Blindauer, C. A.; Stewart, A. J.; Chruszcz, M.; Minor, W. Circulatory Zinc Transport Is Controlled by Distinct Interdomain Sites on Mammalian Albumins. *Chem. Sci.* **2016**, *7* (11), 6635–6648. https://doi.org/10.1039/c6sc02267g.
(49) Pandeya, K.; Patel, R. X-Band Electron Paramagnetic Resonance Spectra of Bovine Serum Albumin-Copper (II) and Bovine Serum Albumin-Copper (II)-Aminoacid Systems. *Indian J. Biochem. Biophys.* **1992**, *29* (3), 245–250.
(50) Peisach, J.; Blumberg, W. E. Structural Implications Derived from the Analysis of Electron Paramagnetic Resonance Spectra of Natural and Artificial Copper Proteins. *Arch. Biochem. Biophys.* **1974**, *165* (2), 691–708. https://doi.org/10.1016/0003-9861(74)90298-7.
(51) Sciortino, G.; Maréchal, J. D.; Fábián, I.; Lihi, N.; Garribba, E. Quantitative Prediction of Electronic Absorption Spectra of Copper(II)–Bioligand Systems: Validation and Applications. *J. Inorg. Biochem.* **2020**, *204*, 110953. https://doi.org/10.1016/j.jinorgbio.2019.110953.
(52) Warren, J. J.; Lancaster, K. M.; Richards, J. H.; Gray, H. B. Inner- and Outer-Sphere Metal Coordination in Blue Copper Proteins. *J. Inorg. Biochem.* **2012**, *115*, 119–126. https://doi.org/10.1016/J.JINORGBIO.2012.05.002.
(53) Ruckthong, L.; Stuckey, J. A.; Pecoraro, V. L. How Outer Coordination Sphere Modifications Can Impact Metal Structures in Proteins: A Crystallographic Evaluation. *Chem. – A Eur. J.* **2019**, *25* (27), 6773–6787. https://doi.org/10.1002/CHEM.201806040.
(54) Sciortino, G.; Lubinu, G.; Maréchal, J. D.; Garribba, E. DFT Protocol for EPR Prediction of Paramagnetic Cu(II) Complexes and Application to Protein Binding Sites. *Magnetochemistry* **2018**, *4* (4), 55. https://doi.org/10.3390/MAGNETOCHEMISTRY4040055.
(55) Hu, X.; Zhang, Q.; Wang, W.; Yuan, Z.; Zhu, X.; Chen, B.; Chen, X. Tripeptide GGH as the Inhibitor of Copper-Amyloid-β-Mediated Redox Reaction and Toxicity. *ACS Chem. Neurosci.* **2016**, *7* (9), 1255–1263. https://doi.org/10.1021/acschemneuro.6b00145.
(56) Meloni, G.; Faller, P.; Vašák, M. Redox Silencing of Copper in Metal-Linked Neurodegenerative Disorders: Reaction of Zn7metallothionein-3 with Cu2+ Ions. *J. Biol. Chem.* **2007**, *282* (22), 16068–16078.

https://doi.org/10.1074/jbc.M701357200.
(57) Lindahl, E.; Nyman, U.; Melles, E.; Sigmundsson, K.; Ståhlberg, M.; Wahren, J.; Öbrink, B.; Shafqat, J.; Joseph, B.; Jörnvall, H. Cellular Internalization of Proinsulin C-Peptide. *Cell. Mol. Life Sci.* **2007**, *64* (4), 479–486. https://doi.org/10.1007/s00018-007-6467-6.
(58) Unnerståle, S.; Mäler, L. PH-Dependent Interaction between C-Peptide and Phospholipid Bicelles. *J. Biophys.* **2012**, *2012*. https://doi.org/10.1155/2012/185907.
(59) Luppi, P.; Geng, X.; Cifarelli, V.; Drain, P.; Trucco, M. C-Peptide Is Internalised in Human Endothelial and Vascular Smooth Muscle Cells via Early Endosomes. *Diabetologia* **2009**, *52* (10), 2218–2228. https://doi.org/10.1007/S00125-009-1476-7.
(60) Frei, E. Albumin Binding Ligands and Albumin Conjugate Uptake by Cancer Cells. *Diabetol. Metab. Syndr.* **2011**, *3* (1), 11. https://doi.org/10.1186/1758-5996-3-11.
(61) Bjørklund, G.; Dadar, M.; Pivina, L.; Doşa, M. D.; Semenova, Y.; Aaseth, J. The Role of Zinc and Copper in Insulin Resistance and Diabetes Mellitus. *Curr. Med. Chem.* **2019**, *27* (39), 6643–6657. https://doi.org/10.2174/0929867326666190902122155.
(62) Lowe, J.; Taveira-da-Silva, R.; Hilário-Souza, E. Dissecting Copper Homeostasis in Diabetes Mellitus. *IUBMB Life* **2017**, *69* (4), 255–262. https://doi.org/10.1002/IUB.1614.
(63) Tanaka, A.; Kaneto, H.; Miyatsuka, T.; Yamamoto, K.; Yoshiuchi, K.; Yamasaki, Y.; Shimomura, I.; Matsuoka, T. A.; Matsuhisa, M. Role of Copper Ion in the Pathogenesis of Type 2 Diabetes. *Endocr. J.* **2009**, *56* (5), 699–706. https://doi.org/10.1507/endocrj.k09E-051.
(64) Kim, S.; Kang, S. Serum Albumin Levels: A Simple Answer to a Complex Problem? Are We on the Right Track of Assessing Metabolic Syndrome? *Endocrinol. Metab.* **2013**, *28* (1), 17. https://doi.org/10.3803/ENM.2013.28.1.17.
(65) Jun, J. E.; Lee, S. E.; Lee, Y. Bin; Jee, J. H.; Bae, J. C.; Jin, S. M.; Hur, K. Y.; Lee, M. K.; Kim, J. H. Increase in Serum Albumin Concentration Is Associated with Prediabetes Development and Progression to Overt Diabetes Independently of Metabolic Syndrome. *PLoS One* **2017**, *12* (4), e0176209. https://doi.org/10.1371/journal.pone.0176209.
(66) Gu, S.; Wang, A.; Ning, G.; Zhang, L.; Mu, Y. Insulin Resistance Is Associated with Urinary Albumin-Creatinine Ratio in Normal Weight Individuals with Hypertension and Diabetes: The REACTION Study. *J. Diabetes* **2020**, *12* (5), 406–416. https://doi.org/10.1111/1753-0407.13010.

CHAPTER 4

Glycation of serum albumin alters binding with C-peptide and copper

4.1 Introduction

Type 1 diabetes (T1D) is an autoimmune disease defined as the destruction of pancreatic beta-cells that lead to a decrease in hormone secretion such as insulin. These patients undergo insulin treatments to regulate glucose levels. However, the long-term complications with the kidneys (nephropathy), nerves (neuropathy), and eyes (retinopathy) are insulin-independent, suggesting a need for additional therapeutic strategies for T1D patients.[1–3]

C-peptide is a 31-mer peptide that is cleaved from the prohormone of insulin, and has demonstrated a range of beneficial effects such as blood flow regulation, glucose uptake, and cell growth.[4] While the peptide is a potential candidate for the treatment of T1D-associated long-term complications, its molecular mechanisms remain elusive. The hinderance in therapeutic advancements may be due to overlooked secondary factors associated with C-peptide. Our group has demonstrated that C-peptide binds to several metal ions such as Cr(III), Cu(II), and Zn(II).[5,6] Furthermore, we have shown that C-peptide forms a ternary complexation with Cu(II) and serum albumin, which impacts the biochemical behavior of the peptide as well as C-peptide clinical immunoassays (Chapter 3).

Serum albumin is an abundant protein carrier that can transport metabolites, metals, fatty acids, and drugs; therefore, the protein plays a crucial role in regulating the bioavailability of these species in the body.[9–12] However, albumin contains a high number of lysine and arginine residues, making the protein prone to glycation, a non-enzymatic mechanism of glucose binding to proteins.[13–15] Termed as the Maillard reaction, glucose

or fructose will spontaneous react with these amine-containing amino acid residues on albumin.[16–18] After 21 days, the end products become irreversibly formed leading to advances glycation end (AGE) products. Figure 4.1 is adapted from Anguizola et. al. and displays both the Maillard reaction as well as AGE formation.[17]

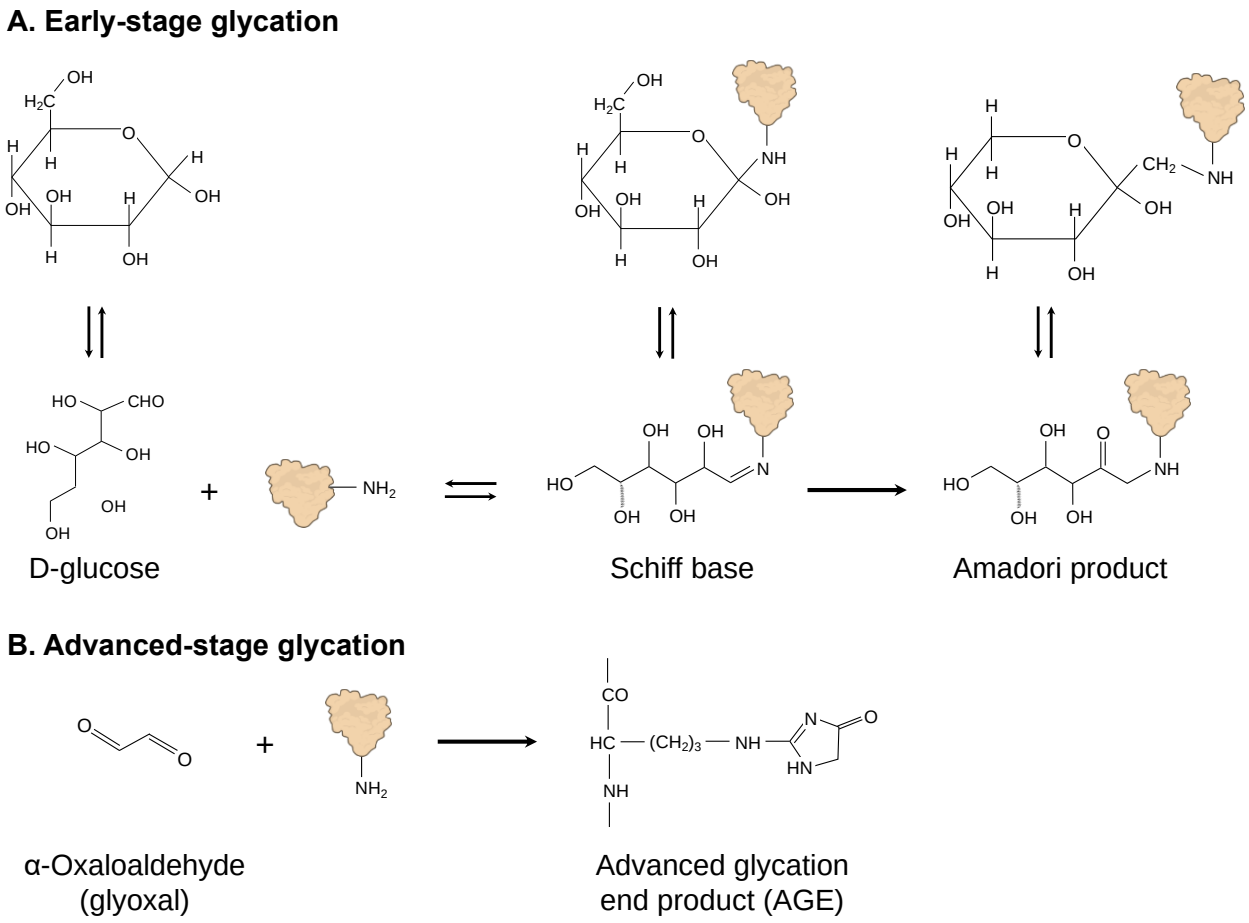

Figure 4.1. Stages of glycation. (A) Early-stage glycation is initiated via the Malliard reaction involving the conjugation of a reducing sugar such as D-glucose to a free amine group such as Lys and Arg on albumin to form a reversible Schiff base, followed by an Amadori product. This stage occurs over a span of hours to weeks. Open- and closed-

chain forms of glucose are interchangeable. (B) Advanced-stage glycation follows to generate advanced glycation end products (AGEs). This stage happens over a course of a few weeks to months, leading to browning (fluorescence), cross-linking, and aggregation.

Because T1D patients have persistent hyperglycemic conditions, AGE formation is accelerated, leading to a shift in structure and function of albumin. This holds clinical implication in two-fold: (1) albumin glycation as a biomarker for diabetes,[19,20] and (2) alteration of drug or peptide binding to albumin at various stages of the autoimmune disease. For example, recent studies focused on how albumin glycation may impair peptide binding with liraglutide and C-peptide.[21,22]

As we have previously characterized the formation of ternary complexes (S1 and S2; see Chapter 3) between C-peptide, Cu(II), and bovine serum albumin (BSA) in Chapter 3, it is also important to investigate how these interactions may change in the presence of glycated bovine serum albumin. Here, our work shows that glycated BSA shifts both the biochemical activities and structure-function of C-peptide. The biochemical activities characterized for S1 and S2 displayed opposing shifts with the addition of glycated BSA. The inflated measurements of S1 and S2 observed in C-peptide clinical immunoassays are reduced, and the enhanced effects of peptide internalization following S2 are reversed. When investigating the mechanistic drive of these complexes with glycated albumin, UV-Visible electronic absorption displayed broadening spectral characteristics of S1 and S2, with S2 showing a shift in the Cu(II)-coordination environment. The spectra pointed to aggregation formation, to which the turbidity assays and circular dichroism confirmed. Altogether, this work highlights how the structural

changes of albumin post-glycation impacts C-peptide activity. This information will help improve our molecular understanding about C-peptide and how it may behave in hyperglycemic conditions associated with T1D.

4.2 Results and Discussion

4.2.1 Glycated albumin perturbs the biochemical activities of C-peptide with Cu(II) and albumin

To determine whether glycated BSA impacts C-peptide activity following the copper-bridged C-peptide/BSA complexes, we generated glycated BSA to add into solutions following S1 and S2.[23,24] Prior to experimental use, we incubated 10 mg/mL BSA in high glucose conditions (500 mM glucose) for 21 days then filtered the solutions to remove any excess glucose. To make direct comparisons between normal and glycated conditions, we compared BSA incubated with high glucose (500 mM) for 0 days (no glycation expected), termed as “nBSA” to BSA exposed to high glucose for 21 days (glycation expected), termed “gBSA”.

We reported in Chapter 3 that both S1 and S2 ternary species registers increased C-peptide levels by enzyme-linked immunosorbent assay (ELISA) in comparison to C-peptide in the absence of BSA. As these clinical kits are used for the diagnosis of diabetes using C-peptide as a secondary biomarker for insulin, it is important to understand whether parameters such as glycemic status may impact C-peptide measurements following S1- and S2-based complexation. To probe these differences, we compared the detection of C-peptide with Cu(II) following nBSA and gBSA conditions. The presence of

high glucose with or without Cu(II) does not impact C-peptide measurements. In Chapter 3, we observed that S1 and S2 inflates C-peptide measurements; addition of nBSA (S1 BSA and S2 nBSA) parallels these changes, showing that the presence of glucose does not alter this inflation. Interestingly, when the samples are prepared via S1 and S2 but with gBSA instead (S1 gBSA and S2 gBSA), detected C-peptide levels decreases by a 2.2- and 2.1-fold compared to S1 nBSA and S2 gBSA, respectively (Figure 4.2). Together, these measurements show that quantification of these biomarkers may vary by glycemic status.

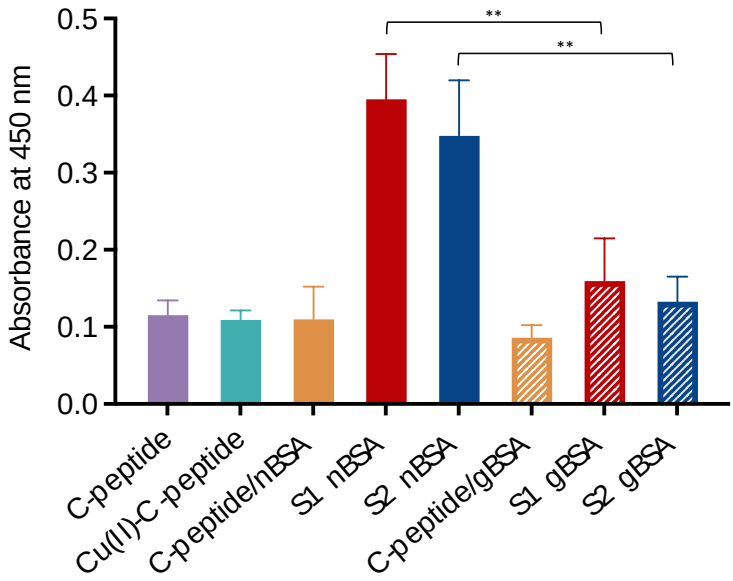

Figure 4.2. C-peptide ELISA (abs. at 450 nm) measurements by antibody recognition in samples with 50 pg/mL apo-C-peptide, Cu(II), nBSA, and gBSA. ELISA detection was normalized to apo-C-peptide. The presence of high glucose did not shift C-peptide detection alone (purple), with Cu(II) (teal), or with the addition of apo-nBSA (orange) or

apo-gBSA (orange, striped). When C-peptide is copper-bridged with gBSA by S1 (red, striped) or S2 (blue, striped), registered C-peptide levels decrease compared to nBSA. Significance is analyzed by unpaired t test; ** $p < 0.01$. Data is displayed as mean ± SD with n = 3.

Next, we accessed whether the presence of glycated albumin may impact C-peptide internalization in HEK-293 (human embryonic kidney) at 30 minutes by endocytosis. We previously characterized that Cu(II)-C-peptide inhibits C-peptide internalization (Stevenson 2019), and with the addition of the S2 complex with BSA in the absence of glucose, peptide internalization was significantly enhanced (Chapter 3). To determine the effects of albumin glycation on affecting C-peptide internalization, HEK-293 cells were stimulated for 30 minutes then fixed, permeabilized, and incubated with primary C-peptide antibodies. Secondary antibodies conjugated to Alexa Fluor 488 fluorophore were added to the fixed cells, then the mean pixel intensities (MPI) of each stimulation condition were determined to detect any shifts in peptide internalization (Figure 4.3). Sample conditions containing apo-C-peptide and the S1-type complexes minimally shifted between addition of nBSA and gBSA. However, while an enhancement was observed with S2 nBSA, this was reverted to be comparable to BSA-absent samples for S2 gBSA. This shift suggests that an alteration in albumin structure from glycation may lead to a shift in C-peptide internalization.

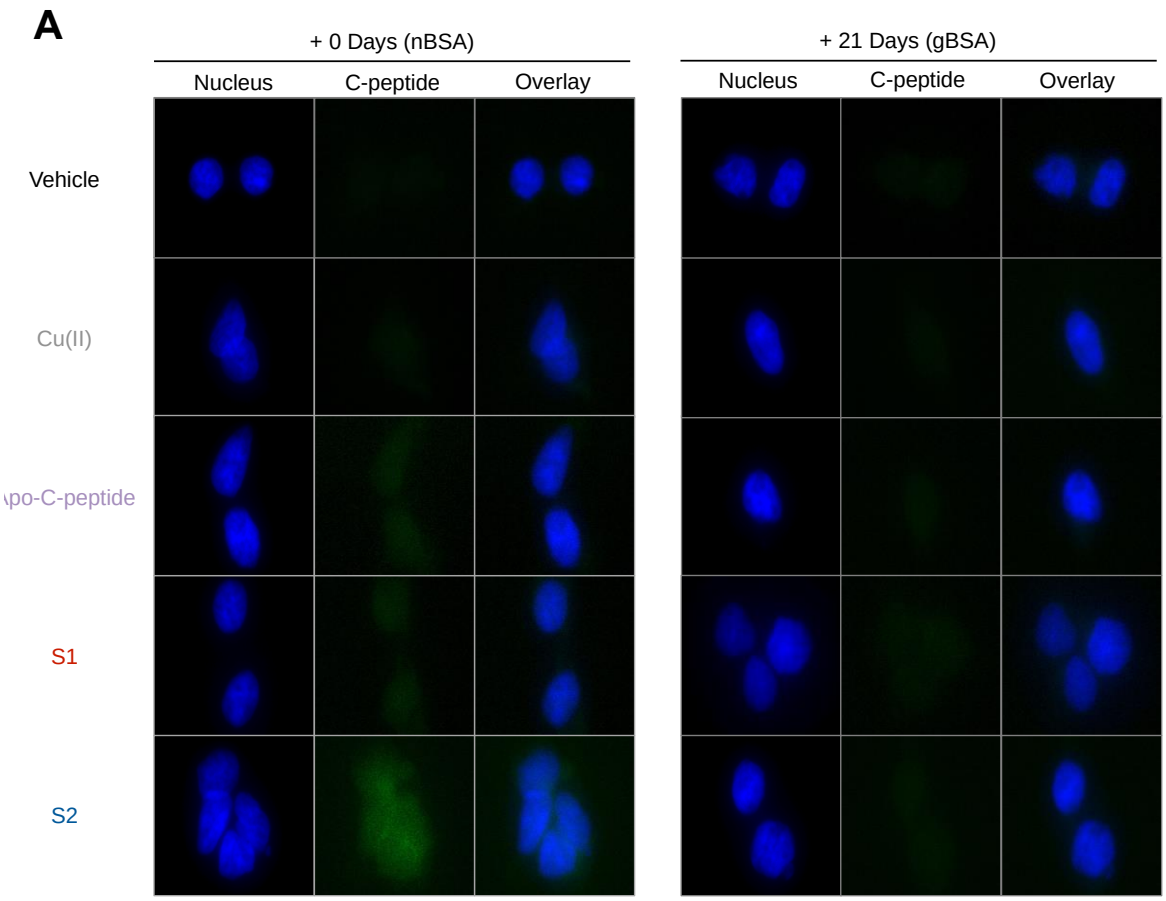
A
+ 0 Days (nBSA)
+ 21 Days (gBSA)
Nucleus
C-peptide
Overlay
Nucleus
C-peptide
Overlay
Vehicle
Cu(II)
Apo-C-peptide
S1
S2

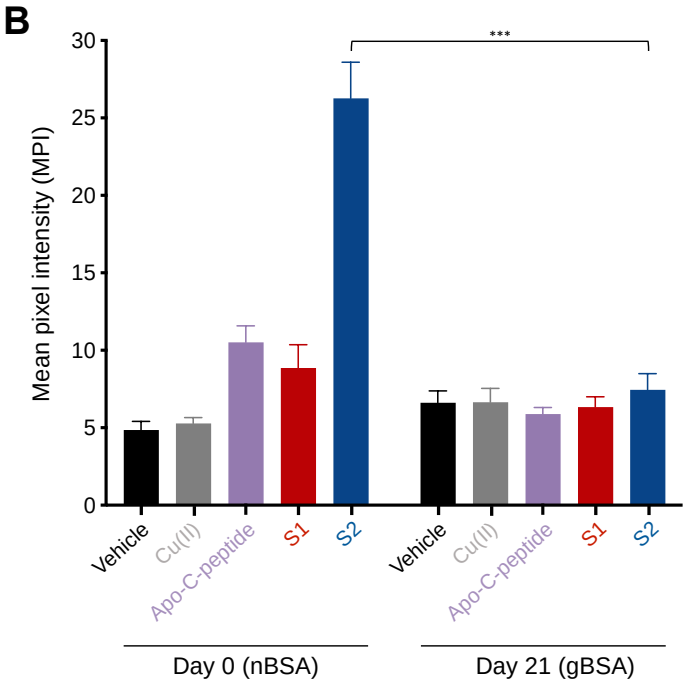
B
Mean pixel intensity (MPI)
30
25
20
15
10
5
0
***
Vehicle
Cu(II)
Apo-C-peptide
S1
S2
Vehicle
Cu(II)
Apo-C-peptide
S1
S2
Day 0 (nBSA)
Day 21 (gBSA)

Figure 4.3. Monitoring C-peptide uptake into serum-free HEK-293 cells using immunofluorescence. (A) Stimulation conditions include 10 μM C-peptide and 11 μM $CuCl_2$ with the addition of either Day 0 gBSA (100 μM BSA + 250 mM glucose) or Day 21 gBSA (100 μM gBSA incubated with 250 mM glucose for 21 days at 37°C). C-peptide primary antibodies were added to fixed cells followed by secondary antibodies conjugated to Alexa Fluor 488. (B) Mean pixel intensities were quantified within cell regions of interest using ImageJ and mean ± SD with n = 3. Significance is determined by unpaired t test; *** $p < 0.005$. Uptake of S2 gBSA decreases in comparison to the control with nBSA.

4.2.2 Shifts in spectroscopic signatures of C-peptide ternary complexes with glycated albumin may be driven by aggregate formation

In Chapter 3, we confirmed by EPR and TDDFT that the ternary complexations may be occurring at the MBSA of BSA. In addition, electronic absorption spectroscopy established that S1 and S2 are in fact, distinct ternary complexes— S1 is a red-shifted complex and S2 is a blue-shifted complex relative to the spectrum of 2:1 Cu(II)-BSA. We used the same experimental conditions as used in Chapter 3 for electronic absorption spectroscopy, as well as the same data processing by subtraction of apo-gBSA + apo-C-peptide spectrum (Figure 4.4A) from the S1 and S2 spectra, to determine whether gBSA species impact these spectral characteristics. The S1 complex at two equivalents Cu(II) in the presence of nBSA interestingly displayed shifts at both Cu(II)-binding sites. The NTS peak red-shifted from 556 nm to 545 nm and the MBSA peak blue-shifted from 678 nm to 686 nm (Figure 4.4B, Table 4.1). In contrast, S2 following nBSA addition only blue-

shifted the NTS peak from 530 nm to 540 nm (Figure 4.4C, Table 4.1). The shifts detected with the addition of the nBSA species following S1 and S2 may point to reversible non-enzymatic reactions occurring with high glucose exposure (Figure 4.1A). With the addition of gBSA, the spectrum of S1 appears to broadened, causing a loss of distinction in both d-d bands. When gBSA is complexed via S2, a broad-like d-d band at 653 nm emerges. The broadening spectral characteristics observed with gBSA following S1 and S2 suggests formation of aggregates in solution due to long-term high glucose exposure (Figure 4.4B).

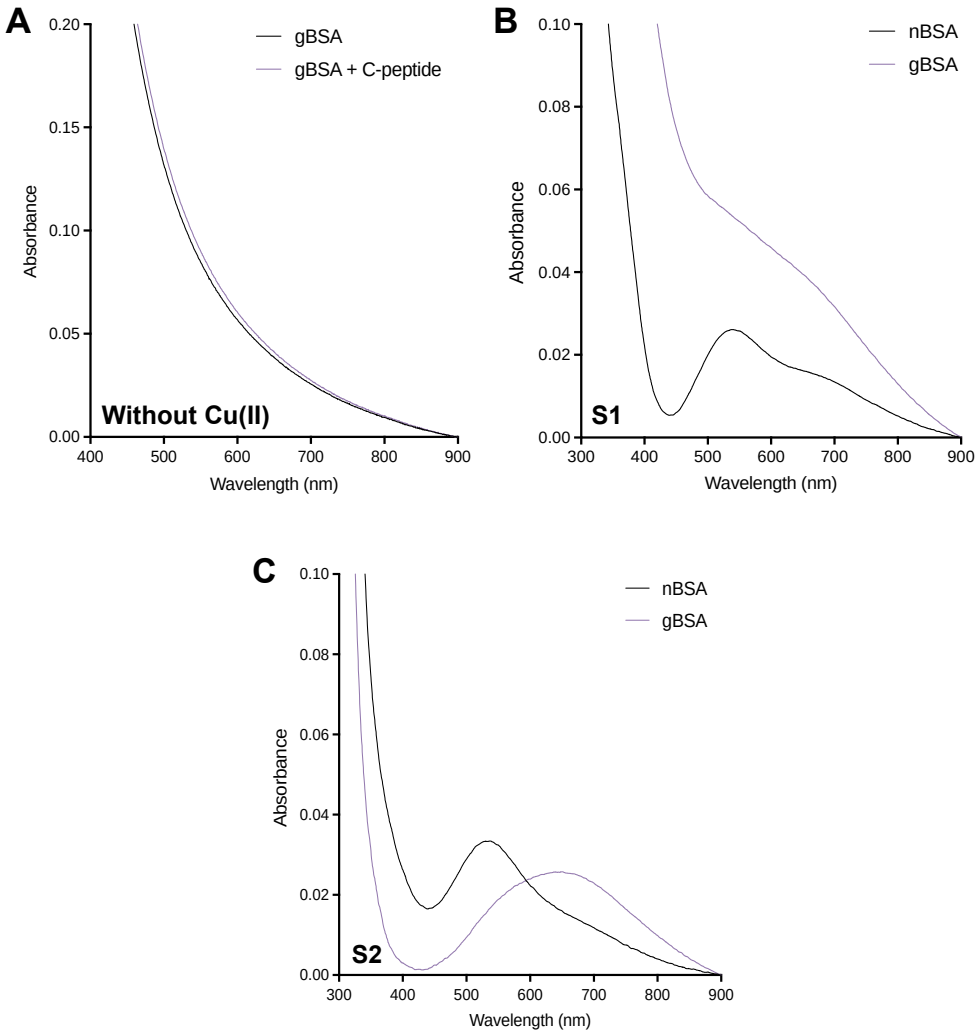

Figure 4.4. Electronic absorption spectra comparing the addition of nBSA and gBSA following S1 and S2 at two equivalents of Cu(II). (A) The addition of C-peptide (purple) does not shift apo-gBSA (black), thus closely overlapping in spectra. (B) S1 displays a broadening spectrum with the addition of gBSA (purple) but not with nBSA (black). (C) gBSA shifts S2 to form new peak, suggesting a modification in the coordination complex as a result of glycation. Maxima values of (A) and (B) are labeled in Table 4.1.

Table 4.1. Maximum absorbance values of the UV-Vis spectra with the addition of two equivalents of Cu(II).

Sample	S1, Abs_{max}		S2, Abs_{max}	
nBSA	545	686	540	691
gBSA	—		560	653

We tested our speculation on aggregation formation for S1 and S2 with the addition of gBSA using a turbidity assay. Turbidity measures the presence of particles in solution that will scatter light. Scattering of light impacts the ratio of incident light (I_o) to transmitted light (I) by decreasing transmitted light and therefore, increasing absorbance. Protein aggregates are particles that scatter light in solution and results in apparent absorbance that can be detected at 450 nm. Samples detected at higher values of absorbance, or greater turbidity, will contain larger protein aggregates. The addition of nBSA following S1 and S2 conditions exhibited very minimal turbidity in comparison to the addition of gBSA.

S1 and S2 displayed about a 3.5-fold increase in turbidity, implicating an increased presence in protein aggregation (Figure 4.5).

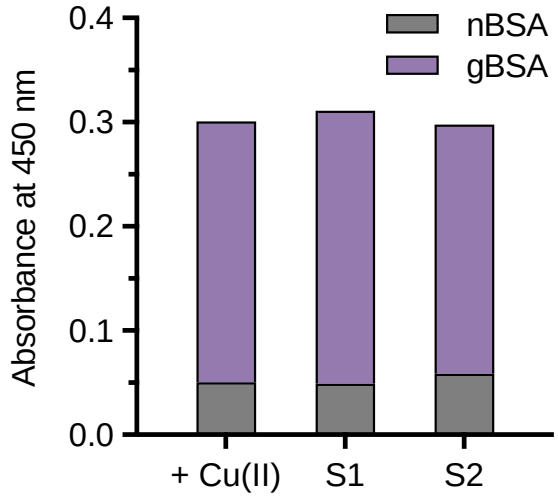

Figure 4.5. Turbidity assay (absorbance at 450 nm) to measure presence of protein aggregation in sample solution. The presence of nBSA displays very minimal turbidity in both S1 and S2 solutions. gBSA increases turbidity in both schematics.

In Chapter 3, we used circular dichroism (CD) to compare changes in alpha-helical content of BSA based on the stoichiometric addition of Cu(II), as well as the order of addition with C-peptide and BSA. CD detected subtle shifts in alpha helical content at 212 and 222 nm revealed differences in conformational structure. With the addition of nBSA, the CD spectra displayed no change in helical content (Figure 4.6, dashed spectra). The addition of 2 equivalents Cu(II) to gBSA show two peaks at 208 and 219 nm, with a large

reduction in ellipticity at 208 nm. This reduction may suggest a shift towards beta-sheet character, where a broadening peak is typically observed in the 210-220 nm region (greenfield 2005). The addition of apo-C-peptide to 2:1 Cu(II)/gBSA following S1 exhibits shifts in wavelength values at both alpha helical peaks and increases in negative ellipticity. The first alpha helical peak shifts from 208 to 209 nm, and the measured ellipticity increases from -3 to -8 millidegrees. The second alpha helical peak shifts from 219 to 222 nm, and the detected ellipticity increases from -12 to -14 millidegrees. In contrast, the addition of 2:1 Cu(II)-C-peptide to apo-gBSA following S2 displays a loss of the first helical peak and a broadening of the second helical peak, with a shift in wavelength from 219 to 223 nm (Figure 4.6, solid spectra). Altogether, all gBSA spectra implicate beta-sheet structure, and the wavelength shift in negative bands compared to nBSA suggest aggregation. These observations support both the electronic absorbance data and the turbidity readouts.

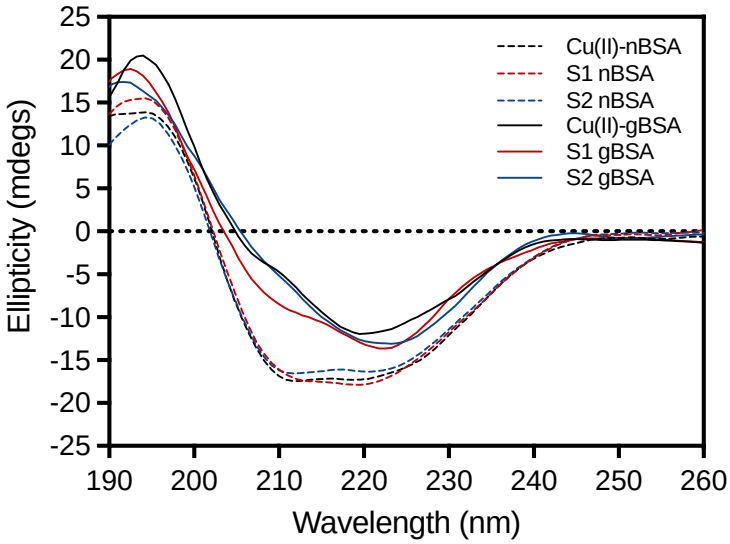

Figure 4.6. Circular dichroism spectra of 2 μM nBSA and gBSA detect differences in structure by shifts in ellipticity and wavelength. Dashed-line spectra show 2 equivalents Cu(II) with nBSA (black), S1 (red), and S2 (blue). Helical content is shown to resemble that of Chapter 3 data. Prominent reduction of negative ellipticity is observed in all gBSA spectra (solid line) with 2:1 Cu(II) (black), S1 (red), and S2 (blue). Particularly, shifts in wavelength values are observed in Cu(II)/gBSA and S2 spectra, pointing to beta-sheet content.

4.2.3 Future work in exploring AGE formation and aggregation with Cu(II), C-peptide, and glycated albumin

It is reported that there may be a cross-talk between protein aggregation and AGE formation.[15,25] For example, the islet amyloid polypeptide (IAPP) is determined to be heavily glycated, leading to formation of toxic amyloid-like aggregates.[26] Metal ions have shown to either inhibit or promote protein/peptide aggregation.[27,28] Particularly, both C-peptide and BSA contain literature precedence in displaying self-aggregation.[29,30] As both

biomolecules display Cu(II)-binding characteristics, and the lab characterized Cu(II)-bridging ternary complexes between C-peptide and BSA, we hypothesized that the presence of Cu(II) plays a role in aggregation with C-peptide and BSA. To test this hypothesis, we prepared the solutions containing high glucose (200 mM) and 30 μM BSA with the following additions: 2 equivalents Cu(II), 1 equivalents C-peptide, or both Cu(II) and C-peptide. All samples were incubated for 21 days at 37°C, then detected for AGE fluorescence, or "browning." Our preliminary work shows that with incubation of Cu(II), AGE formation is accelerated (Figure 4.7).

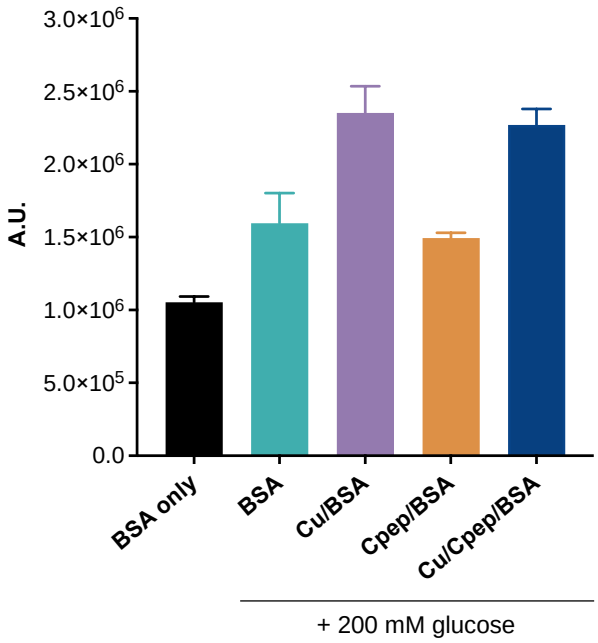

Figure 4.7. AGE fluorescence assay (ex. 350 nm, em. 425 nm; *n* = 3) to measure AGE formation after 21 days at 37°C in solutions containing 30 μM BSA with 2 equivalents

Cu(II), apo-C-peptide, or both in 10 mM phosphate buffer at pH 7.4. The presence of Cu(II) accelerates AGE formation. Data is displayed as mean ± SD with n = 3.

To determine if Cu(II) plays a role in the cross talk between AGE formation and aggregation, we used a turbidity assay to detect if protein aggregation occurs between Cu(II), C-peptide, and BSA. Tsiolaki and colleagues showed characterization of C-peptide aggregation in acidic conditions at room temperature for 7 days. To expand on their work, samples containing 1 mg/mL C-peptide with equivalent solutions of Cu(II) and BSA were added in nanopure H_2O with pH adjusted to 5.5 to observe if aggregation may be detected. Interestingly, Cu(II) increased protein aggregation when added to BSA and C-peptide/BSA. This preliminary work warrants follow-up studies to monitor this process over time up to 21 days using both turbidity and Thioflavin (Tht) assays in high glucose, as well as single molecule fluorescence microscopy, to better understand the molecular mechanisms that drive the observations seen in Figure 4.8.

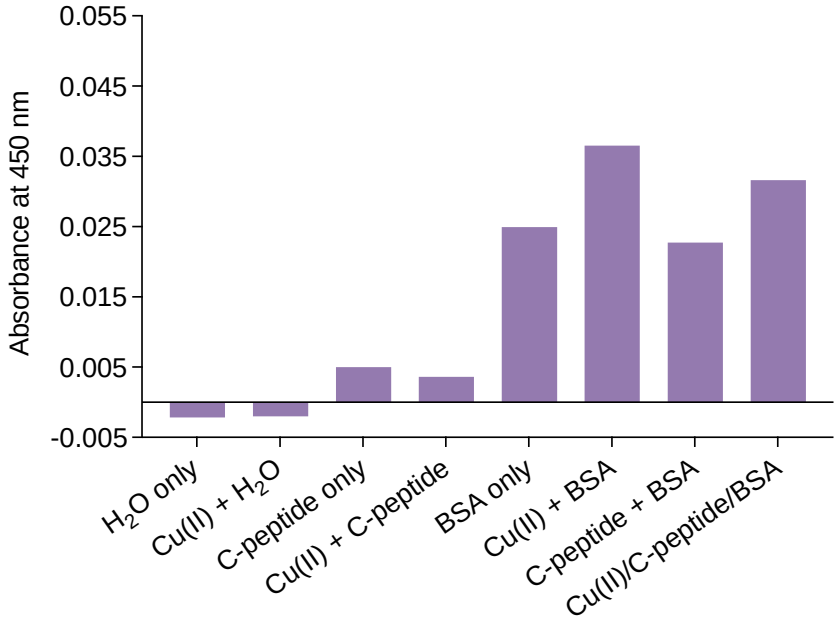

Figure 4.8. Turbidity assay (absorbance at 450 nm) to measure presence of protein aggregation in sample solution. The presence of Cu(II) displays an increase in turbidity, suggesting a higher detection of protein aggregation in Cu(II) + BSA and Cu(II)/C-peptide/BSA.

4.3 Materials and Methods

All chemicals and reagents, as well as use of purified C-peptide, were adapted from Chapter 3. Preparation of samples following S1 and S2 with the addition of nBSA and gBSA for CD, UV-Vis spectroscopy, IF, and ELISA were also adapted from Chapter 3.

Preparation of nBSA samples. nBSA samples were prepared the day of experiment to represent as Day 0. Concentrations of BSA and 500 mM glucose (Sigma) were first determined by molecular weight, then dissolved in 10 mM phosphate buffer (Fisher) at pH 7.4 for CD, UV-Vis spectroscopy, and in DPBS (Gibco) for IF and ELISA.

Preparation of gBSA samples. Prior to experimental use, solutions of 10 mg/mL BSA were incubated in high glucose conditions (500 mM glucose) for 21 days, then filtered using centrifugal filter columns (Amicon, 50 kDa cutoff) to remove any excess glucose. gBSA samples are then diluted by either phosphate buffer or DPBS.

Turbidity assay for measuring protein aggregation. Samples were diluted in 10 mM phosphate buffer at pH 7.4 then added to a 96-well microplate (Greiner Bio-One). Turbidity of each solution was measured at 450 nm for absorbance using a platereader (Molecular Devices i3x). Statistics were performed on Prism 9.1 (GraphPad).

AGE fluorescence assay to detect AGE formation. All samples contain 30 μM BSA and were diluted in 10 mM phosphate buffer (n = 3). Sample conditions include apo-BSA only and BSA + glucose (200 mM) as controls, and experimental solutions contain 200 mM glucose with the addition of 2:1 Cu(II)-BSA, C-peptide/ BSA, or Cu(II)/C-peptide/BSA.

All samples were incubated for 21 days at 37°C, then measured for AGE fluorescence, with an excitation of 350 nm and emission of 425 nm. Data is displayed as mean ± SD with n = 3.

4.4 References

(1) Cooper, M. E. Pathogenesis, Prevention, and Treatment of Diabetic Nephropathy. *Lancet (London, England)* **1998**, *352* (9123), 213–219. https://doi.org/10.1016/S0140-6736(98)01346-4.

(2) Fong, D. S.; Aiello, L. P.; Ferris, F. L.; Klein, R. Diabetic Retinopathy. *Diabetes Care* **2004**, *27* (10), 2540–2553. https://doi.org/10.2337/DIACARE.27.10.2540.

(3) Forbes, J. M.; Cooper, M. E. Mechanisms of Diabetic Complications. *Physiol. Rev.* **2013**, *93* (1), 137–188. https://doi.org/10.1152/PHYSREV.00045.2011.

(4) Wahren, J.; Ekberg, K.; Jörnvall, H. C-Peptide Is a Bioactive Peptide. *Diabetologia* **2007**, *50* (3), 503–509. https://doi.org/10.1007/s00125-006-0559-y.

(5) Stevenson, M. J.; Farran, I. C.; Uyeda, K. S.; San Juan, J. A.; Heffern, M. C. Analysis of Metal Effects on C-Peptide Structure and Internalization. *ChemBioChem* **2019**, *20* (19), 2447–2453. https://doi.org/10.1002/cbic.201900172.

(6) Stevenson, M. J.; Janisse, S. E.; Tao, L.; Neil, R. L.; Pham, Q. D.; Britt, R. D.; Heffern, M. C. Elucidation of a Copper Binding Site in Proinsulin C-Peptide and Its Implications for Metal-Modulated Activity. *Inorg. Chem.* **2020**, *59* (13), 9339–9349. https://doi.org/10.1021/acs.inorgchem.0c01212.

(7) Liu, Y.; Chen, C.; Summers, S.; Medawala, W.; Spence, D. M. C-Peptide and Zinc Delivery to Erythrocytes Requires the Presence of Albumin: Implications in Diabetes Explored with a 3D-Printed Fluidic Device. *Integr. Biol. (United Kingdom)* **2015**, *7* (5), 534–543. https://doi.org/10.1039/c4ib00243a.

(8) Geiger, M.; Janes, T.; Keshavarz, H.; Summers, S.; Pinger, C.; Fletcher, D.; Zinn, K.; Tennakoon, M.; Karunarathne, A.; Spence, D. A C-Peptide Complex with Albumin and Zn2+ Increases Measurable GLUT1 Levels in Membranes of Human Red Blood Cells. *Sci. Rep.* **2020**, *10* (1). https://doi.org/10.1038/s41598-020-74527-6.

(9) Beigoli, S.; Sharifi Rad, A.; Askari, A.; Assaran Darban, R.; Chamani, J. Isothermal Titration Calorimetry and Stopped Flow Circular Dichroism Investigations of the Interaction between Lomefloxacin and Human Serum Albumin in the Presence of Amino Acids. *https://doi.org/10.1080/07391102.2018.1491421* **2018**, *37* (9), 2265–2282. https://doi.org/10.1080/07391102.2018.1491421.

(10) Peters, T. The Albumin Molecule: Its Structure and Chemical Properties. *All About Albumin* **1995**, 9–II. https://doi.org/10.1016/B978-012552110-9/50004-0.

(11) Merlot, A. M.; Kalinowski, D. S.; Richardson, D. R. Unraveling the Mysteries of Serum Albumin-More than Just a Serum Protein. *Front. Physiol.* **2014**, *5 AUG*, 299. https://doi.org/10.3389/FPHYS.2014.00299/BIBTEX.

(12) Curry, S.; Brick, P.; Franks, N. P. Fatty Acid Binding to Human Serum Albumin: New Insights from Crystallographic Studies. *Biochim. Biophys. Acta* **1999**, *1441* (2–3), 131–140. https://doi.org/10.1016/S1388-1981(99)00148-1.
(13) Furusyo, N.; Hayashi, J. Glycated Albumin and Diabetes Mellitus. *Biochim. Biophys. Acta - Gen. Subj.* **2013**, *1830* (12), 5509–5514. https://doi.org/10.1016/J.BBAGEN.2013.05.010.
(14) Qiu, H.-Y.; Hou, N.-N.; Shi, J.-F.; Liu, Y.-P.; Kan, C.-X.; Han, F.; Sun, X.-D. Comprehensive Overview of Human Serum Albumin Glycation in Diabetes Mellitus. *World J. Diabetes* **2021**, *12* (7), 1057. https://doi.org/10.4239/WJD.V12.I7.1057.
(15) Rondeau, P.; Bourdon, E. The Glycation of Albumin: Structural and Functional Impacts. *Biochimie*. Elsevier April 1, 2011, pp 645–658. https://doi.org/10.1016/j.biochi.2010.12.003.
(16) Coussons, P. J.; Jacoby, J.; McKay, A.; Kelly, S. M.; Price, N. C.; Hunt, J. V. Glucose Modification of Human Serum Albumin: A Structural Study. *Free Radic. Biol. Med.* **1997**, *22* (7), 1217–1227. https://doi.org/10.1016/S0891-5849(96)00557-6.
(17) Anguizola, J.; Matsuda, R.; Barnaby, O. S.; Joseph, K. S.; Wa, C.; DeBolt, E.; Koke, M.; Hage, D. S. Review: Glycation of Human Serum Albumin. *Clin. Chim. Acta.* **2013**, *0*, 64. https://doi.org/10.1016/J.CCA.2013.07.013.
(18) Mohamadi-Nejad, A.; Moosavi-Movahedi, A. A.; Hakimelahi, G. H.; Sheibani, N. Thermodynamic Analysis of Human Serum Albumin Interactions with Glucose: Insights into the Diabetic Range of Glucose Concentration. *Int. J. Biochem. Cell Biol.* **2002**, *34* (9), 1115–1124. https://doi.org/10.1016/S1357-2725(02)00031-6.
(19) Ahmed, N. Advanced Glycation Endproducts - Role in Pathology of Diabetic Complications. *Diabetes Research and Clinical Practice*. Elsevier January 1, 2005, pp 3–21. https://doi.org/10.1016/j.diabres.2004.09.004.
(20) Freitas, P. A. C.; Ehlert, L. R.; Camargo, J. L. Glycated Albumin: A Potential Biomarker in Diabetes. *Arch. Endocrinol. Metab.* **2017**, *61* (3), 296–304. https://doi.org/10.1590/2359-3997000000272.
(21) Soudahome, A. G.; Catan, A.; Giraud, P.; Kouao, S. A.; Guerin-Dubourg, A.; Debussche, X.; Le Moullec, N.; Bourdon, E.; Bravo, S. B.; Paradela-Dobarro, B.; Álvarez, E.; Meilhac, O.; Rondeau, P.; Couprie, J. Glycation of Human Serum Albumin Impairs Binding to the Glucagon-like Peptide-1 Analogue Liraglutide. *J. Biol. Chem.* **2018**, *293* (13), 4778–4791. https://doi.org/10.1074/jbc.M117.815274.
(22) Jacobs, M. J.; Geiger, M. K.; Summers, S. E.; DeLuca, C. P.; Zinn, K. R.; Spence, D. M. Albumin Glycation Affects the Delivery of C-Peptide to the Red Blood Cells. *ACS Meas. Sci. Au* **2022**, *2* (3), 278–286. https://doi.org/10.1021/ACSMEASURESCIAU.2C00001.
(23) Qian, M.; Liu, M.; Eaton, J. W. Transition Metals Bind to Glycated Proteins

Forming Redox Active “Glycochelates”: Implications for the Pathogenesis of Certain Diabetic Complications. *Biochem. Biophys. Res. Commun.* **1998**, *250* (2), 385–389. https://doi.org/10.1006/bbrc.1998.9326.

(24) Eaton, J. W.; Qian, M. *Interactions of Copper with Glycated Proteins: Possible Involvement in the Etiology of Diabetic Neuropathy*; 2002; Vol. 234.

(25) Rondeau, P.; Navarra, G.; Cacciabaudo, F.; Leone, M.; Bourdon, E.; Militello, V. Thermal Aggregation of Glycated Bovine Serum Albumin. *Biochim. Biophys. Acta - Proteins Proteomics* **2010**. https://doi.org/10.1016/j.bbapap.2009.12.003.

(26) Milordini, G.; Zacco, E.; Percival, M.; Puglisi, R.; Dal Piaz, F.; Temussi, P.; Pastore, A. The Role of Glycation on the Aggregation Properties of IAPP. *Front. Mol. Biosci.* **2020**, *7*. https://doi.org/10.3389/FMOLB.2020.00104.

(27) Rizvi, A.; Furkan, M.; Naseem, I. Physiological Serum Copper Concentrations Found in Malignancies Cause Unfolding Induced Aggregation of Human Serum Albumin in Vitro. *Arch. Biochem. Biophys.* **2017**, *636*, 71–78. https://doi.org/10.1016/J.ABB.2017.11.001.

(28) Navarra, G.; Tinti, A.; Leone, M.; Militello, V.; Torreggiani, A. Influence of Metal Ions on Thermal Aggregation of Bovine Serum Albumin: Aggregation Kinetics and Structural Changes. *J. Inorg. Biochem.* **2009**, *103* (12), 1729–1738. https://doi.org/10.1016/j.jinorgbio.2009.09.023.

(29) Tsiolaki, P. L.; Louros, N. N.; Zompra, A. A.; Hamodrakas, S. J.; Iconomidou, V. A. Unraveling the Aggregation Propensity of Human Insulin C-Peptide. *Biopolymers* **2017**, *108* (2). https://doi.org/10.1002/BIP.22882.

(30) Maciążek-Jurczyk, M.; Janas, K.; Pożycka, J.; Szkudlarek, A.; Rogóż, W.; Owczarzy, A.; Kulig, K. Human Serum Albumin Aggregation/Fibrillation and Its Abilities to Drugs Binding. *Mol. 2020, Vol. 25, Page 618* **2020**, *25* (3), 618. https://doi.org/10.3390/MOLECULES25030618.

CHAPTER 5

Copper interactions with C-peptide shifts intracellular copper metabolism and peptide uptake

5.1 Introduction

Proinsulin C-peptide is released in equimolar amounts with active insulin from pancreatic β-cells and has been shown to possess beneficial hormone-like roles such as glucose uptake, blood flow regulation, and increased cell growth.[1,2] With over a decade of work supporting its beneficial physiological effects,[3,4] its therapeutic advances are hindered by a lack of mechanistic understanding of C-peptide.[3] Therefore, a molecular investigation on C-peptide and its structural functions will help identify connections between the physiological and biological activities of the peptide.

In determining the peptide's mode of action, previous studies have shown that C-peptide function depends on the co-addition of essential divalent metal ions. In the presence of Zn(II), C-peptide can prevent islet amyloid polypeptide (IAPP) aggregation in pancreatic β-cells.[5] C-peptide activation of ATP release from erythrocytes is enhanced when in the presence of Cr(III), Fe(II), or Zn(II).[6–8] Further work showed that serum albumin, an abundant circulating protein in the bloodstream,[9] is required for transport of both Zn(II) and C-peptide from pancreatic β-cells to erythrocytes.[10,11] Recently, we demonstrated that Cu(II) can alter peptide internalization by directly binding to E3 and D4 of C-peptide.[12,13] Moreover, the wild-type sequence of C-peptide is necessary for precise binding of Cu(II) to C-peptide, and that mutations or truncations of the peptide lead to non-specific metal ion binding.[13]

Cu(II) is of particular interest as the dysregulation of intracellular copper homeostasis is linked to tissue damage in type 2 diabetes (T2D) due to elevated copper levels,[14] and is correlated with the inflammatory or fibrotic progression in non-alcoholic

fatty liver disease (NAFLD) as a result of decreased copper status.[15] As C-peptide has been highlighted as a potential biomarker for Cu(II)-related diseases,[15] the direct binding of Cu(II) with full-length C-peptide raises the question of whether this metal/peptide complexation contains the ability to shift intracellular copper levels, to which could impact the aforementioned Cu(II)-related disease states. To uncover the link between C-peptide and copper metabolism, long-term signaling effects of C-peptide must be elucidated. As serum albumin has been identified as a potential chaperone for C-peptide, and is the second major constituent of exchangeable copper pool in blood plasma behind ceruloplasmin,[9] we probed the role serum albumin may have on C-peptide mechanisms by focusing on copper status.

In this work, we investigate the outcomes of C-peptide activity based on its wild-type and mutated variant structures. Interestingly, these peptides display cell-line based differences in altering copper biomarkers as well as peptide uptake mechanisms. Given the relationship between C-peptide, Cu(II), and albumin (see Chapter 3), cell-based assays were also performed in the presence and absence of albumin. Overall, the presented data may point to C-peptide activity that involves shifts in intracellular copper status, and by extension, Cu(II)-related diseases.

5.2 Results

5.2.1 Wild-type C-peptide shifts copper metabolism and serum albumin alters peptide activity

Because Cu(II) directly binds to C-peptide and inhibits peptide internalization,[12,13] we interrogated whether the Cu(II)-bound complex could impact copper trafficking and homeostasis within the cell. To assess copper status, we used two cell lines, the human hepatic line (HepG2) and the human embryonic kidney line (HEK-293), on account of reported effects of C-peptide on liver and kidney tissues.[16–18] We monitored the effects of C-peptide addition *via* protein levels of the copper chaperone for superoxide dismutase (CCS), a well-established biomarker used for tracking copper homeostasis.[19,20] An increase in CCS levels is indicative of a decrease in intracellular copper levels, while a decrease in CCS is associated with an increase in intracellular copper levels. Cells were stimulated with either Cu(II), wild-type C-peptide only (apo-C-peptide), or C-peptide preincubated with Cu(II) (Cu(II)-C-peptide) in starvation media (serum-free) for 24 hours (Figure 5.1A), then lysates were analyzed by Western blotting. Only apo-C-peptide increased CCS levels in both HepG2 and HEK-293 (Figure 5.1B and 5.1C), insinuating a decrease of cytosolic copper levels. Because serum albumin is a potential chaperone for C-peptide,[10,11] we determined whether the copper modulatory ability of C-peptide is influenced by the addition of commercially available bovine serum albumin (BSA). In Figure 5.1b, BSA enhances the apo-C-peptide effect on cytosolic copper status in HepG2, but surpasses this effect in HEK-293 (Figure 5.1C). However, when Cu(II) is pre-bound to C-peptide then added to a solution containing BSA, it decreased CCS expression in both HepG2 and HEK-293 (Figure 5.1B and 5.1C), suggesting that the order in which

Cu(II) was added plays a role in shifting CCS levels. To confirm that the observed shifts in CCS levels in both cell lines are due to decreased cytosolic copper status and is independent of copper export, we looked at ATP7B in HepG2 and ATP7A in HEK-293 cells to track copper exporter levels.[21–23] We showed that ATP7B and ATP7A protein levels shift when exogenous copper is added in solution (Figure 5.1D and 5.1E). Copper exporter levels did not change with apo-C-peptide, but shifted with Cu(II)-bound C-peptide. C-peptide/BSA slightly increased copper exporters in both HepG2 and HEK-293 (Figure 5.1D and 5.1E). Together, the lack of notable shifts in ATP7B and ATP7A expression confirmed that the effects on cytosolic copper status observed with apo-C-peptide and C-peptide/BSA are independent of copper export.

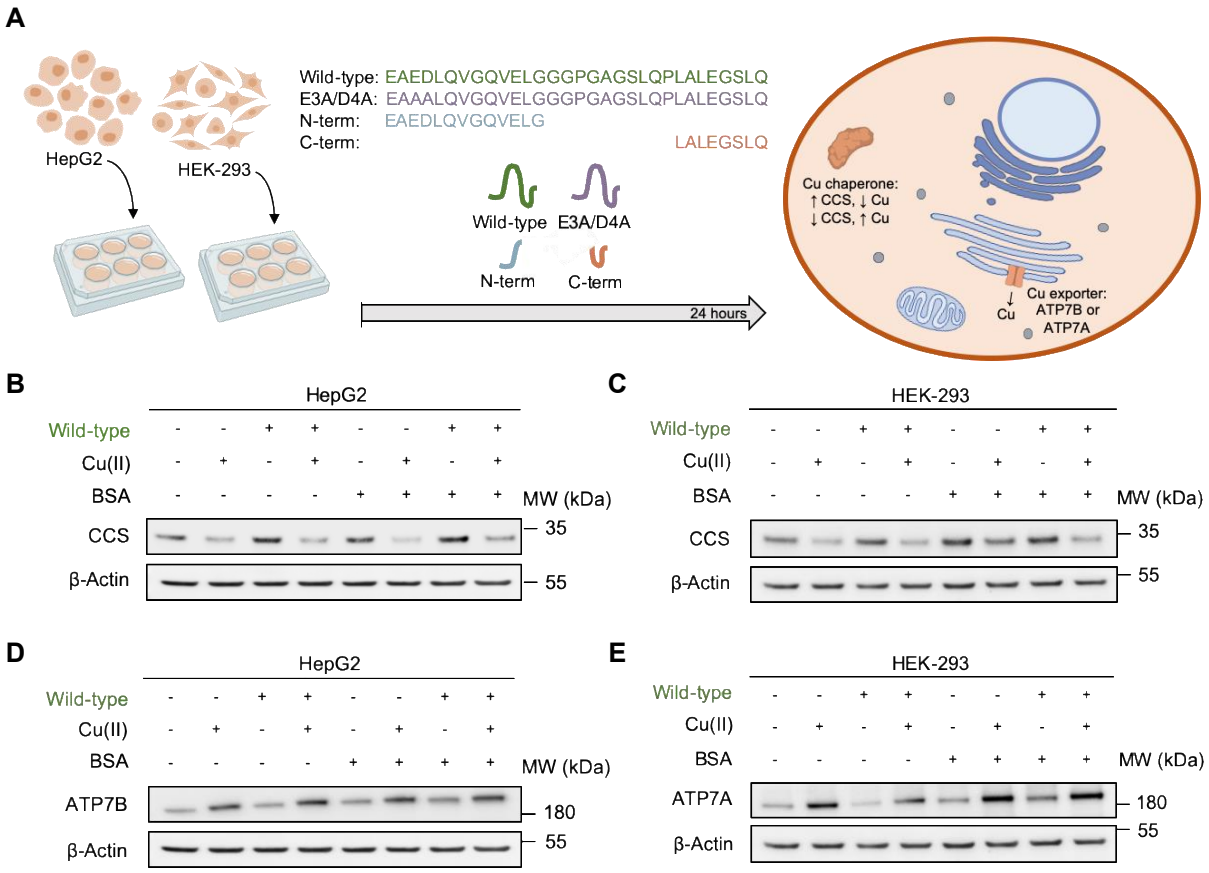

Figure 5.1. Wild-type C-peptide with and without BSA shifts cytosolic copper status. (A) Graphical representation depicting the workflow of 24 hour peptide stimulations using both wild-type and mutated C-peptide in HepG2 and HEK-293 to investigate shifts in cytosolic copper levels *via* CCS, a copper chaperone, and ATP7B or ATP7A, which are copper exporters. (B, C, D, E) Sample conditions containing 10 µM wild-type apo-C-peptide or preformed Cu(II)-C-peptide in solution with and without BSA following Western blot (WB) analysis of CCS levels in HepG2 and HEK-293, and ATP7B levels in HepG2 and ATP7A levels in HEK-293. (B) Comparison of biomarker levels are in reference to the negative control WB band or apo-BSA WB band. Apo-C-peptide increased CCS levels

in HepG2, and this effect was increased further in the presence of BSA. (C) Apo-C-peptide increased CCS in HEK-293, but this effect was surpassed when C-peptide is added with BSA. (D, E) Apo-C-peptide with and without BSA did not influence ATP7B levels in HepG2 and minimally shifted ATP7A expression in HEK-293.

5.2.2 C-peptide mutants reveal cell-line based differences in copper trafficking

We reported that the Cu(II)-C-peptide interaction requires the full-length peptide for precise copper binding at the E3 and D4 amino acid residues, and that either replacing both residues to generate a double mutant (E3A/D4A), or truncating the peptide to the N-terminus segment (N-term, E1G13) or the C-terminus segment (C-term, L24Q31) results in non-specific copper binding.[13] We herein evaluate whether disrupted copper binding of these mutants impacts the observed prominent effects of wild-type C-peptide with or without BSA on copper trafficking in HepG2 and HEK-293. All three C-peptide mutants with or without BSA did not display any notable changes in both CCS levels and ATP7B levels (Figure 5.2A & 5.2C) of HepG2, suggesting that the full length of C-peptide is necessary to observe prominent shifts in cytosolic copper levels. In HEK-293, CCS levels increased following the addition of each apo-mutant (Figure 5.2B), indicating that non-specific binding of Cu(II) still allows for similar changes in CCS levels as in wild-type C-peptide. When these mutants are added with BSA, only the N-term increases CCS levels (Figure 5.2B), pointing to the importance of the Cu(II)-binding residues of C-peptide when BSA is present. ATP7A levels slightly change in HEK-293 with each apo-mutant both with

and without BSA (Figure 5.2D). Altogether, the observed changes with CCS in both cell models do not correlate with copper export.

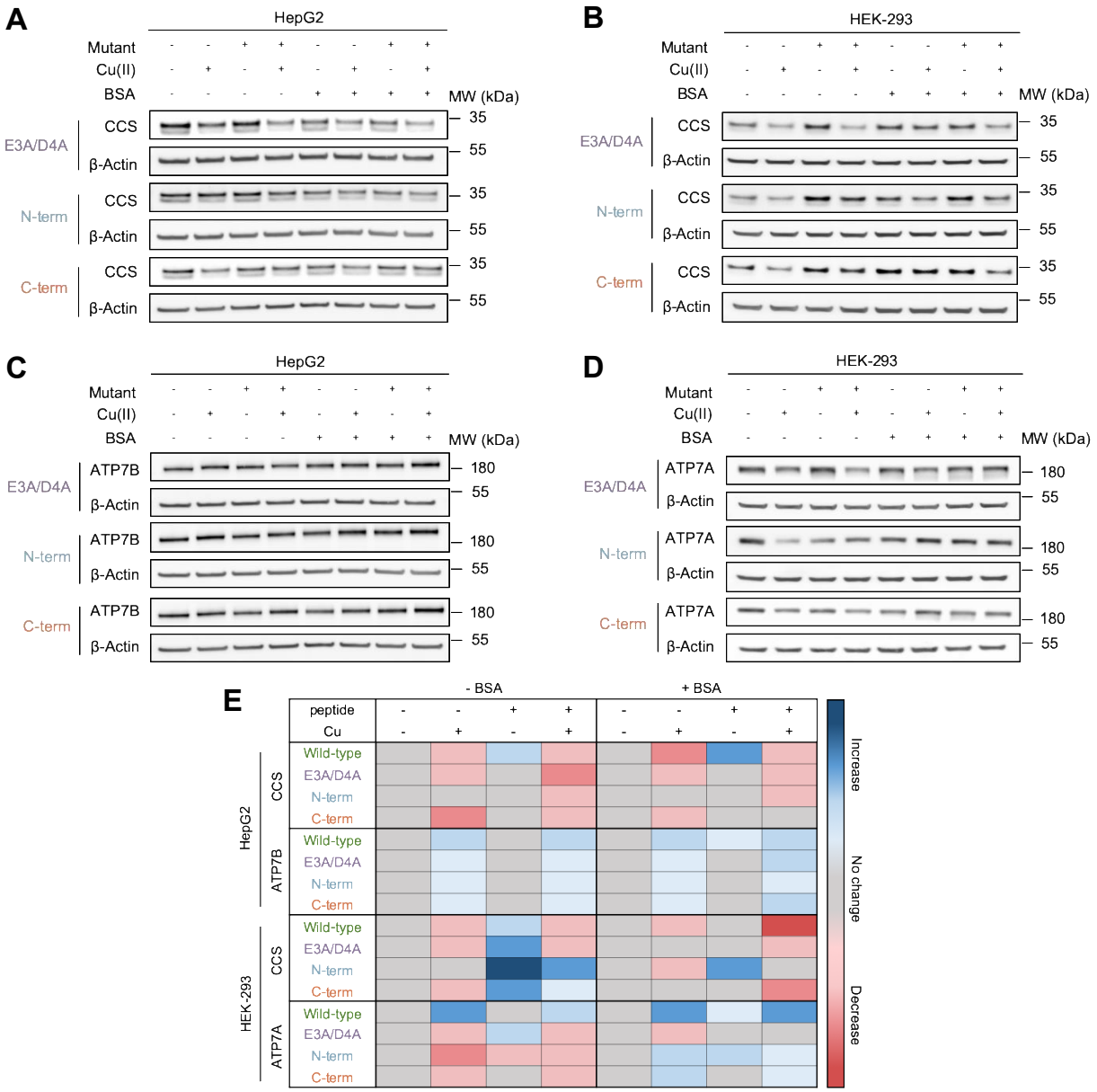

Figure 5.2. C-peptide mutants reveal cell-line based differences in copper biomarker responses and mode of peptide uptake. Sample conditions include 10 µM C-peptide

mutants (E3A/D4A, N-term, C-term) following the same Western blot analysis as wild-type C-peptide with or without BSA. (A) All three apo-mutants did not shift CCS levels with and without BSA in HepG2. Pre-bound Cu(II)-peptide mutants slightly decreased CCS levels with and without BSA. (C) ATP7B did not change with any apo-mutant with and without BSA. In HEK-293, all three apo-mutants increased CCS. (B) When Cu(II) or BSA is added with N-term, CCS levels seem to only increase with this specific peptide mutant. (D) ATP7A levels slightly shift in HEK-293 in comparison to HepG2. (E) Summary table of Western blots that include wild-type C-peptide and all C-peptide mutants tested in various conditions for comparison (Figure 5.1B-E and Figure 5.2A-D). Blue indicates an increase in protein levels, while red points to a decrease in protein levels. Grey represents either the control WB band or no change observed with respect to the control WB band.

5.2.3 Mode of C-peptide uptake is cell-line dependent

Because cell-line based differences were observed between the wild-type and mutated peptides, we questioned if the differences in functionality stem from preference in the mode of C-peptide uptake that leads to these distinctive changes. Both cell lines were stimulated with solutions containing apo-C-peptide or Cu(II)-C-peptide with the addition of BSA in starvation media (serum-free) at 30 minutes, 4 hours, or 24 hours to detect peptide uptake over time. Cells were fixed, permeabilized, and incubated with C-peptide primary antibodies, followed by secondary antibodies conjugated with Alexa Fluor 488 fluorophore. Mean pixel intensities of each sample condition was used to determine any shifts in C-peptide internalization. As previously reported, HEK-293 at 30 minutes

displayed an increase in the internalization of apo-C-peptide.[16] Whereas, the presence of Cu(II) causes a decrease in C-peptide internalization.[12] Interestingly, Cu(II)-C-peptide greatly increased internalization in the presence of BSA in comparison to Cu(II)-C-peptide in starvation media (Figure 5.3), demonstrating that BSA reverts the process of Cu(II) inhibition with C-peptide internalization. At 4 and 24 hours, C-peptide internalization was not observed in HEK-293 cells. In HepG2 cells, peptide internalization was not observed at any of the timed stimulations, suggesting that C-peptide was not internalized *via* endocytosis in HepG2 in comparison to HEK-293.

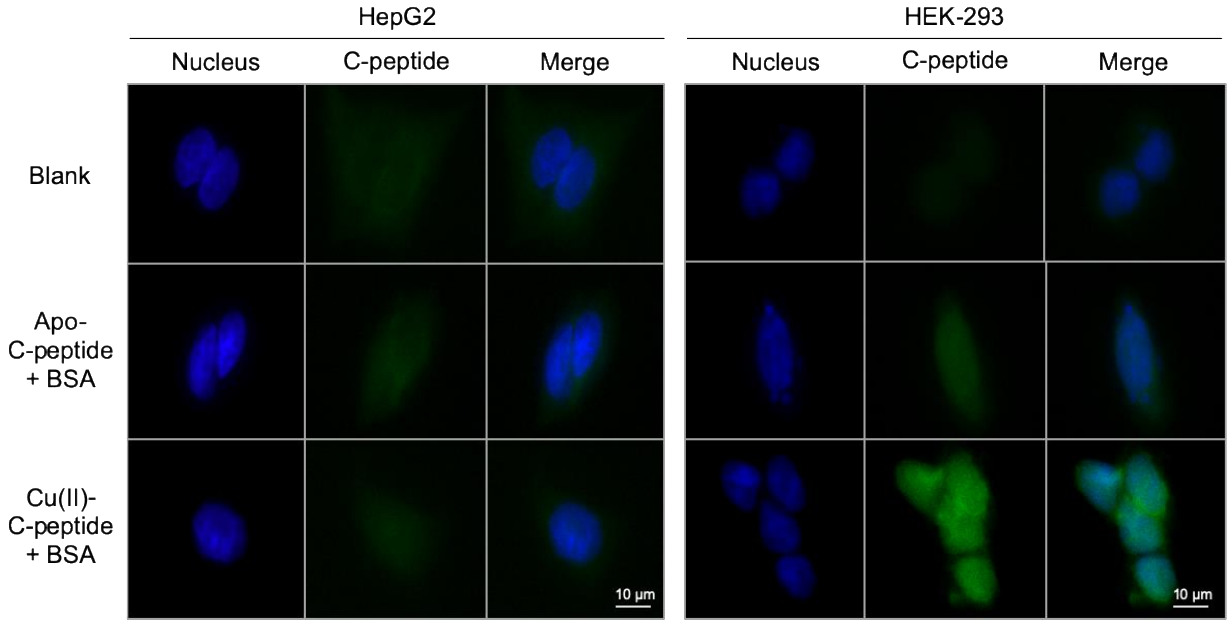

Figure 5.3. Representative immunofluorescence images (n = 3) show that wild-type C-peptide/BSA and Cu(II)-C-peptide/BSA does not increase peptide internalization in HepG2, but notably increases when wild-type Cu(II)-C-peptide/BSA is added to HEK-293 cells.

5.3 Discussion

Our work highlights new mechanistic effects of C-peptide in regulating copper metabolism. We observe cell-line based differences in cytosolic copper responses between two cell-line models, HepG2 and HEK-293, which have been used in previous C-peptide studies,[16–18] and presented as well-characterized models for metabolic processing and copper trafficking responses.[21–23] Full-length apo-C-peptide induces a shift in cytosolic copper status after 24 hours by increasing CCS levels, and as a result, decreases copper levels in HepG2 and HEK-293. Furthermore, the data highlights a crosstalk between C-peptide and BSA, a potential chaperone, as BSA enhances the C-peptide effect on decreasing copper levels in HepG2. This shift in copper status points to a potential restoration in copper homeostasis for Cu(II)-related diseases associated with elevated copper levels, such as T2D.[14] On the other hand, when C-peptide is pre-complexed with Cu(II), we observe an opposite effect where CCS decreases, and therefore, copper levels increase. BSA enhances this effect with HepG2, and even further with HEK-293. As the onset of NAFLD, another Cu(II)-related disease, progress due to a copper deficient state (Wang 2020), Cu(II)-C-peptide/BSA could help regulate cytosolic copper status by increasing intracellular copper levels.

When the copper binding residues (E3, D4) of C-peptide are mutated, or the full-length peptide is truncated to its N-term (E1G13) or C-term (L24Q31) segment, we observe that these mutations were able to reproduce increased shifts in CCS levels as full-length C-peptide in HEK-293, but this effect was absent in HepG2. This outcome suggests that the peptide uptake mechanism of C-peptide may vary by endocrine target. Various modes of C-peptide uptake have been studied such as C-peptide internalization as demonstrated

by Lindahl and colleagues,[16] and C-peptide uptake by receptor mediation *via* GPR146 as screened by Yosten and co-workers.[17] Time-dependent Immunofluorescence studies revealed that HEK-293 increases C-peptide internalization when added with Cu(II) and BSA at the 30-minute timepoint; whereas, HepG2 does not internalize C-peptide following all sample conditions at 30 minutes, 4 hours, or 24 hours. Therefore, it is possible that HepG2 binds to C-peptide *via* a GPR receptor, while HEK-293 internalizes the peptide by endocytosis. These cell-line based differences by mode of peptide uptake warrants further investigation.

Referring back to the ternary complexations discussed in Chapter 3, Scheme 1 (Cu(II)-BSA + apo-C-peptide) and Scheme 2 (apo-BSA + Cu(II)-C-peptide), we questioned if the different Cu(II)-coordination modes between Scheme 1 and 2 point to possible preferences in binding modes depending on the trends seen between cell-line or endocrine targets. Because we observe an increased shift in intracellular copper levels with C-peptide/BSA particularly in HepG2, the binding mode that pairs with this trend follows Scheme 1 as BSA has a higher binding affinity for Cu(II) than C-peptide, and therefore Cu(II) must bind to the protein chaperone first. In HEK-293, intracellular copper levels increased with preformed Cu(II)-C-peptide and BSA, to which follows the binding formation of Scheme 2 In addition, peptide internalization increased only with Scheme 2 in HEK-293 cells, but no changes are seen in HepG2 cells in all proposed schematics. Therefore, the binding modes between Schemes 1 and 2 may also play a role in method of C-peptide uptake (Figure 5.4).

Overall, our work highlights new mechanistic insights with C-peptide in regards to shifting copper metabolism and peptide uptake. The distinctions in copper biomarker

responses based on cell lines, addition of BSA, and Cu(II)-binding modes can pave the way for understanding the interplay of these diseases with potential applications in both therapeutic and diagnostic advances.

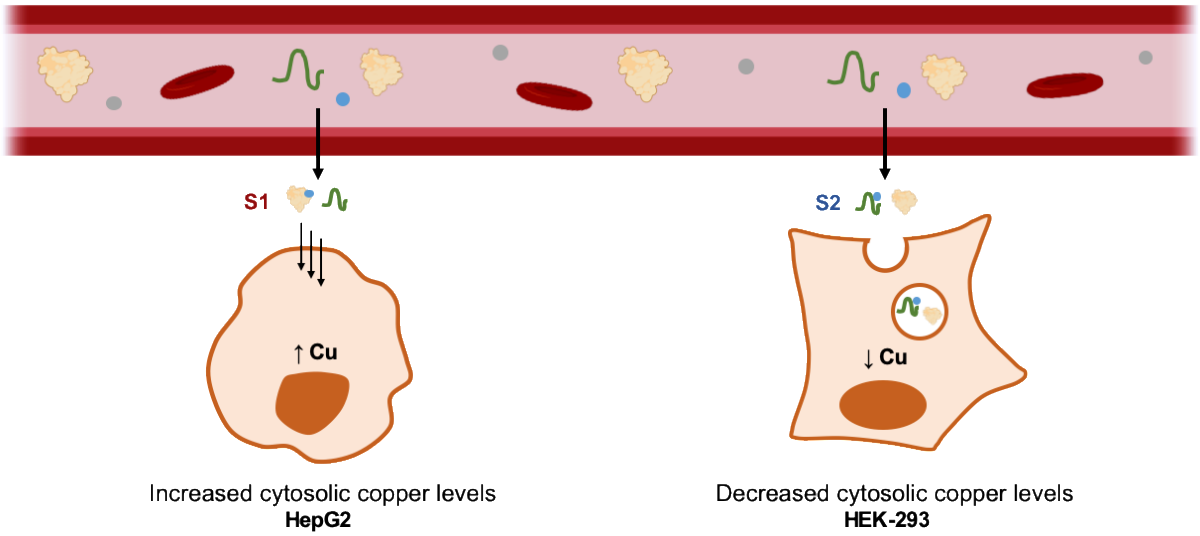

Figure 5.4. Proposed scheme displaying possible mechanisms of C-peptide and BSA in shifting copper metabolism within HepG2 and HEK-293. Intracellular copper levels are typically balanced by homeostasis, however, a disruption in copper levels lead to copper-related disease states. When C-peptide/BSA enters HepG2 possibly by receptor mediation, Cu(II) bridges these biomolecules following Scheme 1, which leads to increased intracellular copper levels in HepG2. Conversely, when preformed Cu(II)-C-peptide and BSA enters HEK-293 by endocytosis, this leads to the formation of Scheme 2. As a result, HEK-293 is put in a state of decreased intracellular copper levels. Blue circle Copper; Green biomolecule C-peptide; Protein Serum albumin; Gray circle metabolites; Cu Copper

***When replicating these blots for HepG2, biomarker expression changes with passage numbers. These cells are cultured in 4.5 g/L glucose, and the changes observed by Western blotting seem to correlate to long-term exposure of glucose. Blots shown in this chapter are done between P18-22. Blots completed between P12-15 exhibit different protein expression.*

5.4 Materials and Methods

Chemicals and reagents. All chemicals and reagents were purchased from Fisher Scientific. Dimethylformamide (DMF), 4-methylpiperidine, *N,N*-diisopropylethylamine (DIEA), dichloromethane (DCM), *N,N,N′,N′*-tetramethyl-O-(1H-benzotriazol-1-yl)uronium hexafluorophosphate (HBTU), 2,2,2-trifluoroacetic acid (TFA), diethyl ether, methanol, formic acid (FA), dimethylsulfoxide (DMSO), $CuCl_2$, Na_2HPO_4, NaOH, HCl, coumarin-3-carboxylic acid (3-CCA), L-ascorbic acid (Asc), and bovine serum albumin fatty acid-free powder (BSA) were purchased from ThermoFisher. Wang resin preloaded with Fmoc-Gln(Trt)-OH and Fmoc-Gly-OH, along with Fmoc-protected amino acids were purchased from ThermoFisher but manufactured by ChemImpex. All buffered solutions and copper salt solutions were created using Direct-Q 3 deionized water (>18 MΩ, Millipore).

Peptide synthesis of wild-type C-peptide & mutants. Human wild-type C-peptide (EAEDLQVGQVELGGGPGAGSLQPLALEGSLQ), E3A/D4A C-peptide, and N-terminus (N-term, E1-G13) and C-terminus (C-term, L24-Q31) truncations were synthesized at a 0.2 mmol scale using a heated Fmoc-based solid-phase peptide synthesis (SPPS) method. For wild-type, E3A/D4A, and C-term, Wang resin with preloaded Fmoc-Gln(Trt)-OH was swelled overnight in 5x DMF. Resin was washed 10 times with DMF. The N-terminal residue was deprotected with 25% 4-methylpiperidine in DMF, first hand-shaken for 1 minute then placed on the shaker for 10 minutes. The resin was washed 10x with 2x resin volume of DMF. Amino acids (4 eq.) and HBTU (3.9 eq.) were dissolved in minimal DMF, then DIEA (10 eq.) was added. Resin was suspended in the amino acid/HBTU/DIEA solution and heated for 5 minutes at 95°C, shaken, and incubated again at 95 °C for another 5 minutes. The solution was placed on a shaker to cool for 2 minutes.

The resin was washed 10x with 2x resin volume with DMF. The protocol was repeated from the Fmoc deprotection step for each additional amino acid. After the last amino acid coupling, the resin was washed 10x with 2x resin volume of DMF, followed by 10x washes with 2x resin volume of DCM and dried overnight. Cleavage of the protecting groups and peptide from the resin was carried out in minimal solution of 95:5 TFA:H_2O with 1-4 hours shaking. The solution was poured into chilled diethyl ether to precipitate, then the suspension was centrifuged at 3900 rpm for 10 minutes at 4°C. The supernatant was decanted and the pellet was washed again with chilled diethyl ether followed by centrifugation after each wash (3x). The pellet was dried under a stream of air overnight.

Preparation of samples following each schematic. Pre-aliquoted C-peptide and BSA were dissolved in DPBS (Gibco) for Western blot and immunofluorescence experiments, or in 10 mM PO_4 buffer (Fisher) at pH 7.4 for CCA assays, CD, UV-Vis, pH titrations, and EPR. $CuCl_2$ (Fisher) was dissolved in Milli-Q water followed by solutions containing C-peptide and/or BSA to achieve 1 or 2 eq. Cu(II). Treatments following each schematic include: (S1) 30 minute incubation of preformed Cu(II)-BSA at 1 or 2 eq. Cu(II) in solution followed by the addition of C-peptide for another 30 minutes incubation (S2) 30 minute incubation of preformed Cu(II)-C-peptide at 1 or 2 eq. Cu(II) in solution followed by the addition of BSA for another 30 minute incubation, and (S3) separate 30 minute incubations of preformed Cu(II)-BSA and Cu(II)-C-peptide at 0.5 or 1 eq. Cu(II), followed by the combination of these preformed solutions for an additional 30 minutes to reach final concentrations of 1 or 2 eq. Cu(II) in solution.

Cell line maintenance and Western blot treatment conditions. Human embryonic kidney (HEK-293) cells and human hepatocyte carcinoma (HepG2) cells were grown in

complete DMEM media + 4.5 g/L high glucose (ThermoFisher Scientific) with the addition of 10% Avantor Seradigm Premium Grade Fetal Bovine Serum (VWR), 1 mM sodium pyruvate (ThermoFisher Scientific), 100 IU penicillin and 100 µg/mL streptomycin (ThermoFisher Scientific), and 2 mM L-glutamine (Gibco). Cells were subcultured every 2 to 3 days at 70 to 90% confluence. All experiments were performed on HEK-293 cells between passage 5 and 35, and HepG2 cells between passage 10 and 20. Cells were maintained in a sterile environment and grown in 5% CO2 at 37°C in a Heracell 150l incubator (ThermoFisher Scientific). The following treatments for both cell lines at 30 minutes, 4 hours, or 24 hours include (1) $CuCl_2$ diluted in serum-free media to final concentration of 11 µM Cu(II), (2) 10 µM C-peptide diluted with serum-free media, (3) preformed Cu(II)-C-peptide diluted in serum-free media to final concentrations of 10 µM C-peptide and 11 µM Cu(II), (4) 100 µM BSA diluted in serum-free media, (5) preformed Cu(II)-BSA diluted with serum-free media to make 100 µM BSA and 11 µM Cu(II), (6) 30 minute incubation of preformed C-peptide-BSA followed by dilution with serum-free media to make 10 µM C-peptide and 100 µM BSA, and (7) 10 µM C-peptide, 11 µM Cu(II), and 100 uM BSA following (S2) conditions. C-peptide mutants (E3A/D4A, N-term, C-term) were also dissolved in DPBS following the same treatment conditions (1-7) as wild-type C-peptide.

Western blot analysis. Cells were plated at 400,000 and 300,000 cells per well in a 6-well plate for HEK-293 and HepG2 cells, respectively. Media was aspirated and washed with PBS at RT, then cells were serum-starved overnight. The following treatments for both cell lines at 30 minutes, 4 hours, or 24 hours include (1-7) for both wild-type C-peptide and C-peptide mutants (E3A/D4A, N-term, C-term). After a timed stimulation was

completed at 30 minutes, 4 hours or 24 hours, cells were washed with cold DPBS, then lysed (150 mM NaCl, 1% NP-40, 0.5% sodium deoxycholate, 0.1% SDS, 50 mM Tris-Cl pH 7.4) with EDTA-free protease inhibitor (ThermoFisher Scientific) and phosphatase inhibitor (MilliporeSigma). Lysates were vortexed on ice for 20 minutes then cleared by centrifugation at 15,000 x G at 4°C. Lysates were frozen at -20°C overnight, then quantified using a BCA assay (Invitrogen). 10 µg protein was prepared with 2-mercaptoethanol (BioRad), DPBS (Gibco), and LDS sample buffer (NP0007, Invitrogen), and loaded into a 4-12% Bis-Tris 15-well gel (Invitrogen). Gels were run in MES buffer at 100 V for 1 hour then transferred onto a PVDF membrane using a Trans-Blot Turbo Transfer System (BioRad). Membranes were blocked in 5% BSA in TBST solution (Cell Signaling Technology) for 1 hour at RT and blotted in primary antibody overnight at 4°C. Membranes were washed 3x for 5 minutes with TBST at room temperature and blotted with a secondary antibody in 5% BSA in TBST. Membranes were washed 3x for 5 minutes in TBST and imaged on a Chemidoc MP Imager (BioRad). Primary antibodies included anti-CCS (1:1000 Santa Cruz Biotechnology), anti-ATP7B (1:2000 Abcam), anti-ATP7A (1:2000 Santa Cruz Biotechnology), anti-β-Actin (1:5000 Cell Signaling Technology), and anti-α-tubulin (1:5000 ThermoFisher). For secondary antibodies, anti-rabbit IgG HRP-conjugated antibody (1:2000 Cell Signaling Technology) was used for ATP7B, anti-mouse IgG HRP-conjugated antibody (1:1000 Cell Signaling Technology) for ATP7A, anti-mouse IgG AlexaFluor 800 (1:5000 Invitrogen) for CCS, anti-rabbit IgG AlexaFluor 555 (1:5000 Invitrogen) for β-Actin, and anti-rat IgG AlexaFluor 647 (1:5000 Invitrogen) for α-tubulin. Images were processed using the ImageLab software (Biorad).

Immunofluorescence. The immunofluorescence protocol was adapted from Stevenson et al.[1] HEK-293 cells were plated into 12-well plates with acid-washed coverslips at 200,000 cells/well and HepG2 cells were plated at 100,000 cells/well. Both cell lines were grown to 50-70% confluence, then serum-starved overnight. Cells were washed with DPBS and treated with the same treatments used in Western blot stimulations (1-7) with wild-type C-peptide at 30 minutes, 4 hours, and 24 hours. Cells were then fixed with 4% paraformaldehyde at RT for 10 minutes, then washed twice with cold DPBS. Cells were permeabilized with 0.3% Triton X-100 (Fisher) in DPBS at RT for 10 minutes, then washed thrice with cold DPBS. HEK-293 cells were blocked with 3% BSA (Fisher) and HepG2 cells were blocked with 10% BSA at RT for one hour. Both blocking solutions also contain 10 mM HEPES (Gibco) and 0.3% Triton X-100 in DPBS. Cells were incubated overnight with primary anti-human C-peptide antibody (4593, Cell Signaling Technology) at 1:400 dilution in blocking buffer at 4°C. Cells were rinsed thrice with DPBS at 5 minutes each, incubated with Alexa Fluor 488 goat anti-rabbit ReadyProbes secondary antibody (Invitrogen) for 30 minutes, then washed twice with DBPS. Cells were stained with NucBlue Live ReadyProbes (Hoescht 33342, R37605, Invitrogen), washed twice with DPBS, then mounted with ProLong Gold Antifade Mountant (Invitrogen). Cells were imaged on an EVOS FL microscope with 40x magnification using DAPI and GFP Fluorescent light cubes (Invitrogen). ImageJ was used for image processing such as contrasting the DAPI and GFP channels, overlaying images, and zooming images by 200%. ImageJ was also used to determine the mean pixel intensity of treated cells.

5.5 References

(1) Wahren, J.; Ekberg, K.; Jörnvall, H. C-Peptide Is a Bioactive Peptide. *Diabetologia* **2007**, *50* (3), 503–509. https://doi.org/10.1007/s00125-006-0559-y.

(2) Marques, R. G.; Fontaine, M. J.; Rogers, J. C-Peptide: Much More than a Byproduct of Insulin Biosynthesis. *Pancreas* **2004**, *29* (3), 231–238. https://doi.org/10.1097/00006676-200410000-00009.

(3) Pinger, C. W.; Entwistle, K. E.; Bell, T. M.; Liu, Y.; Spence, D. M. C-Peptide Replacement Therapy in Type 1 Diabetes: Are We in the Trough of Disillusionment? *Molecular BioSystems*. Royal Society of Chemistry 2017, pp 1432–1437. https://doi.org/10.1039/c7mb00199a.

(4) Washburn, R. L.; Mueller, K.; Kaur, G.; Moreno, T.; Moustaid-moussa, N.; Ramalingam, L.; Dufour, J. M. C-peptide as a Therapy for Type 1 Diabetes Mellitus. *Biomedicines*. MDPI AG 2021, pp 1–24. https://doi.org/10.3390/biomedicines9030270.

(5) Ge, X.; Kakinen, A.; Gurzov, E. N.; Yang, W.; Pang, L.; Pilkington, E. H.; Govindan-Nedumpully, P.; Chen, P.; Separovic, F.; Davis, T. P.; Ke, P. C.; Ding, F. Zinc-Coordination and C-Peptide Complexation: A Potential Mechanism for the Endogenous Inhibition of IAPP Aggregation. *Chem. Commun.* **2017**, *53* (68), 9394–9397. https://doi.org/10.1039/C7CC04291D.

(6) Meyer, J. A.; Froelich, J. M.; Reid, G. E.; Karunarathne, W. K. A.; Spence, D. M. Metal-Activated C-Peptide Facilitates Glucose Clearance and the Release of a Nitric Oxide Stimulus via the GLUT1 Transporter. *Diabetologia* **2008**, *51* (1), 175–182. https://doi.org/10.1007/s00125-007-0853-3.

(7) Keltner, Z.; Meyer, J. A.; Johnson, E. M.; Palumbo, A. M.; Spence, D. M.; Reid, G. E. Mass Spectrometric Characterization and Activity of Zinc-Activated Proinsulin C-Peptide and C-Peptide Mutants. *Analyst* **2010**, *135* (2), 278–288. https://doi.org/10.1039/b917600d.

(8) Medawala, W.; McCahill, P.; Giebink, A.; Meyer, J.; Ku, C. J.; Spence, D. M. A Molecular Level Understanding of Zinc Activation of C-Peptide and Its Effects on Cellular Communication in the Bloodstream. *Review of Diabetic Studies*. Society for Biomedical Diabetes Research September 2009, pp 148–158. https://doi.org/10.1900/RDS.2009.6.148.

(9) Bal, W.; Sokołowska, M.; Kurowska, E.; Faller, P. Binding of Transition Metal Ions to Albumin: Sites, Affinities and Rates. *Biochimica et Biophysica Acta - General Subjects*. 2013, pp 5444–5455. https://doi.org/10.1016/j.bbagen.2013.06.018.

(10) Liu, Y.; Chen, C.; Summers, S.; Medawala, W.; Spence, D. M. C-Peptide and Zinc Delivery to Erythrocytes Requires the Presence of Albumin: Implications in Diabetes Explored with a 3D-Printed Fluidic Device. *Integr. Biol. (United Kingdom)* **2015**, *7* (5), 534–543. https://doi.org/10.1039/c4ib00243a.

(11) Geiger, M.; Janes, T.; Keshavarz, H.; Summers, S.; Pinger, C.; Fletcher, D.; Zinn, K.; Tennakoon, M.; Karunarathne, A.; Spence, D. A C-Peptide Complex with Albumin and Zn2+ Increases Measurable GLUT1 Levels in Membranes of Human Red Blood Cells. *Sci. Rep.* **2020**, *10* (1). https://doi.org/10.1038/s41598-020-74527-6.

(12) Stevenson, M. J.; Farran, I.; Uyeda, K.; San Juan, J.; Heffern, M. C. Analysis of Metal Effects on C-peptide Structure and Internalization. *ChemBioChem* **2019**. https://doi.org/10.1002/cbic.201900172.

(13) Stevenson, M. J.; Janisse, S. E.; Tao, L.; Neil, R. L.; Pham, Q. D.; Britt, R. D.; Heffern, M. C. Elucidation of a Copper Binding Site in Proinsulin C-Peptide and Its Implications for Metal-Modulated Activity. *Inorg. Chem.* **2020**, *59* (13), 9339–9349. https://doi.org/10.1021/acs.inorgchem.0c01212.

(14) Squitti, R.; Mendez, A. J.; Simonelli, I.; Ricordi, C. Diabetes and Alzheimer's Disease: Can Elevated Free Copper Predict the Risk of the Disease? *J. Alzheimer's Dis.* **2017**, *56* (3), 1055. https://doi.org/10.3233/JAD-161033.

(15) Wang, N.; Wang, Y.; Zhang, W.; Chen, Y.; Chen, X.; Wang, C.; Li, Q.; Chen, C.; Jiang, B.; Lu, Y. C-Peptide Is Associated with NAFLD Inflammatory and Fibrotic Progression in Type 2 Diabetes. *Diabetes. Metab. Res. Rev.* **2020**, *36* (2), 1–8. https://doi.org/10.1002/dmrr.3210.

(16) Lindahl, E.; Nyman, U.; Melles, E.; Sigmundsson, K.; Ståhlberg, M.; Wahren, J.; Öbrink, B.; Shafqat, J.; Joseph, B.; Jörnvall, H. Cellular Internalization of Proinsulin C-Peptide. *Cell. Mol. Life Sci.* **2007**, *64* (4), 479–486. https://doi.org/10.1007/s00018-007-6467-6.

(17) Yosten, G. L. C.; Kolar, G. R.; Redlinger, L. J.; Samson, W. K. Evidence for an Interaction between Proinsulin C-Peptide and GPR146. *J. Endocrinol.* **2013**, *218* (2). https://doi.org/10.1530/JOE-13-0203.

(18) Rossiter, J. L.; Redlinger, L. J.; Kolar, G. R.; Samson, W. K.; Yosten, G. L. C. The Actions of C-Peptide in HEK293 Cells Are Dependent upon Insulin and Extracellular Glucose Concentrations. *Peptides* **2022**, *150*. https://doi.org/10.1016/j.peptides.2021.170718.

(19) J, B.; M, I.; MR, L. Copper Deficiency Induces the Upregulation of the Copper Chaperone for Cu/Zn Superoxide Dismutase in Weanling Male Rats. *J. Nutr.* **2003**, *133* (1), 28–31. https://doi.org/10.1093/JN/133.1.28.

(20) Brady, D. C.; Crowe, M. S.; Turski, M. L.; Hobbs, G. A.; Yao, X.; Chaikuad, A.; Knapp, S.; Xiao, K.; Campbell, S. L.; Thiele, D. J.; Counter, C. M. Copper Is Required for Oncogenic BRAF Signalling and Tumorigenesis. *Nat. 2014 5097501* **2014**, *509* (7501), 492–496. https://doi.org/10.1038/nature13180.

(21) Barnes, N.; Bartee, M. Y.; Braiterman, L.; Gupta, A.; Ustiyan, V.; Zuzel, V.; Kaplan, J. H.; Hubbard, A. L.; Lutsenko, S. Cell-specific Trafficking Suggests a New Role for Renal ATP7B in the Intracellular Copper Storage. *Traffic* **2009**, *10*

(6), 767. https://doi.org/10.1111/J.1600-0854.2009.00901.X.
(22) S, L. Copper Trafficking to the Secretory Pathway. *Metallomics* **2016**, *8* (9), 840–852. https://doi.org/10.1039/C6MT00176A.
(23) S, L. Human Copper Homeostasis: A Network of Interconnected Pathways. *Curr. Opin. Chem. Biol.* **2010**, *14* (2), 211–217. https://doi.org/10.1016/J.CBPA.2010.01.003.